The Department of Radiation Therapy and Radiation Oncology
Medical Faculty, University of Saarland
Homburg/Saar, Germany

The role of histone variant H2A.J in radiation dermatitis

Submission of thesis to the Medical Faculty in fulfilment of
for the degree of
Doctor of Philosophy (Ph.D.)
Medical Faculty,
UNIVERSITY OF SAARLAND
2023

Submission by: Gargi Tewary
Date of Birth: 12.08.1993
Place: Noida, U.P, India

Date of Promotion: 25.08.2023

Dekanat: Univ-Prof. Dr.med. Michael D.Menger

Supervisors: Prof. Dr. rer. nat. Klaus Römer
                          Univ-Prof. Dr. med. Thomas Volk

Declaration

I hereby declare that the Ph.D thesis entitled **"The role of histone variant H2A.J in radiation dermatitis"** is a presentation of my original research work. All external sources of information have been acknowledged. No portion of this work has been submitted in support of any other degree or qualification.

Place: Homburg, Germany

Date:

Gargi Tewary

Table of contents

List of abbreviations

µl	Microliter
µm	Micrometer
53BP1	p53-binding protein 1
Ab	Antibody
CT	Computed tomography
CPG	Cytosine phosphate guanine
DAPI	4′,6-Diamidin-2-phenylindole
DAB	3,3'-Diaminobenzidin-Tetrahydrochloride
DDR	DNA damage response
dH2O	deionized water
DMF	N,N-Dimethylformamide
DMSO	Dimethylsulfoxide
DNA	Deoxyribonucleic acid
ELISA	Enzyme linked immunosorbent assay
g	Gravity
Gt	Goat
Gy	Gray
GM-CSF	Granulocyte macrophage - colony stimulating factor
h	Hour
HFSC	Hair follicle stem cells
H2A.J	Histone variant H2A.J
H_2O_2	Hydrogen peroxide
IR	Ionizing radiation
IFM	Immunofluorescence microscopy

IHC	Immunohistochemistry
IL-6	Interleukin-6
IVC	Individually ventilated cage
J	Joule
kg	Kilogram
KO	Knock-out
meV	Megaelectronvolt
mGy	Milli gray
min	minute
mm	Millimetre
MMP	Matrix- Metallo-Proteinases
MPO	Myeloperoxidase
MCP-1	Monocyte chemoattractant protein-1
NaCl	Sodium chloride
NET	Neutrophil extracellular traps
NHEJ	Non-homologous end- joining
non-IR	Non-irradiated
PBS	Phosphate buffer saline
PDGF	Platelet derived growth factor
PFA	Paraformaldehyde
pg	Picogram
pH	Potential of hydrogen
p-value	Probability value
Rb	Rabbit
RT	Room temperature
S	Sievert

SASP	Senescence associated secretory phenotype
SA-β-GAL	Senescence-associated beta galactosidase
SEM	Standard error of mean
SD	Standard deviation
TNF	Tumor necrosis factor
w	Week
WT	wild-type

Summary

Histone variant H2A.J is connected with premature senescence following ionizing radiation (IR) and modifies senescence-associated secretory phenotype (SASP). Using a preclinical in-vivo model the role of H2A.J was investigated in the acute phase of radiation dermatitis. H2A.J wild-type (WT) and knock-out (KO) mice were exposed to moderate (1x or 5x 2Gy, whole-body IR) or high doses (10Gy or 20Gy, dorsal skinfold IR). Radiation-induced skin reactions were analysed at 24h/ 72h/ 1w/ 2w post-IR at the macroscopic (skin lesions) and microscopic level (hair follicle density, epidermal thickness). H2A.J and other senescence markers (SA-β-Gal, laminB1) were analysed in epidermal keratinocytes by immunohistochemistry and immunofluorescence microscopy. ELISA measurements showed higher cytokine expression in conditioned medium acquired from skin cultures of KO and WT mice.

In WT skin epidermal keratinocytes showed a time- and dose-dependent H2A.J accumulation following IR exposure. Unexpectedly, significantly stronger radiation reactions were observed in irradiated KO versus WT skin with stronger inflammatory reactions and hair follicles loss. Clearly more radiation-induced senescence was observed in epidermal keratinocytes of KO versus WT skin after moderate and high IR doses. Among various keratinocyte populations significant differences in senescence induction were observed, with hair follicle stem cells (HFSCs) in bulge regions of KO skin being particularly badly damaged at high doses, leading to increased hair follicle atrophy. Neutrophil-derived myeloperoxidase led to increased tissue damage in irradiated KO skin, and subsequently to excessive proliferation and abnormal differentiation of keratinocytes, probably through regulatory mechanisms of transcription-factor JunB, eventually leading to more pronounced epidermal hyperplasia.

In conclusion, through epigenetic regulation of pro-inflammatory genes in response to IR exposure, H2A.J expression in epidermal keratinocytes plays an obligatory role in balancing the innate immune response during radiation dermatitis.

Zusammenfassung

Die Histonvariante H2A.J ist mit vorzeitiger Seneszenz nach ionisierender Strahlung (IR) assoziiert und moduliert den Seneszenz-assoziierten sekretorischen Phänotyp (SASP). Anhand eines präklinischen in-vivo-Modells wurde die Rolle von H2A.J in der akuten Phase der Strahlendermatitis untersucht. H2A.J-wild-typ (WT) und knock-out (KO) Mäuse wurden moderaten (1x oder 5x 2Gy, Ganzkörper-IR) oder hohen Dosen (10Gy oder 20Gy, dorsale Hautfalten-IR) ausgesetzt. Strahleninduzierte Hautreaktionen wurden 24h/ 72h/ 1w/ 2w post-IR auf makroskopischer (Hautläsionen) und mikroskopischer Ebene (Haarfollikeldichte, epidermale Dicke) analysiert. H2A.J und andere Seneszenzmarker (SA-β-Gal, LaminB1) wurden in epidermalen Keratinozyten durch Immunhistochemie und Immunfluoreszenzmikroskopie analysiert. In WT-Haut zeigten epidermale Keratinozyten eine zeit- und dosisabhängige H2A.J-Akkumulation nach IR Exposition. Unerwarteterweise wurden signifikant stärkere Strahlenreaktionen bei bestrahlter KO versus WT Haut mit stärkeren Entzündungsreaktionen und Haarfollikelverlust beobachtet. Deutlich mehr strahleninduzierte Seneszenz wurde in epidermalen Keratinozyten von KO im Vergleich zu WT Haut nach moderaten und hohen IR-Dosen beobachtet. Unter verschiedenen Keratinozyten-Populationen wurden signifikante Unterschiede in der Seneszenz-Induktion beobachtet, wobei Haarfollikel-Stammzellen (HFSCs) in Bulge-Regionen der KO Haut bei hohen Dosen besonders stark geschädigt wurden, was zu einer erhöhten Haarfollikel-Atrophie führte. Aus Neutrophilen stammende Myeloperoxidase führte zu einer erhöhten Gewebeschädigung in bestrahlter KO Haut und anschließend zu einer übermäßigen Proliferation und abnormalen Differenzierung von Keratinozyten, wahrscheinlich durch regulatorische Mechanismen des Transkriptionsfaktors JunB, was schließlich zu einer ausgeprägteren epidermalen Hyperplasie führte.

Zusammenfassung

Zusammenfassend lässt sich sagen, dass die strahleninduzierte H2A.J Expression in epidermalen Keratinozyten die Entzündungsreaktionen im Rahmen der Strahlendermatitis durch epigenetische Regulationsmechanismen wesentlich beeinflusst.

1. <u>Introduction</u>

1.1. Skin physiology

The skin is a multi-layered epithelium that surrounds the entire organism and thus protects it from external influences and stimuli throughout life (Cotsarelis, 2006). The skin consists of three main units: First the subcutis, which consists mainly of connective tissue and stored fatty tissue. Above the subcutis is the dermis (Cotsarelis, 2006; Cotsarelis et al., 1990; Fuchs, 2008) including collagen and elastic fibers, and a variety of sensory receptors and blood vessels that nourish the overlying epidermis. The epidermis is the outermost layer of skin (Fuchs & Segre, 2000; Kaur, 2006). It consists almost entirely of keratinocytes (corn-forming cells) linked by desmosomes that are detached from the surface of cornified squamous epithelial cells (Kaur, 2006; R. J. Morris et al., 2004). In order to carry out its lifelong protective function, the epidermis must constantly renew itself (Ohyama et al., 2006) to replace shed or dead cells (Fuchs & Segre, 2000). This skin tissue homeostasis is achieved by stem cells in the basal cell layer that have the ability to form rapidly dividing daughter cells, also called transiently amplifying cells (Cotsarelis, 2006; Cotsarelis et al., 1990). These cells rapidly divide a few times before differentiating on their way to the skin surface. This route from the basal cell layer to the surface of the epidermis in the murine skin takes about 8-9.5 days (Rando, 2006; Trempus et al., 2003). The epidermis is broken through by hair follicles in hairy skin regions. In mice the hair follicle is fully formed between the 5-9 days after birth. This requires an interaction between the dermis and the basal cell layer of the epidermis (Trempus et al., 2003).
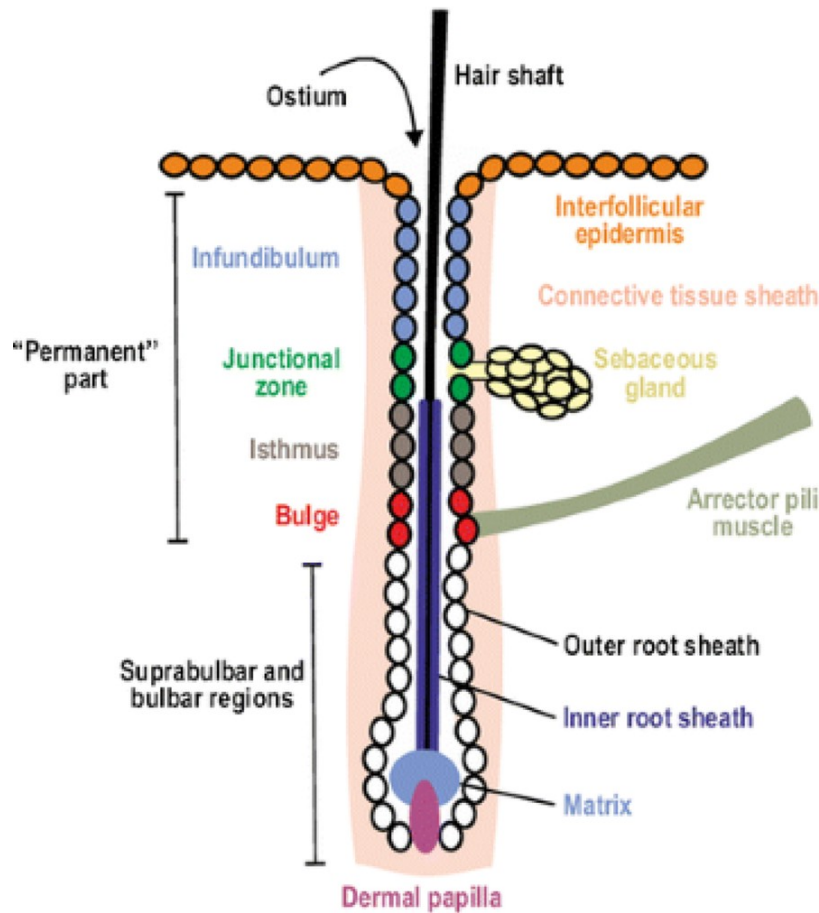
Figure 1. Structure of the hair follicle. Schematic representation of different parts of the murine hair follicle. The bulge region (red) is the reservoir of CD34 positive hair follicle stem cells which are known to be multipotent stem cells crucial for wound healing and epidermal rejuvenation (Panteleyev, 2018).

The hair follicle is made up of several layers. Each layer, from the innermost, the hair medulla, to the outermost, the outer root sheath, has a defined function (Potten, 1974; Trempus et al., 2003). The actively dividing cells are confined to the outer root sheath, the secondary germinal region, and the hair bulb (lowest part of the hair follicle) (Oshima et al., 2001; Paus et al., 1998; Potten, 2009; Trempus et al., 2003). As further seen in Fig 1, the hair follicle is divided into two areas, the permanent area - from the base of the epidermis to below the ridge - and the cyclic area, which extends from the secondary germinal region to the tip of the hair follicle (Ohyama et al., 2006; Oshima et al., 2001). Different stem cell populations can be identified in the hair follicle, which lie inside the bulge region (R. J. Morris et al., 2004). The primordial stem cells of the epidermis, the hair follicle stem cells (HFSCs), which were the first adult stem cells to be isolated, are located on the basement membrane of the

bulge (Trempus et al., 2003). This cell population was identified as label-retaining cells based on their rare dividing activity and also subsequently identified as stem cells using microdissected hair follicles and subsequent transplantation under the renal capsule of hairless mice (Oshima et al., 2001; Paus et al., 1998). These can form all cells of the hair follicle, the sebaceous gland and the epidermis (Paus et al., 1998). In addition, they have the potential to also form non-epithelial cells such as neurons, blood vessel cells or Schwann cells, reflecting the pluripotent character of these stem cells (Kaur, 2006; R. J. Morris et al., 2004; Myung & Ito, 2012). In murine skin HFSCs can be specifically detected using CD34 (Kaur, 2006; Trempus et al., 2003).

1.2. Clinical radiotherapy

Radiotherapy is prescribed for about 60-70% of people with cancer, alone or in combination with other treatments (Woodhouse et al., 2018). The extent of clinical radiation dermatitis depends on external factors like total dose, dose per fraction, quality of beam (LET), radiation technique (bolus), volume and surface area of the irradiated skin (skin folds) and individual sensitivity to radiation (Bray et al., 2016).

Total radiation dose is a key factor for the development of skin toxicity. For example total dose ($\geq$20Gy) can result in development of skin toxicity, but if the dose is fractionated the total dose can be raised up to 30 or 40Gy before radiation induced skin toxicity develops (Dowling et al., 2017; Mazeron et al., 2014). Therefore fractionated radiation treatment increases radiation tolerance. However the time before clinical manifestations occur is not dependent on the radiation dose, but is actually connected to the timing of normal cell turnover. Which means that the total dose delivered affects the time that the skin requires to clinically heal (Dowling et al., 2017; Ford & Dieterich, 2017). In addition, the usage of boost doses that create overlying treatment fields as well as bolus materials are methods of radiotherapy that escalate radiation doses in the skin, thus resulting in increased risk of skin toxicity (Chang et al., 2014; Malicki et al., 2014).

Acute skin damage is also affected by the quality of radiation beam (Bray et al., 2016). The type of particle that is emitted by source of radiation affects the depth of infiltration in the skin tissue, thereby affecting the extent of damage (Bray et al., 2016; Woodhouse et al., 2018). In addition, the size of the skin area is directly proportional to the risk of acute skin reactions caused by high radiation doses. In order to overcome this issue new external beam modalities, such as intensity-modulated-radiotherapy (IMRT), are used to reduce the radiation hotspots in the skin by supplying more homogenous dose distributions (Dowling et al., 2017; Mazeron et al., 2014). Moreover, IMRT has also been shown to reduce the occurrence of late radiation-induced skin effects, such as telangiectasia in breast cancer patients (Chang et al., 2014; Ford & Dieterich, 2017).

The extent of radiation-induced skin reactions is both, treatment as well as patient related. For instance, factors like smoking, poor nutritional habits, obesity and overlapping skin folds contribute to the predisposition towards acute radiation dermatitis (Bray et al., 2016; Chang et al., 2014; Ford & Dieterich, 2017).

1.3. Radiation-induced skin toxicity

Exposure of skin to ionizing radiation leads to cutaneous reactions in the irradiated skin. Various factors as mentioned in section 1.2 affect the biological response of the skin, such as radiation quality, dose rate, and total dose (Bray et al., 2016). Skin damage caused by ionizing radiation involves effects that last from hours to years after radiation exposure. These effects occur at single doses higher than 4 Gy or normo-fractionated doses higher than 30-40Gy (Chu et al., 2021; Jaschke et al., 2017). Histopathological findings of late skin effects include telangiectasia, dermal fibrosis, atrophy of sebaceous glands, and reduction in hair follicles numbers. Due to increased or reduced melanin production in melanocytes, irradiated skin often shows pigmentation disorders (Janko et al., 2012; Multhoff & Radons, 2012).

Another essential factor that contributes to radiation-induced skin damage is the loss of functional skin tissue stem cells. Missing or non-functional stem cells cannot adequately

replace the damaged cells in the context of tissue homeostasis (Spałek, 2016). Impairment of the survival and proliferation of stem cells takes place within days after irradiation and an increased rate of apoptosis in these cells persists for months (Bolderston et al., 2006; Janko et al., 2012).

Irradiation of skin leads to the production of cytokines by various skin cells, such as keratinocytes, thereby initiating an pro-inflammatory and pro-fibrotic cascade during all stages of cutaneous radiation reactions (Bray et al., 2016; Woodhouse et al., 2018). Studies have shown that senescence-associated cytokine signalling of IL-1 and IL-6 along with upregulation of IL-17 within murine hair follicles, basal keratinocytes and dermal fibroblasts are major mediators of radiation-induced alopecia and dermatitis (IRIAD) (Bray et al., 2016; Liao et al., 2017; Mazeron et al., 2014). Therefore, some of the major cytokines that have found to be involved in radiation-induced skin response are IL-1, IL-6, tumor-necrosis-factor (TNF)-α and transforming-growth-factor (TGF)-β (Bray et al., 2016).

IL-1, existing in two forms IL-1α and IL-1β, is one of the most significant pro-inflammatory cytokines and involved in the acute phase of inflammatory response (Bray et al., 2016; Müller, hematology, et al., n.d.). IL-1 primarily secreted by monocytes, macrophages, keratinocytes, fibroblasts and endothelial cells plays an vital role in the stimulation of keratinocyte proliferation and the induction of matrix-metallo-proteinases (MMP's) and collagen synthesis (Liao et al., 2017; Müller & Meineke, 2011). In a study it was found that in C57BL/6 mice irradiated with a single dose of 30Gy that keratinocytes are the major cells type responsible for production of IL-1. One of the isoforms of IL-1 that is IL-1β has been shown to be responsible for elevated expression of MMP's (Jaschke et al., 2017; Müller, hematology, et al., n.d.; Yang et al., 2020). The biological role of these proteases are connected to a complex regulatory system that involves specific tissue inhibitors of MMPs (TIMP) (Bray et al., 2016). The MMP/TIMP counterbalancing system plays an essential role

in pathological skin conditions like fibrosis. Thus IL-1 signalling has been found to show an important role in radiation-induced dermatitis and skin fibrosis (Bray et al., 2016).

IL-6 is a pluripotent cytokine that acts as major mediator during acute inflammatory response. IL-6 is produced by keratinocytes and fibroblasts, but particularly by phagocytic mononuclear cells, T and B lymphocytes and endothelial cells (Bray et al., 2016; Liao et al., 2017; Paldor et al., 2022). IL-6 has been found to have a huge number of DNA binding sites for transcription factors like nuclear-factor (NF)-κB, activator-protein (AP)-1 and cAMP-responsive element binding protein (CREB). Induction of IL-6 by ionizing radiation leads to the induction of binding activity of theses transcription factors (Liao et al., 2017; Paldor et al., 2022).

Tumor-necrosis-factor (TNF)-α is a cytokine majorly released by phagocytes, neutrophils, lymphocytes and natural killer (NK) cells. TNF- α is one of the key mediators of the cellular immune response (Borish & Steinke, 2003; Bray et al., 2016; Schaue et al., 2012). Additionally keratinocytes also express TNF receptors on their cell surface (Bray et al., 2016). Upon radiation exposure synthesis of TNF-α by keratinocytes leads to induction of autocrine and paracrine mechanisms and secretion of cytokines (Bray et al., 2016; Okunieff et al., 2006; Schaue et al., 2012). Both TNF-α and IL-1 have the capability for the induction of IL-6 expression and these three cytokines are major mediators of the inflammatory response which is a main event in cutaneous radiation reactions (Gallet et al., 2011; Okunieff et al., 2006).

Tumor-growth-factor (TGF)-β is a family of peptides that exists in three isoforms TGF-β1, TGF-β2, TGF-β3 (Bray et al., 2016; Rübe et al., 2004). This multifunctional cytokine is produced by different cell types like macrophages, fibroblasts, and keratinocytes and involved in cellular processes like growth, differentiation, apoptosis and production of extracellular matrix production (ECM) (Bray et al., 2016; Schaue et al., 2012). TGF-β1 plays an important role in the development and normal wound healing. During fibrosis TGF-β1 is involved in the deposition and remodelling of extracellular matrix (ECM) and the production of matrix proteins like collagen and fibronectin. Deregulation in TGF-β1 causes fibroproliferative

disorders (Borish & Steinke, 2003; Schaue et al., 2012). TGF-β1 plays a central role in inflammatory and fibrotic diseases, such as radiation-induced skin fibrosis (Gallet et al., 2011). Initiation of TGF-β was observed in mouse skin after single-dose irradiation of 50Gy, during both the acute inflammatory phase and the late fibrosing phase of radiation-induced skin damage (Borish & Steinke, 2003; Bray et al., 2016; Schaue et al., 2012).

1.3.1 Radiation-induced dermatitis

Radiation dermatitis is a well-known side effect of ionizing radiation that is given to the skin during cancer treatment (Dormand et al., 2005). Radiation dermatitis is also the most communal side effect in patients getting radiation therapy for sarcoma, breast and head and neck cancer (Spałek, 2016; Xue et al., 2017). The majority of cancer patients that receive radiation therapy show some form radiation dermatitis such as erythema, dry or moist desquamation. Erythema is the first visible sign of radiation dermatitis seen in 90% of these patients followed by moist desquamation seen in 30% of the patients (Jaschke et al., 2017; Xue et al., 2017).

The pathogenesis of radiation dermatitis involves inflammatory responses,that affects the cellular components in the epidermis, dermis and vasculature (Gallet et al., 2011; Hymes et al., 2006a). Radiation exposure leads to immediate tissue damage due to the production of reactive oxygen species (ROS) as well as the direct effects of IR, leading to DNA damage that affects cellular structures such as like cell membranes and nuclear DNA (Gallet et al., 2011; Xiao et al., 2020).

Damage to the skin triggered by ionizing radiation also disturbs the proliferation of keratinocytes (Hymes et al., 2006a; Jaschke et al., 2017; Xue et al., 2017). The epidermis therefore tries to compensate this damage by increasing the rate of mitosis in the basal keratinocyte layer. But because the generation of new cells is faster than the shedding of the old cells (corneocytes) this results in thickened scaly skin or dry desquamation (Yang et al., 2020). Due to this the basal layer is not able to recover and an exudate is released from the

basal layer, which is referred to as moist desquamation (Almendral et al., 1988; Martin et al., 2016; Yang et al., 2020). Thus, variable degrees of such damage affect the integrity of the physical barrier provided by the skin (Yang et al., 2020).
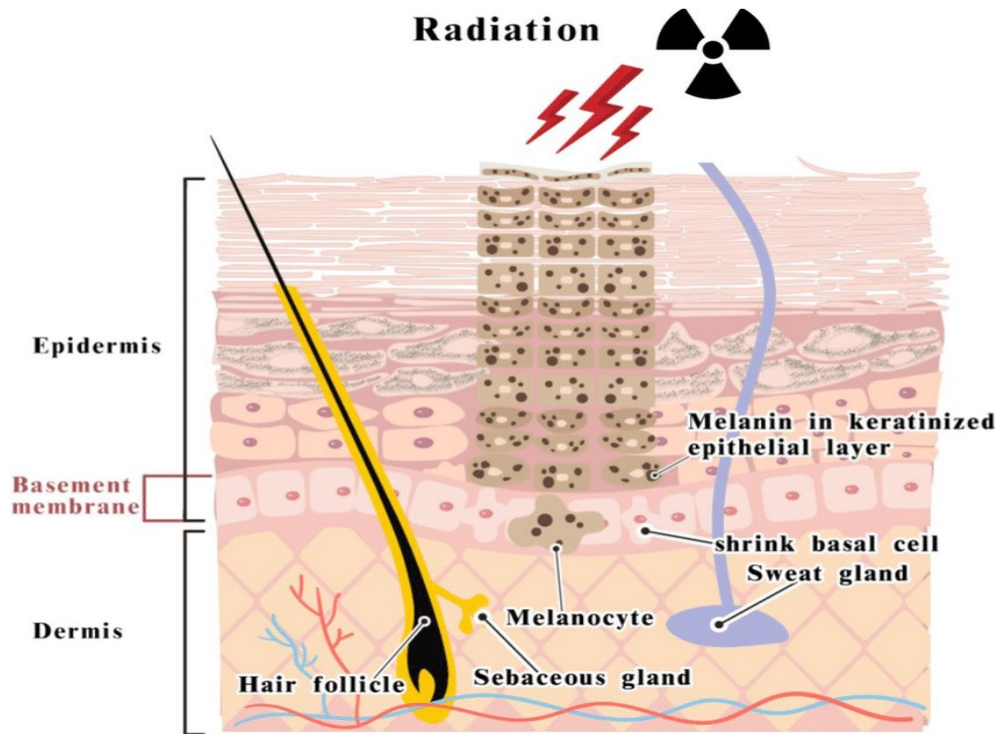
Figure 2 Pathophysiological mechanism of radiation-induced skin injury: Ionizing radiation causes damage to skin appendages such as hair follicles, sweat and sebaceous glands, which might lead to their atrophy. The activation of melanocytes can lead to hyperpigmentation (Chu et al., 2021).

The mechanism of radiation-induced dermatitis involves stimulation of immune cells in the epidermal and dermal layer by keratinocytes (Friedman, 2005; Guarino et al., 2009). This involves a cascade of activating signals from cytokines and chemokines like interleukin-1α (IL-1α), interleukin-1β (IL-1β), tumor necrosis factor (TNF)-α, IL-6, C-C motif chemokine ligand -4 (CCL-4), C-X-C motif chemokine ligand-10 (CXCL-10) , CCL-2. The production of MMP's and their endogenous inhibitors (TIMPs) may lead to the degradation of dermal components. The activation of vascular endothelial cells causes increase in adhesion molecules, such as intercellular adhesion molecules (ICAM-1), vascular cell adhesion molecule (VCAM-1) and E-selectin (Dormand et al., 2005; Spałek, 2016). These adhesion

molecules play a central role for the migration of immune cells to the site of radiation-induced skin injury (Spałek, 2016).

1.4. Role of 53BP1 in regulation of DNA double strand break repair

DNA double strand break repair is significant for stabilizing genomic integrity and upholding cellular homeostasis (IM Ward, 2003; Lieber, 2010). An imperative regulator of DSB signalling is p53-binding protein 1 (53BP1) (LB Schultz, 2000; N Dimitrova, 2008). 53BP1 plays an important role in promoting checkpoint signalling by amplifying ATM activity in response to DNA damage (TA Mochan, 2004; B. Wang, 2002).
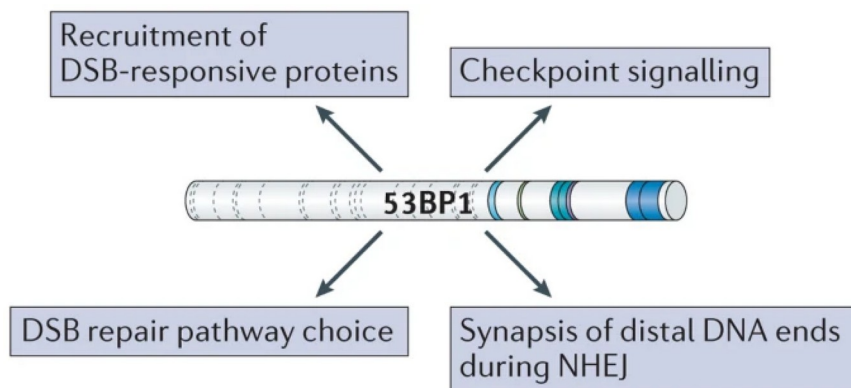
Figure 3: Functions of 53BP1 in the DNA damage response (1) DSB signalling at DNA damage sites, (2) promoting ATM-mediated checkpoint signalling, (3) key player in choosing DSB repair pathway, (4) promoting distal DNA end synapsis during NHEJ (B. Wang, 2002).

53BP1 is mainly associated with non-homologous end joining (NHEJ) that involves re-joining of broken ends of DNA molecules (Lieber, 2010; Panier & Boulton, 2013). 53BP1 protects the double-strand break ends from processing by DNA end-resection during G1 phase of the cells cycle (L Anderson, 2001; TA Mochan, 2004). When DSBs are detected, 53BP1 immediately starts accumulating on the chromatin that surrounds the damaged site of DNA. (Difilippantonio, 2008; Manis, 2004).

This signalling cascade is started by ATM-mediated phosphorylation of histone H2A (H2A) variant H2A.X (γH2A.X) which is followed by recruitment of mediator of DNA damage checkpoint protein 1 (MDC1) and activation of RNF8-RNF168-dependent chromatin ubiquitylation (AA Goodarzi, 2013; Manis, 2004). ATM-mediated phosphorylation of the

53BP1 N-terminus initiates the association with molecular factors RAP1-interacting factor1 (RIF1) and PAX transactivation activation domain-interacting protein (PTIP) that blocks the end-processing, thus channelling the DSB repair by NHEJ in G1 phase (Bunting, 2010; IM Ward, 2003; Lieber, 2010). Recruitment of 53BP1 can be studied microscopically for tracking the formation of subnuclear foci in damaged chromatin, thus 53BP1 is commonly used as a marker of DSB repair (Callen, 2013; Ditullio, 2002).

1.4.1. Radiation-induced senescence

The term senescence was first originated by Hayflick and Moorhead in 1961, which defines the finite capacity of a cell's life (Hayflick & Moorhead, 1961). Whether a cell undergoes senescence is dependent on multiple factors such as cell type, extent of DNA damage, duration of exposure to DNA damaging agent, etc. (Campisi, 2013; Chen et al., 2019).

Cellular senescence is usually characterized by the amplified expression of CDKNA's, such as p16INK4a and p21, reduced expression of lamin B1, and senescence-associated heterochromatin foci (SAHF) (Birch & Gil, 2020; Li et al., 2018a). Senescent cells are also marked by a flat morphology with an large lysosomal compartment, marked by the expression of senescence associated β-galactosidase (SA-β-Gal) (Mongiardi et al., 2021).

Exposure to ionizing radiation can cause irreparable DSB's, that lead to delay in the DNA damage response (DDR) and trigger premature senescence (Kuilman et al., 2010). DDR leads to the temporary arrest of the cell cycle through ATR, ATM kinase, p53/p21 and p16INK4a/Rb-regulated pathways (Chen et al., 2019; Rodier et al., 2009). Following DSB induction ATM and ATR kinase act as mediators for the phosphorylation of downstream targets of the DDR, such as histone H2AX and p53, and mediate distinct kinase signaling cascades such as CHK1 and CHK2 pathways, modulating cell cycle checkpoints (Nagineni et al., 2021; Peng et al., 2020). The degree of DNA damage repair by these downstream effectors shows an essential role in regulating the cell outcome, that can be premature senescence or apoptosis (McCart et al., 2017).

**1.4.2. Senescence-associated secretory phenotype (SASP)**

Senescence-associated secretory phenotype (SASP) is one of the most commonly used markers for detection of senescence, which is secreted in senescent cells (Birch & Gil, 2020). SASP contributes via autocrine and paracrine signalling mechanisms to the stabilization of the senescent phenotype (Rodier et al., 2009). SASP plays a key role in recruiting immune cells, such as natural killer (NK) cells, neutrophils, monocyte-derived macrophages and T cells, that are important for clearing senescent cells (Birch & Gil, 2020). In response to tissue damage the SASP is known to promote cellular reprogramming in neighbouring cells (Campisi, 2013; Mongiardi et al., 2021).

SASP induction involves factors like nuclear factor-κB (NF-κB), CCAAT-enhancer binding protein β (c/EBPβ) and persistent DDR activity, that cause induction of pro-inflammatory SASP factors like insulin-like growth factor binding protein (Igfbp), IL-6 and IL8 (Li et al., 2018b; McCart et al., 2017; Nagineni et al., 2021). Activation of NF- κB is required for promoting SASP activation which is regulated by activation of member of mitogen activated protein kinase p38 (Eriksson & Stigbrand, 2010). Additionally, recruitment of ATM to DSBs activates NF-κB, that further encourages expression of pro-inflammatory genes of SASP factors, such as IL1α/β, IL-6, TGF-β, TNF-α (Eriksson & Stigbrand, 2010; Salminen et al., 2012). Moreover, SASP composition is also regulated by NOTCH1 based on immunosuppressive or inflammatory function (Birch & Gil, 2020).

1.5. Histone variants

Histones have a major functional importance for packaging and organization of DNA inside the nucleus. Moreover, histones show a pivotal role in the epigenetic guideline of genes expression (Rossetto et al., 2012; Strahl & Allis, 2000). For this purpose, histones have an

unique protein sequences and selection of specific chaperone organizations and chromatin remodelling complexes that control their localization in the genome (Rossetto et al., 2012).
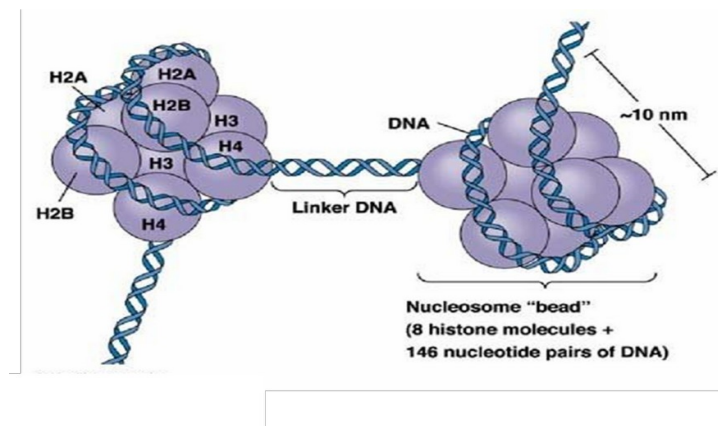
Figure 4. Structure of histone octamer and nucleosome. Association of 146 bp of DNA with histone octamer to form a nucleosome. Histones are crucial for nucleosome compaction, about 50 bp of linker DNA is present between each nucleosome (Gion, Wendy & Adams, David et al. 2023).

The nucleosome consists of 4 pair of core histones, H2A, H2B, H3 and H4 and DNA consisting of 145-147 base pairs (bp) (Celeste et al., 2003; Downs et al., 2004). In addition to this, histones have structurally similar isoforms that might play a central role in regulation of gene expression (Fernandez-Capetillo et al., 2004; Karagiannis & El-Osta, 2007).

The replacing of canonical histones by histone variants is one of the mechanisms evolved by cells for chromatin regulation, that increase the complexity of chromatin by creation of specialized nucleosomes (Tamburini & Tyler, 2005; Vidanes et al., 2005). The H2A family has abundance of variants like H2A.X, H2AZ, macroH2A1, macroH2A2, H2AF/Z and H2ABbd that are highly diverse in the C-terminus in relation to amino acid length and sequence (Fernandez-Capetillo et al., 2004; Tamburini & Tyler, 2005; Vidanes et al., 2005). Recruitment of these histone variants on nucleosomes affects the chromatin structure and function in two ways, firstly by the sequence divergence that affects the stability of the nucleosome and secondly by the modifications caused by these sequence divergence (Suganuma & Workman, 2011; Tamburini & Tyler, 2005; van Attikum & Gasser, 2005).

During transcription and replication changes in the chromatin structure take place. This chromatin remodelling is required for increasing the accessibility of proteins to the DNA, and mainly takes place in two ways, by post-translational modifications (covalent histone modifications) or by displacing histones or entire nucleosome (Rossetto et al., 2010, 2012; Yun et al., 2011). Covalent histone modifications are very important epigenetic regulatory elements that function by structural histone changes, electrostatic interactions and recruitment of non-histone proteins to chromatin. These epigenetic changes are marked by phosphorylation, acetylation, methylation and ubiquitination of histones (Rossetto et al., 2012; Strahl & Allis, 2000; Tamburini & Tyler, 2005).

The phosphorylation of histones or histone variants is a hallmark for theDDR. In eukaryotic cells the phosphorylation of the H2AX histone variant takes place at serine 139 (S139) (Fernandez-Capetillo et al., 2004; Vidanes et al., 2005) and leads to the activation of the DDR.

Acetylation is another post translational modification which is involved in transcriptional activation. For instance, it involves histone modification of H3 and H4 at the lysine residue, thereby altering the interactions between histones and DNA (Celeste et al., 2003; Downs et al., 2004).

Histone modifications are also marked by methylation of lysine and arginine residues. Depending on the type of histone involved histones can be mono-, di- or tri-methylated, indicating transcriptionally active or inactive chromatin (Suganuma & Workman, 2011; Tamburini & Tyler, 2005). For instance, methylation of lysine H3K4, H3K79 and H3K36 leads to the transcriptional activation; however, methylation of H3K9, H4K20 and H3K27 leads to the repression of transcription (Suganuma & Workman, 2011; van Attikum & Gasser, 2005).

Finally the largest post-translational modification is the conjugation of ubiquitin to lysine residues; such modification takes place in three stages, that is activation, conjugation and ligation that mono-ubiquitinate or poly-ubiquitinate polypeptides for specific function in histones (Celeste et al., 2003; Downs et al., 2004). For instance, ubiquitination of histone H2A leads to gene silencing, while ubiquitination of histone H2B leads to both, gene activation and silencing (Rossetto et al., 2010; Tamburini & Tyler, 2005).

1.5.1 Histone variant H2A.J

Until this time, there are 11 canonical H2A and 8 H2A variants found in the human genome encoded by 26 genes (Khare et al., 2012). The major difference between Histone variant H2A.J and canonical H2A is the protein sequence (only by alanine-valine substitution at position 11) and the presence of an SQ motif near the C-terminus (Contrepois et al., 2017a). The H2Afj gene is located on chromosome 12 near the H4 gene (Tanaka et al., 2020) and shows two commonly known isoforms, the first ensuing from splicing of 2 introns and the latter, which does not involve intronic splicing (Ota et al., 2004; Strausberg et al., 2002).

Previous in-vivo studies have shown that H2A.J was highly expressed in luminal epithelial cell of multiple glands in mouse (Redon et al., 2021). Moreover, knock-out of H2AfJ gene in luminal breast cancer cells lead to reduction of estrogen-responsive gene expression, thus suggesting a role in luminal breast cancer (Redon et al., 2021). H2A.J has shown to accumulate in epidermal keratinocytes during human skin ageing (Rübe et al., 2021). In response to ionizing radiation (IR) H2A.J has been shown to be involved in senescence-associated growth arrest and SASP regulation (Isermann et al., 2020). Additionally, in response to ionizing radiation differentiated keratinocytes showed low H2A.J expression in murine hair follicle at different time-points indicating that H2A.J might play an important role in maturation of keratinocytes (Hippchen et al., 2022).

2. __Aim of work__

The aim of this study is to understand the pathophysiological role of H2A.J in murine skin after moderate and high IR doses, in order to clarify the molecular and cellular events that drive acute radiation-induced dermatitis.

Here, using C57BL/6N wild-type and corresponding h2afj$^{-/-}$ knock-out mice we investigated the role of H2A.J regarding DNA damage response, senescence induction and SASP secretion during radiation dermatitis.

3. <u>Materials & Methods</u>

Table 1: Reagents and chemicals for experiments	
Acufirm wound suture needles	Dreieich, Germany
Ammonium persulphate	Thermo Fisher, USA
Asid-med depilation cream	Asid Bonz, Herrengerg, Germany
Chloroform	Fluka Gmbh, Germany
Citric acid	Merck, USA
Dako mounting medium (IHC)	Agilent, Germany
Dako REAL target retrieval solution (S1699)	Agilent, Germany
Dimethylsulfoxide (DMSO)	Carl Roth Gmbh, Germany
Doxycycline hydrochloride	Sigma-Aldrich, USA
Ethanol (100 %)	Sigma-Aldrich, USA
Fetal bovine serum (FBS)	Sigma-Aldrich, USA
Immersion oil	Merck, USA
Isopropanol	Hedinger, Germany
NaCL solution	B.Braun, Germany
N,N-Dimethylformamide (DMEM)	Sigma-Aldrich, USA
Magnesium chloride hexahydrate	Applichem, Germany
Paraformaldehyde	Sigma-Aldrich, USA
Paraplast paraffin	Carl Roth, Germany
Penicillin	Merck, USA

pH 7.0 buffer solution	Hanna Instruments, Germany
Potassium ferricyanide	Sigma-Aldrich, USA
Potassium ferrocyanide	Sigma-Aldrich, USA
Rompun	Bayer, Germany
Immunoblock	Carl Roth, Germany
Milipore filter	Carl Roth, Germany
Diaminobenzidine tablet	Sigma-Aldrich, USA
Sodium chloride	Carl Roth Gmbh
Sodium Pyruvate	Sigma-Aldrich, USA
Trizol reagent	Invitrogen, USA
ketaminhydrochloride (100mg/ml)	Zoetis, Germany
Ultra sound gel (250 ml)	Geithain, Germany
Mounting medium (IFM)	Vector Laboratories, UK
X-Gal	Applichem, Germany
Xylol	Hedinger, Germany

Table 2: Preparation for intracardial Perfusion	
Anesthesia	120µg urostamin/ Ketamin per 16µg Rompun
Anti-coagulative	1% Heparin in PBS
Fixative	4% paraformaldehyde

Table 3: Reagents prepared for IHC	
Antigen retrieval buffer	1ml of buffer in 9ml of distilled Water (1:10)
Blocking buffer	Immunoblock 1:10 in distilled water
Citrate buffer	Dilute in 1:10 ratio in distilled water
Potassium ferricyanide	100mM in PBS
Potassium ferrocyanide	100mM in PBS
X-gal solution (senescence)	2% PFA + 0.2% glutaraldehyde in PBS
β-gal stock	1mg/ml X-Gal in DMF
β-gal stain	5ml: 4.6ml citratebuffer + 100µl X-Gal + 250µl $K_3(Fe(CN)_6$ + 250µl $K_4(Fe(CN)_6$

Table 4: Laboratory equipments	
Cell culture multiwell plates (6 well)	Greiner Bio-one, Germany
Centrifuge tubes	Sarstedt Gmbh Germany
Coverslips	Burgdorf, Germany
Filter discs (90mm)	Sartorius, Germany
microscope slides	Marienfeld ,Germany
Tissue embedding cassette	Neo Lab Gmbh, Germany
Syringe (10 & 20ml)	B.Braun Gmbh, Germany
Parafilm	Bemis, USA
Razor blades	Plano, Germany
Centrifugation tube	Eppendorf, Germany

Perfusion needle	Sarstedt, Germany
Standard pipette tips	Sarstedt, Germany
Surgical blades	B.Braun, Germany
Microscope slides	Carl Roth, Germany
Nitrogen supply	VWR, Germany
LINAC (linear accelerator)	Siemens Medical Solutions, USA
Weighing Balance	Sartorius, Germany
Centrifuge	Eppendorf, Germany
Dissection instruments (scalpel, forceps, scissors)	C. Bruno, Germany

Table 5:Device & Instruments	
Fridge (4°C)	Bosch , Germany
Heating chamber	Binder, Tuttlingen, Germany
Pipettes (P10, P100, P200 P1000)	Eppendorf, Germany
Plexiglass cylinder	Uniklinikum Homburg, University of Saarland
Plexiglass plate	Uniklinikum Homburg, University of Saarland
Microtome	Leica, Wetzlar, Germany
Nikon Eclipse, TS100 light microscope	Nikon Instruments, Amsterdam
Thermoshaker	Ditabis, Pforzheim, Germany
CO_2 incubation chamber	Heraeus Gmbh, Germany

Table 6: Software	Company

GraphPad	GraphPad Software, San Diego, CA, USA
Microsoft Office	Microsoft Corporation, Redmond, WA, USA
NIS Elements Basic Research software	Nikon Instruments Europe, Netherlands
Affinity Photoshop CS3	Adobe, USA

Table 7: Primary antibodies					
Marker	**Host**	**Batch**	**Company**	**Fluorescence**	**Histology**
Primary antibodies					
Anti-53BP1	Rb	NB-100-304	Novus Biologicals	1:5000	-
Anti-CD34+	Rt	551387	BD Pharmingen	1:50	-
Anti-H2A.J	Rb	61793	Active motif	-	1:1000
Anti-ki67	Rb	15580	Abcam	1:200	-
Anti-lamin B1	Rb	133741	Abcam	1:100	-
Anti-JunB	Rb	C3759	Cell signalling	1:100	-
Anti-myloperoxidase	Rb	AF3667	R & D systems	-	1:100

Table 8: Secondary antibodies					
Alexa Fluor 488/568 anti-rat	Donkey	175475	Abcam	1:400	-
Alexa Fluor 568nm anti-rabbit	Gt	A11036	Invitrogen, USA	1:1000	-
Alexa Fluor 488nm	Gt	A11034	Invitrogen, Carlsbad,	1:1000	-

anti-rabbit			CA, USA		

| **Table 9: Cytokines for Enzyme Linked Immunosorbent Assay (ELISA)**		
Cytokines	**Product no.**	**Company**
IL-6	Ab100713	Abcam, Germany
GM-CSF	Ab231665	Invitrogen, Thermofisher Scientific, Germany
MCP-1	Ab208979	Abcam, Germany

3.1. Animal Experiments

3.1.1 C57BL/6N

Wild-type, male C57BL/6N mice were attained from Charles River Laboratories (Sulzfeld, Germany). The 8-week-old C57BL6 mice were sent in litters and kept together for one week in animal facility after which they were used for experiments.

3.1.2. H2Afj/N

H2Afj/N KO mice were generated and obtained from Carl Mann's Laboratory, France. Two pairs of male and female mice were obtained that were used for further breeding and experiments. All animal experiments and animal husbandry were supported with accordance to the Animal Welfare Act and the specifications of the State Office for Consumer Protection - Department 'Official Veterinary Service, Food Control' of the Saarland. Three to six mice were kept in IVC cages under identical, standardized laboratory conditions (temperature 22°C ±2°C, humidity 55% ±10% and a constant day-night rhythm of 12h to 12h) in the animal husbandry of the experimental surgery department of the Medical Faculty of Saarland University. The corresponding test protocols were permitted by the animal welfare officer of Saarland University and the State Office for Consumer Protection and are listed under the test numbers 27/2021 and 29/2020.

3.2. Experimental planning

For whole-body irradiation of 2Gy & 5x 2Gy four time points were planned including control for both WT and KO mice (2Gy: non-IR, 24h, 72h, 1w; 5x2Gy: non-IR, 72h, 1w, 2w). For both treatment groups and each time point 3 biological replicates were used (n=3). For high-dose irradiation with 10Gy and 20Gy, 3 time points were planned including control (non-IR, 1w, 2w); for both treatment groups and for each time point 3 biological replicates were used (n=3).
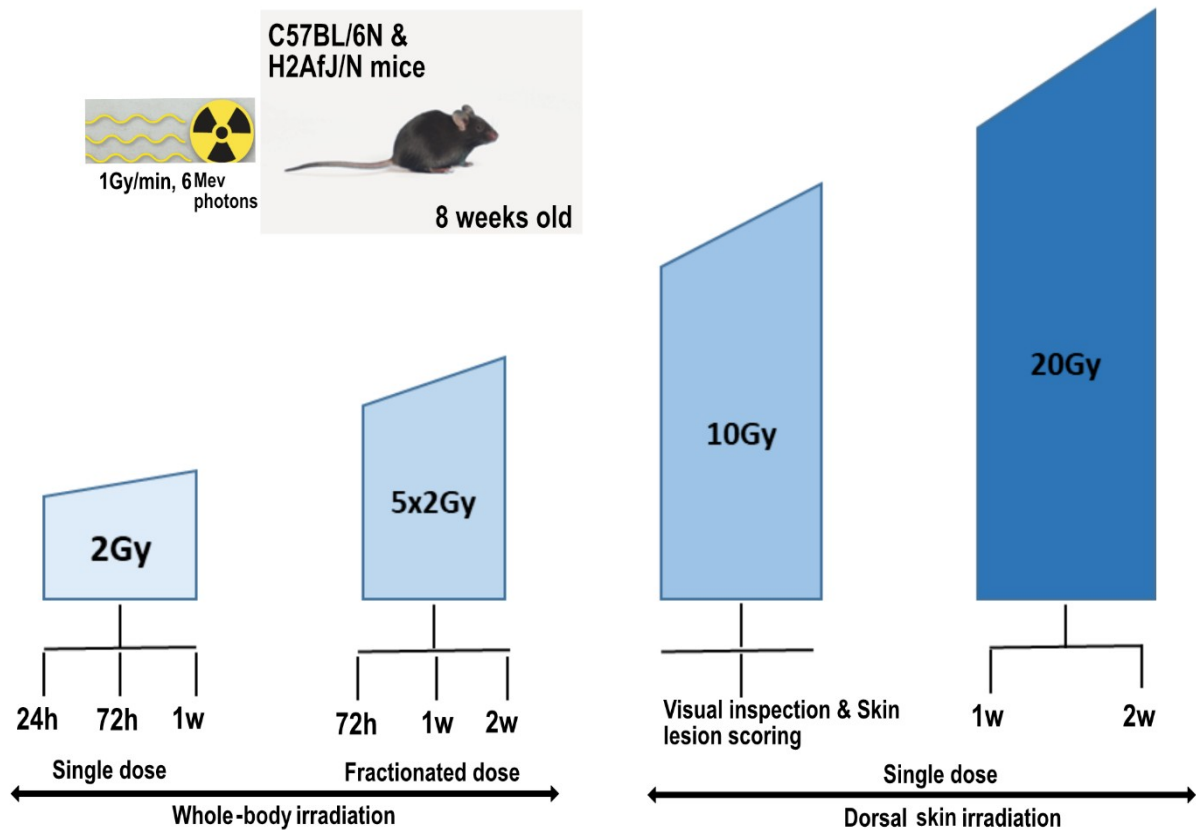
Figure 5. Experimental planning for irradiation of mice Schematic representation of single, fractionated whole-body irradiation and of dorsal skinfold irradiation. For fractionated whole-body IR the mice were exposed once every day from Monday to Friday (5x per week). For every treatment group non-irradiated, age-matched WT and KO mice were analyzed as non-irradiated controls.

3.3. CT planning for dorsal skinfold irradiation
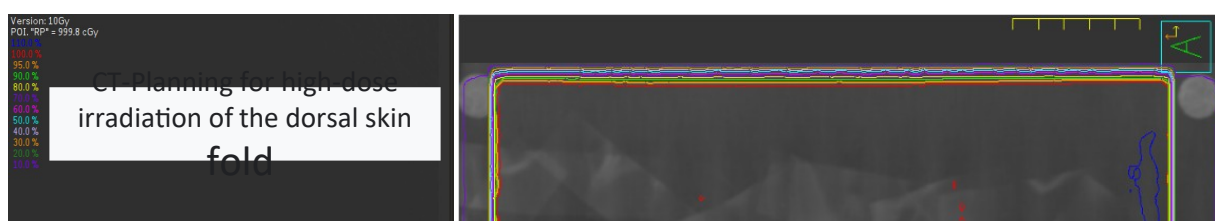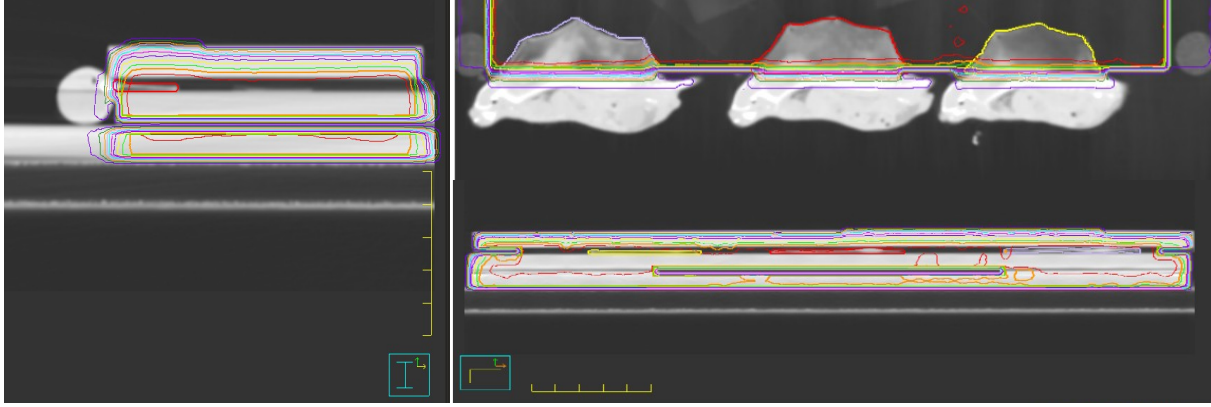
Figure 6: CT-planning for dorsal skinfold irradiation: CT-planned dose distributions using the Pinnacle™ planning system. The dose distribution was calculated using a CT scan of anaesthetized mice in the radiation position. The isodose distributions are shown in all planes.

The planning system (Pinnacle™, Philips Healthcare) provides corresponding isodoses or isolines in each CT section, i.e., lines of the same dose in percent (Fig. 6). The 3D dose distribution shows that with this irradiation technique a skin area of only approx. 10mm is exposed to high doses (100% isodose) and no organs at risk are in the high-dose range. The dose distribution was validated using the Pinnacle™ planning system (Philips, Amsterdam, and The Netherlands). For whole-body irradiation (2Gy, 5x2Gy), the mice were positioned in plexiglas cylinder (19 cm in diameter) under a Plexiglas cover with a thickness of 1.5 cm. A 5 cm cavity for the mice was created through the Plexiglas lid. The irradiation took place with photons (energy level: 6 MeV, dose-rate: 1Gy/min) at the linear accelerator (Artiste™ from Siemens) at the Clinic for Radiation Therapy (Saarland University Hospital).

A   Whole-body irradiation

B   Dorsal skin irradiation
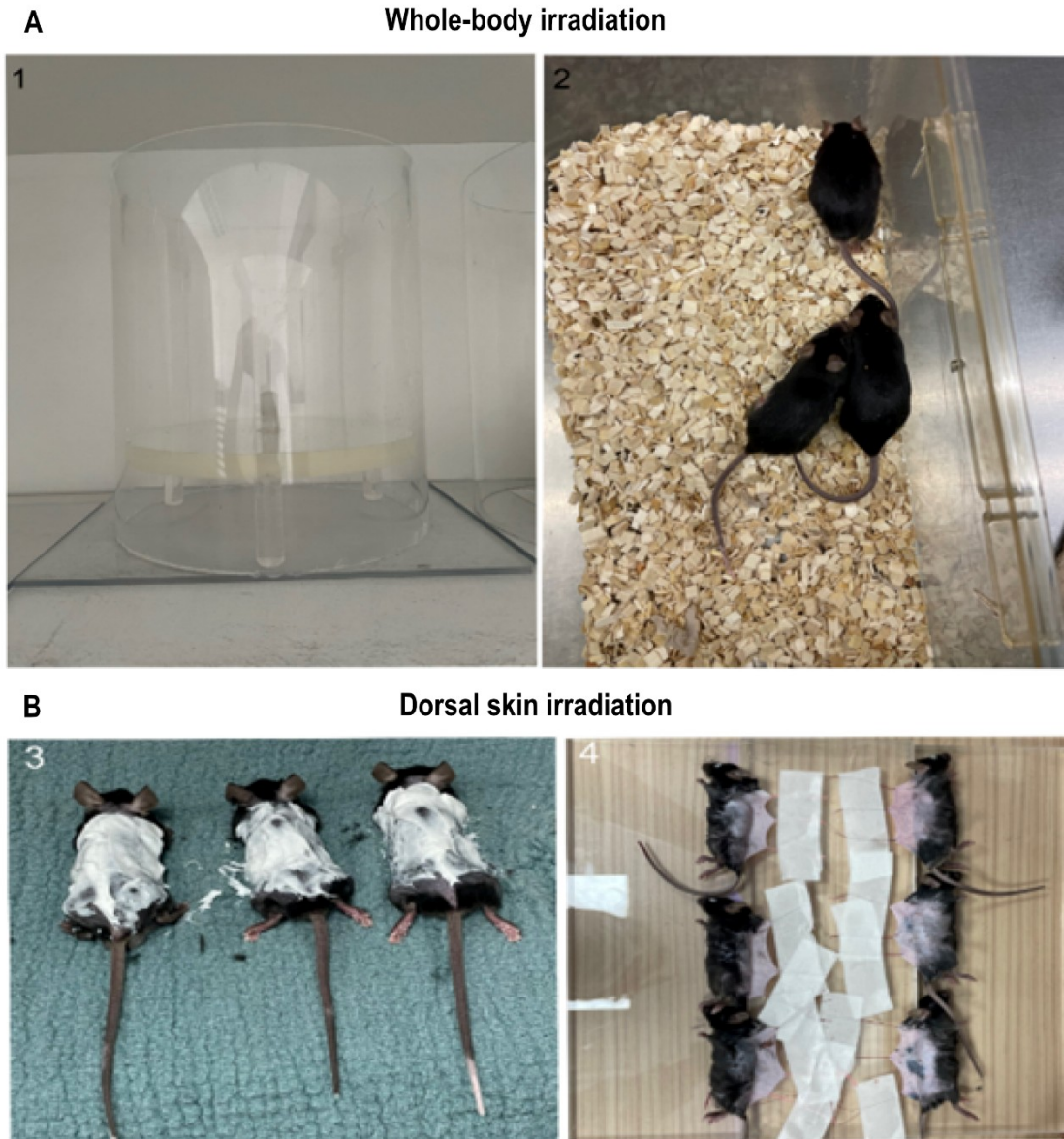
Figure 7: Whole-body and dorsal skinfold irradiation of mice. (A) Arrangement for whole-body irradiation in a group of 3-6 mice using plexiglass cylinder for irradiation. (B) For the dorsal skinfold irradiation, the backs of mice were depilated, and skinfolds were fixed using 3 sutures during irradiation.

For fractionated whole-body IR (5x2Gy) the mice were exposed with 2Gy radiation, once a day from Monday to Friday and always at the same time (8:00 h). At the start of irradiation, the mice were 7 weeks old. For IFM and IHC investigations, the mice were perfused intracardially and the tissues were removed at defined time points after IR exposure. For high-dose irradiation of dorsal skin (10Gy & 20Gy) the mice were first anesthetised by giving intraperitoneal injection (Rompun / ketamine) (0.1 ml / 10 g body-weight) of the muscle relaxant xylazine (Rompun) and the anaesthetic (ketamine) in a 1:2 ratio, diluted in 0.9%

sodium chloride solution. Subsequently, the skin on the back was depilated and skinfolds were stretched along the back for approximately 10 mm and fixed with 3 sutures for the duration of the irradiation (approximately 5-10 minutes). After irradiation, the sutures were immediately undone on the anesthetized animal. Since the skin can be irradiated in isolation with this IR technique, the other organ tissues can be spared.

3.4. Intracardial perfusion

For sample collection, the mice were anesthetized for intracardial perfusion with subsequent tissue removal by intraperitoneal injection of ketamine (120 µg/ g body-weight) and rompun (16 µg/ g body-weight) in 0.9% sodium chloride (NaCl) solution. After reaching surgical tolerance, which was checked by examining the interdigital reflexes, the skin tissue was collected from the dorsal side of the mouse.

Subsequently, abdominal cavities were opened and organs were fixed by intracardial perfusion with 2% paraformaldehyde (PFA). For this purpose, a surgical needle was inserted into the left ventricle of the mouse heart and at the same time the right atrium was opened to allow the blood and excess fixative solution to escape. First, 20 ml flush buffer was injected via the surgical needle and then the mouse was fixed by introducing 40-45 ml 4% PFA. As a result, the blood was completely replaced by fixing solution and at the same time tissue and organs were fixed before decomposition processes occur. After fixation, the mice's organs were removed (brain, heart, lungs, liver, kidneys, small intestine and testicles) and fixed again overnight in 4% PFA for embedding.

3.5. Immunofluorescence staining

Paraffin-embedded tissues were sectioned in 4µm thin slices and incubated at 56°C for 1 hour. To label the sections with different fluorochrome-labelled antibodies, the paraffin was first removed by incubation in xylene (3x7 minutes) and sections were then placed in descending ethanol series (100%, 95%, 90%, 80% and 70%) and rehydrated for three minutes each. To

unmask the epitopes, the paraffin sections were incubated for 1 hour in citrate buffer (pH 6) in 95°C water bath. For the labelling of 53BP1, the paraffin sections were boiled in citrate buffer for 40 minutes. After a cooling time of 20 minutes, a 1-hour incubation was carried out in a blocking solution in order to saturate non-specific binding sites. The blocking solution used for most of the antibodies was a commercially purchased immunoblock working solution (Roti Immunoblock diluted 1:10). The incubation took place in a humidity chamber by adding 100µl of the respective blocking solution to the slide and subsequently sealing it with a cover glass without bubbles. Before incubating the sample with the primary antibody, the coverslip and the blocking solution were removed. The primary antibody was diluted in the corresponding blocking solution according to (table 7) and applied to the slide and tissue sections and sealed with a coverslip. The samples were incubated in a humidity chamber at 4°C overnight.

On the next day, slides were washed three times (each 10 minutes) with PBS to remove the excess primary antibody by washing, followed by incubation with secondary fluorescence antibody (table 8) diluted in the appropriate blocking solution for 1h at room temperature in the dark. The excess antibody was again removed by washing three times with PBS, however, work continued in the dark to protect the fluorescence signal. Finally, the samples were covered with a mounting medium comprising 4',6-diamidine-2-phenylindole (DAPI) and stored at 4°C. The prepared solutions were stored at 4°C in the refrigerator with the exclusion of light until they were examined under the immunofluorescence microscope.

3.6. Immunohistochemical staining

3.6.1. SA-β-Gal staining

Skin tissue samples were collected from the back of the mouse, and pre-fixated for a maximum of 30 minutes in 4% paraformaldehyde (PFA). After 30 minutes PFA was removed and replaced with 2-3ml of washing buffer and placed on a shaker for three times for 7

minutes for removal of remaining PFA from the skin tissue. After washing with wash buffer, staining solution (1-2ml per 15ml falcon) was added to the skin tissues and incubated in dark overnight (12-16h) in the incubator preheated at 37°C. After incubation, tissues were washed twice for 5 minutes with distilled water and fixed completely in 4% PFA for 2h minimum. After incubation the tissues were prepared for embedding and further immunohistological staining.

3.6.2 Immunohistochemical staining for H2A.J

Embedded skin tissues were sectioned in 4μm thickness and incubated at 56°C for 1h to melt off paraffin coating. After incubation, the section of skin tissues was soaked in xylol three times for 10 minutes to remove remaining paraffin. Sections were then soaked in decreasing alcohol baths for 3 minutes (absolute, 96%, 90%, 80% 70%) for rehydration and finally in distilled water. After treating with alcohol, the tissues were immersed in citrate buffer at 95°C for antigen retrieval for 1h. Tissues were briefly immersed in distilled water and then transferred in a solution of hydrogen peroxide for 25 minutes to block the endogenous peroxide activity. Tissues sections were washed in phosphate buffer saline (PBS), 2 times for 10 minutes and then blocked in immunoblock in 1:10 dilution with distilled water for 1h at room temperature. Tissue section were incubated overnight with H2A.J primary antibody in dilution 1:200 at 4°C.

On the second day tissues were washed in PBS two times for 10 minutes and then incubated with biotinylated secondary antibody in a dilution of 1:1000 for 1h at RT. Sections were then washed twice in PBS for 10 minutes and dried thoroughly. After washing, sections were incubated in ABC complex for 30 minutes at room temperature. Slides were again washed three times in PBS. Sections were then incubated in DAB reagent for 5-15 minutes until brown precipitate colour was formed at room temperature. After washing in PBS twice for 5 minutes the sectioned were then counterstained with haematoxylin for 60 seconds and then immediately soaked under running water until colour change was observed. Sections were

38

coated with mounting medium and stored out of light for histological and quantitative analysis.

3.6.3 Quantification analysis

For quantitative analysis ≥500 cells in at least 10 hair follicles or epidermis were registered for each tissue section and H2A.J+, SA-β-GAL+, Lamin B1+, JunB+, CD34+, Ki67+ and MPO+ cells were calculated using Nikon Eclipse NI-E microscope. 53BP1-foci were quantified in immunofluorescence in different parts of the hair follicle until at least 40 foci positive cells were recorded for each time point per tissue section. This was accomplished for three biological replicates as well as three technical replicates. Each irradiated sample was compared to a non-irradiated, age-matched control.

3.7. Enzyme linked immunosorbent assay (ELISA)

Sample acquisition

To detect the cytokine secretion of murine skin, 1 g of dorsal skin from the mice were weighed and placed on membrane filters for secretion of cytokines in 2ml of FBS-free medium at 37°C. Conditioned medium was collected after 48h and then centrifuged at 300g for 5 min to remove any debris, supernatant was removed and filtered through a 0.22µm syringe filter. Conditioned medium was aliquoted and frozen at -80°C.

Preparation of reagents

Wash buffer (1x)

To prepare 1x wash buffer, 50ml of the wash buffer concentrate (20x) was decanted into a clean 1000ml graduated cylinder. The final volume was brought to 1000ml with glass distilled or deionized water.

Assay buffer (1x)

To prepare 1x assay buffer, 5ml of the assay buffer concentrate (20x) was poured into a clean 100ml graduated cylinder. The final volume was brought to 100ml with distilled water.

Biotin-conjugate

A 1:100 dilution of the concentrated Biotin-Conjugate solution with assay buffer (1x) in a clean plastic tube was prepared as needed. The Biotin-Conjugate should be used within 30 minutes after dilution.

Streptavidin-horse radish peroxidase (HRP)

A 1:100 dilution of the concentrated streptavidin-HRP solution with assay buffer (1x) in a clean plastic tube was prepared as needed. The streptavidin-HRP was used within 30 minutes after dilution.

Standard Dilution

Seven tubes were labelled, one for each standard point: S1, S2, S3, S4, S5, S6, and S7. Preparation 1:2 serial dilutions for the standard curve was performed as follows: 225 µl of reconstituted standard (concentration = 500 pg/ml) was pipetted into the first tube labelled S1, mix (concentration of standard 1 = 250 pg/ml). 225 µl of this dilution was pipetted into the second tube labelled S2 and mixed thoroughly before the next transfer. Serial dilutions were repeated 5 more times, thus creating the points of the standard curve. Sample diluent served as blank.

ELISA assay

ELISA was performed on conditioned medium to detect IL-6, GM-CSF and MCP-1, respectively. For performing ELISA, the number of microwell strips required to test the desired number of samples plus appropriate number of wells needed for running blanks and

standards were determined. Each sample, standard, blank and optional control sample was assayed in duplicate.

Microwell strips were washed twice with approximately 400µl wash buffer per well with thorough aspiration of microwell contents between washes. The wash buffer was allowed to sit in the wells for about 10-15 seconds before aspiration. After the last washing step, the wells were emptied and excess wash buffer was removed by tapping microwell strips on absorbent pad or paper towel. The microwell strips were used immediately after washing. 100µl of sample diluent was pipetted in duplicate to the blank wells. After this 50µl of sample diluent and 50µl of each sample in was added in duplicate in sample wells. The microwell plate was covered with an adhesive film and incubated at room temperature (18-25°C) for 2h on a microplate shaker.

After 2h the adhesive was removed and the microwell strip was emptied and washed 4 times with wash buffer. After washing 100µl of Biotin conjugate was added to all the wells. The wells were covered with adhesive film and incubated at room temperature (18-25°C) for 1h on a microplate shaker. After 1h adhesive film was removed and the walls were emptied, the microwell strips were again washed 4 times. After washing 100µl of diluted streptavidin was added to all wells including blank wells. The plates were again covered with an adhesive film and incubated at room temperature (18-25°C) for 30 minutes on a microplate shaker. After 30 minutes the microwell strips were emptied and washed four times. 100µl of TMB substrate solution was added to all wells. The microwell strips were again incubated at room temperature (18-25°C) for about 10 minutes in dark to avoid direct exposure to intense light. After 10 minutes the enzyme reaction was stopped by quickly pipetting 100µl stop solution into each well. Absorbance of each microwell was red on a spectrophotometer using 450nm as the primary wavelength.

3.8. Haematoxylin & eosin staining

To study the histology of the skin tissue, the sections were soaked in xylol three times for 10 minutes to remove remaining paraffin. Sections were then soaked in decreasing alcohol baths for 3 minutes (100%, 96%, 90%, 80% and 70%) for rehydration and finally in distilled water. After this, the skin sections were incubated in haematoxylin and eosin stain solution for about 6 minutes to stain the cell nuclei. In order to wash off the surplus stain the sections were rinsed under tap water for about 10 seconds. The skin tissue sections were then treated with 0.1% hydrochloric acid, afterwards they were rinsed under running tap water for about 6 minutes. The sections were then incubated in eosin solution to stain the cytoplasm and erythrocytes. The sections were then bathed in tap water to wash off the excess stain for 30 seconds and coated with mounting medium and stored out of light for histological and quantitative analysis.

3.9. Scoring of skin lesion

The scoring of skin lesion was done on the 2nd, 4th, 6th, 8th, 10th, 12th and 14th day after irradiating the mice with 10Gy and 20Gy. Based on the table below scoring of skin lesions were done for all the three replicates in each dose group and control group. The sum of the scores for each mouse was added up to achieve the final scoring for each dose group (non-IR, 10Gy, 20Gy) in both WT and KO mice. Finally, the average for each group was plotted for

Table 10: Skin lesion scores

the respective days.

Grading	Significance
0	Normal (no effect)
1	Slight erythema
2	Intense erythema
3	Dry Desquamation
4	Moist Desquamation

5	Inflamed skin tissue few spots of excoriation
6	Inflamed skin tissue with extensive excoriation

3.10. Measurement of epidermal thickness and hair follicle density

To measure the epidermal thickness and hair follicle density at 2 weeks after exposure to 20Gy, skin tissue samples were stained with haematoxylin and eosin. The images for analysis were acquired using Nikon Eclipse NI-E microscope in bright field at 10x magnification. NIS- elements software was used for the analysis by utilising the area measurement tool to measure epidermal thickness. 10 fields were analysed for each technical replicate. To quantify the hair follicles, 5 different regions were analysed in all replicates by counting the hair follicles; hair follicle density was determined by dividing the number of hair follicles by the corresponding skin area.

3.11. Statistical analysis

Statistical analysis was performed using Graphpad Origin Pro program. In order to determine statistically significant differences between the irradiated and non-irradiated, age-matched groups, a two-sample t-test for independent samples was used for normally distributed values and a Mann-Whitney-U for samples with non-normal distribution. The mean and the standard error of three biological and three technical replicates was calculated for normally distributed values. Statistical significance is presented in the figures by * $p < 0.05$; ** $p < 0.01$ and *** $p < 0.001$.

4. <u>Results</u>

4.1. Radiation-induced 53BP1-foci in different hair follicle regions

The 53BP1 is a common DDR marker, positioned to the sites of DNA damage and forms radiation-induced foci. In DNA damage response 53BP1 is categorized as an intermediary that is vital for the processing of the DNA damage response signal.

In order to understand the influence of H2A.J in the DNA damage response, WT (C57BL6/N) and KO (H2AfJ$^{-/-}$) mice were irradiated with a single dose of 2Gy and analysed at different time points following IR exposure (24h, 72h, 1w post-IR). 53BP1-foci were quantified in both WT and KO skin samples in entire hair follicle and in different parts of hair follicle (bulge, papilla and infundibulum) (fig. 8).

In the total hair follicle, the earliest time point used to analyse 53BP1-foci was 24h post-IR which showed significant increase with 0.27 ±0.03 foci/ cell in WT skin in comparison to non-IR which showed 0.034 ± 0.001 foci/ cell. In KO skin 24h post-IR showed similar number of foci/cell 0.26 ± 0.0008 in comparison to the non-IR which showed 0.03 ± 0.0004 foci / cell. After 72h post-IR the foci / cell gradually decreased in WT 0.16 ± 0.008 foci / cell and KO showing 0.15 ± 0.008 foci / cell. However no significant variance was seen between WT and KO at 72h post-IR. After 1w post-IR further decrease in the foci/ cell was observed in WT 0.11 ± 0.011 foci / cell and KO 0.109 ± 0.008 foci / cell, however no significant difference was seen in foci/cell amongst WT and KO mice.
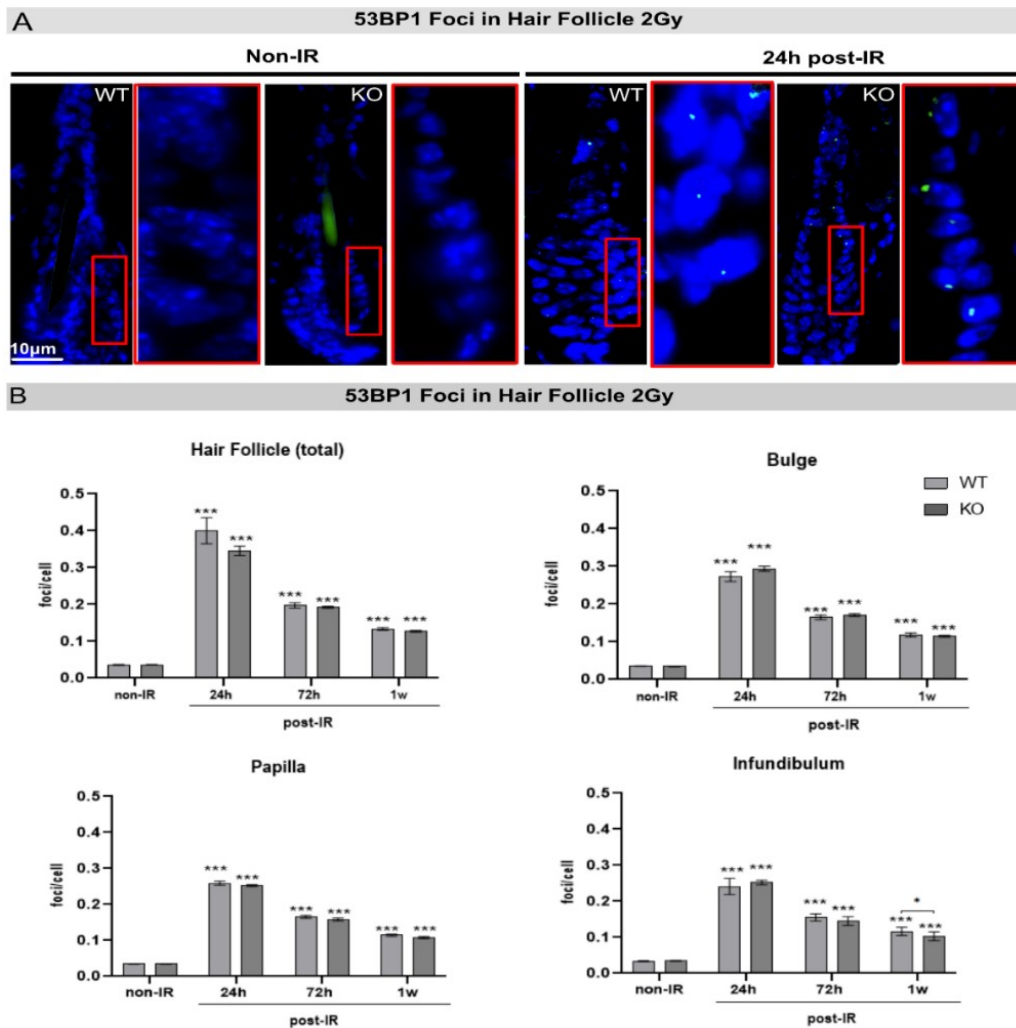
Figure 8. Quantitative analysis of 53BP1-foci following 2Gy irradiation. (A) Overview images of immunofluorescence labeling with 53BP1-foci (green) in different parts of the hair follicle after irradiation (magnification: 20x, scale bar = 10µm). A detailed image of the marked regions (red box) is shown at 60x magnification . **(B)** Quantification of 53BP1-foci in different parts of the hair follicle after irradiation with 2Gy compared to age-matched, non-irradiated controls. Shown are the mean values of the 53BP1-foci per cell and the standard deviation for three biological and three technical replicates (n=3). The significance of the differences between the irradiated and non-irradiated groups was assessed using the unpaired t-test and found to be *$p < 0.05$; **$p < 0.01$ and ***$p < 0.001$ given.

The bulge of the hair follicle known to be the reservoir of multipotent stem cells was analysed 24h post-IR, even though a gradual increase in the foci/cell was witnessed in the WT 0.27 ± 0.03 foci /cell in comparison to non-IR 0.03 ± 0.002 foci / cell and KO 0.29 ± 0.006 foci / cell in comparison to non-IR 0.03 ± 0.001 foci / cell. After 72h post-IR a gradual decrease in the foci/cell in WT i.e 0.16 ± 0.01 foci / cell and knock out i.e 0.17 ± 0.01 foci/ cell was observed

in comparison to their corresponding non-IR but no significant variance was seen between the foci / cell in WT and KO. After 1w post-IR further gradual decrease was observed in WT i.e 0.1 ± 0.01 foci / cell and KO 0.1 ± 0.007 foci / cell in comparison to the respective control.

The dermal papilla are situated at the bottom of the hair follicle and are responsible for hair formation, growth and cycling. After 24h post-IR significant increase was observed in the WT that showed 0.2 ± 0.01 foci / cell in comparison to non-IR 0.03 ± 0.002 foci / cell and knock out showed 0.25 ± 0.01 foci / cell compared to non-IR 0.03 ± 0.001 foci / cell. After 72h post-IR the WT showed 0.16 ± 0.01 foci / cell and KO showed 0.15 ± 0.01 foci / cell. After 1w post-IR the WT showed 0.11 ± 0.009 foci / cell and knock out showed 0.10 ± 0.009 foci / cell. Although a gradual escalation and decrease was observed in the number of foci / cell from earliest to latest time points no significant increase was observed between WT and KO.

The infundibulum further showed 24h post-IR significant increase was observed in the WT that showed 0.2 ± 0.02 foci / cell in comparison to non-IR which showed 0.03 ± 0.001 foci / cell and KO showed 0.25 ± 0.006 foci / cell in comparison to non-IR 0.03 ± 0.001 foci / cell. After 72h post-IR WT showed 0.15 ± 0.009 foci / cell and KO showed 0.14 ± 0.01 foci / cell. Further after 1w post-IR analysis the WT showed 0.1 ± 0.01 foci / cell and knock out showed 0.10 ± 0.01 foci / cell. The infundibulum of the hair follicle showed a similar pattern in the number of foci / cell showing a single in comparison to the control however no change in between WT and KO.

Analysis of these epidermal cell populations revealed significantly increased 53BP1-foci levels at 24h, 72h and even at 1w post-IR compared to non-irradiated controls, showing un- or misrepaired DNA damage (Fig. 1A). However, no significant changes in DSB repair capacities were observed between these epidermal cell populations, nor between WT versus KO skin, suggesting that H2A.J is not a part of acute process of DSB repair.

4.2. H2A.J and SA-β-GAL expression in hair follicles

Senescence-associated beta galactosidase (SA-β-Gal) is a known marker for senescent and aged cells. SA-β-Gal is detectable by beta-galactosidase activity at pH 6.0 in senescent cells. In order to investigate the expression of H2A.J and SA-β-Gal in response to a single dose of 2Gy, immunohistochemistry was performed at different time points (24h, 72h, and 1w post-IR).

To study the expression of histone variant H2A.J (fig. 10), DAB stained H2A.J+ cells were quantified in the bulge, papilla, infundibulum and the total hair follicle. A gradual increase was observed in the percentage of H2A.J+ cells with increasing time in hair follicles of WT skin. Following IR exposure, the number of H2A.J+ cell was already slightly increased at 24h (12.7 ±4.06%), showed a higher percentage at 72h (21.7 ± 4.03%) and the highest increase at 1w post-IR (26.4 ± 4.4%). In contrast, hair follicles in non-irradiated WT skin showed very low H2A.J expression.

In the bulge region of WT hair follicles the non-irradiated control tissue showed 3.9 ±2.5% of H2A.J+ cells, followed by 14.1 ± 5.6% at 24h post-IR, 21.1 ±3.6% at 72h post-IR and 26.9 ± 3.5% at 1w post-IR.

The dermal papilla showed around 4.9 ± 1.3% of H2A.J positive cells in non-IR, further increasing to 8.9 ± 5.1% at 24h post-IR further increasing to 20.3 ± 8.1% and finally showing the highest accumulation at 1w post-IR i.e. 23.8 ± 11.1% H2A.J+ cells.
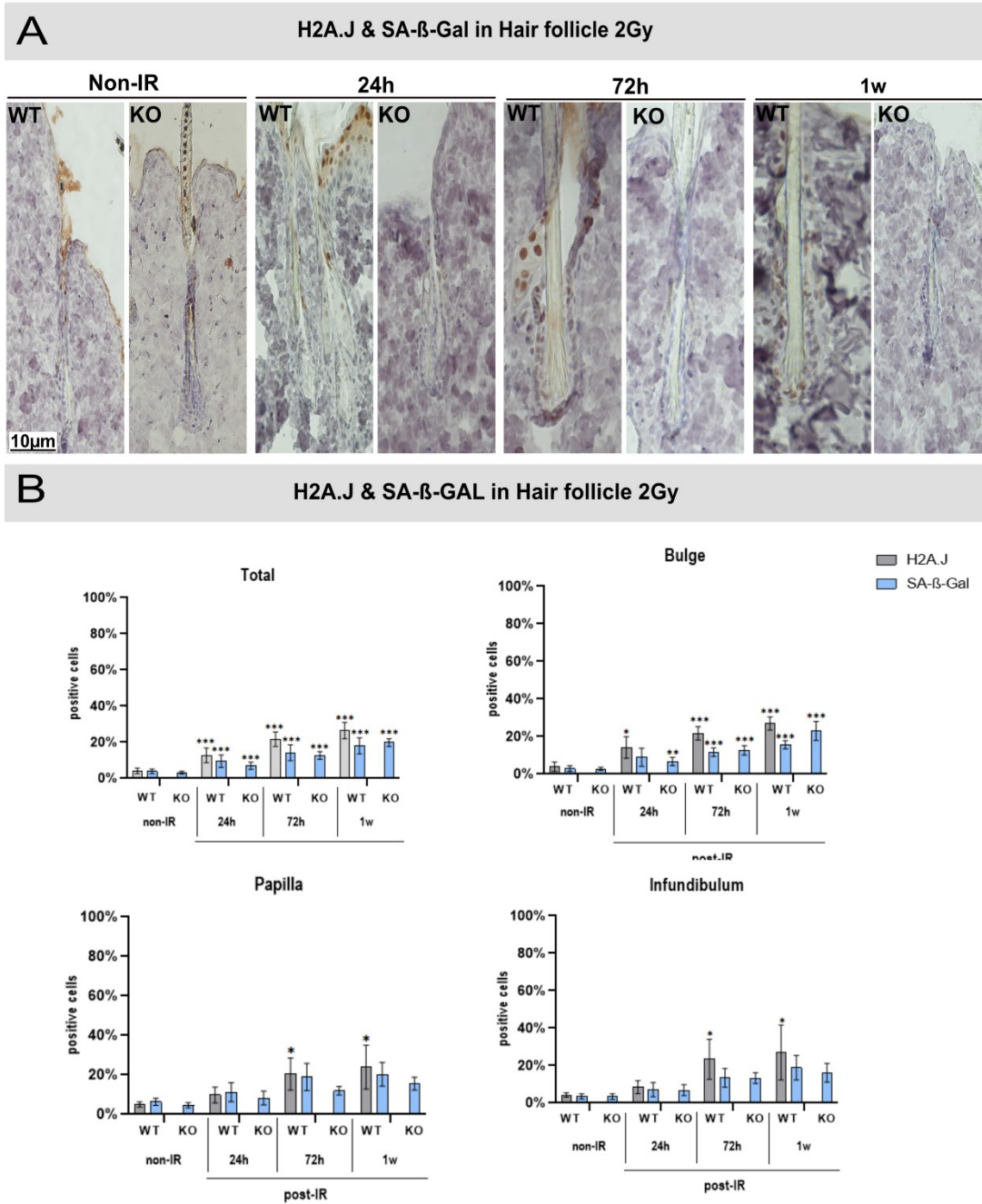
Figure 9 Quantitative analysis of H2A.J and SA-β-Gal after 2Gy irradiation. (A) Overview images of immunohistological staining withwith DAB for H2A.J (brown) and X-gal for senescence (blue) in different parts of hair follicle after irradiation (magnification: 10x, scale bar = 10μm). (B) Quantification of H2A.J+ and SA-β-Gal+ cells in different parts of the hair follicle at different times after irradiation with 2 Gy compared to age-matched, non-irradiated controls. Shown are the mean values of the percentage of H2A.J+ and SA-β-Gal+ cells and the standard deviation for three biological and three technical replicates (n=3). The significance of differences between irradiated and non-irradiated groups were assessed using the Man-Whitney non-parametric unpaired t-test and found to be *p <0.05; **p <0.01 and ***p <0.001.

The infundibulum showed about $4.2 \pm 0.3\%$ accumulation of H2A.J+ cells in the non-IR, further increasing to $8.4 \pm 3.4\%$ of H2A.J+ cells at 24h post-IR, further increasing to $23.3 \pm 10.7\%$ at 72h post-IR and showing highest accumulation at 1w post-IR $26.9 \pm 14.6\%$.

For investigation the manifestation of SA-β-Gal activity in response to 2Gy radiation dose, SA-β-Gal + cells were quantified in the bulge, papilla, infundibulum and the hair follicle.

Referring to fig. 9 the total hair follicle in non-IR WT mice showed $3.8 \pm 1.2\%$ in comparison to the knock out i.e. $3.15 \pm 0.6\%$ of SA-β-Gal. The 24h post-IR showed no significant difference between WT ($9.5 \pm 3.4\%$) and KO ($6.9 \pm 2.01\%$). Similar result was observed at 72h time point where no significant difference was seen between WT showing $14.1 \pm 4.3\%$ and KO showing 12.6 ± 2.1 % of SA-β-Gal+ cells. However, a significant difference was observed in the SA-β-Gal activity after 1w post-IR in WT showing $17.9 \pm 4.4\%$ and KO showing 19.0 ± 2.1 % of SA-β-Gal + cells.

In the bulge region, the SA-β-Gal activity showed no difference between non-IR WT $2.8 \pm 1.5\%$ and non-IR KO $2.6 \pm 1.2\%$. Additionally, at 24h post-IR the WT showed $8.9 \pm 4.8\%$ of SA-β-Gal+ cells and KO showed 6.7 ± 2.2 % of SA-β-Gal + cells thus showing no major difference. At 72h post-IR the WT showed $11.6 \pm 2.2\%$ while KO showed $12.6 \pm 2.5\%$ SA-β-Gal + cells again showing no major difference between WT and KO. However at 1w post-IR a significant difference ($p = 0.001$) was seen in the SA-β-Gal+ cells in the WT which showed $15 \pm 2.2\%$ and KO which showed higher SA-β-Gal + cells that is $22.9 \pm 5.05\%$.

In the papilla region of the hair follicle, a substantial increase was seen in the SA-β-Gal activity of WT and KO where WT showed $6.3 \pm 1.7\%$ of SA-β-Gal + cells and KO showed $4.5 \pm 1.3\%$ SA-β-Gal + cells. At 24h post-IR the WT showed $11.1 \pm 4.7\%$ and KO showed $8.2 \pm 3.5\%$ SA-β-Gal + cells thus showing no big difference. At 72h post-IR the WT showed $18.9 \pm 6.8\%$ and KO showed $11.9 \pm 2.2\%$ SA-β-Gal + cells showing an important difference between them. However, in the 1w post-IR no significant difference was observed where the WT showed $20.2 \pm 6.05\%$ and KO showed $15.4 \pm 3.1\%$ SA-β-Gal + cells.

In the infundibulum of the hair follicle, no major difference was observed between the WT and KO non-IR, where the WT showed 3.5 ± 1.3% and KO showed 3.3 ± 1.5% SA-β-Gal + cells. At 24h post-IR the WT showed 7.07 ± 3.7% and the KO showed 6.8 ± 2.9% SA-β-Gal + cells showing no major significant difference in the SA-β-Gal accumulation. After 72h post-IR the WT showed 13.4 ± 4.9% of SA-β-Gal + cells and the knock out showed 13.2 ± 2.8% SA-β-Gal + cells thus showing no significant difference. After 1w post-IR no substantial difference was observed in the activity of SA-β-Gal + cells between the WT and KO where the WT showed 18.8 ± 6.5% and KO showed 16.2 ± 5.0% SA-β-Gal + cells.

Although a slight increase was observed in the SA-β-Gal activity with increasing time point, very less differences were observed in the percentage of SA-β-Gal between WT and KO.

In order to study the expression and accumulation of H2A.J and SA-β-Gal in the WT and H2A.J knock out mice, fractionated radiation of 5 x 2Gy was performed. After radiation murine skin tissue samples were collected at different time points (72h, 1w and 2w post-IR). H2A.J and SA-β-Gal+ cells were counted in the bulge, papilla, infundibulum and the entire hair follicle. In reference to the fig. 11 after a fractionated radiation dose exposure of 5x2Gy, H2A.J showed to have increased expression in different parts of the hair follicle.

In the total hair follicle, the non-IR showed very low H2A.J that is 1.5 ± 0.4%, however at 72h post-IR showed 37.8 ± 6.4% H2A.J+ cells. The 1w time point showed 51.8 ± 5.6% H2A.J+ cell further increasing to 68.5 ± 3.9% during the 2w post-IR.
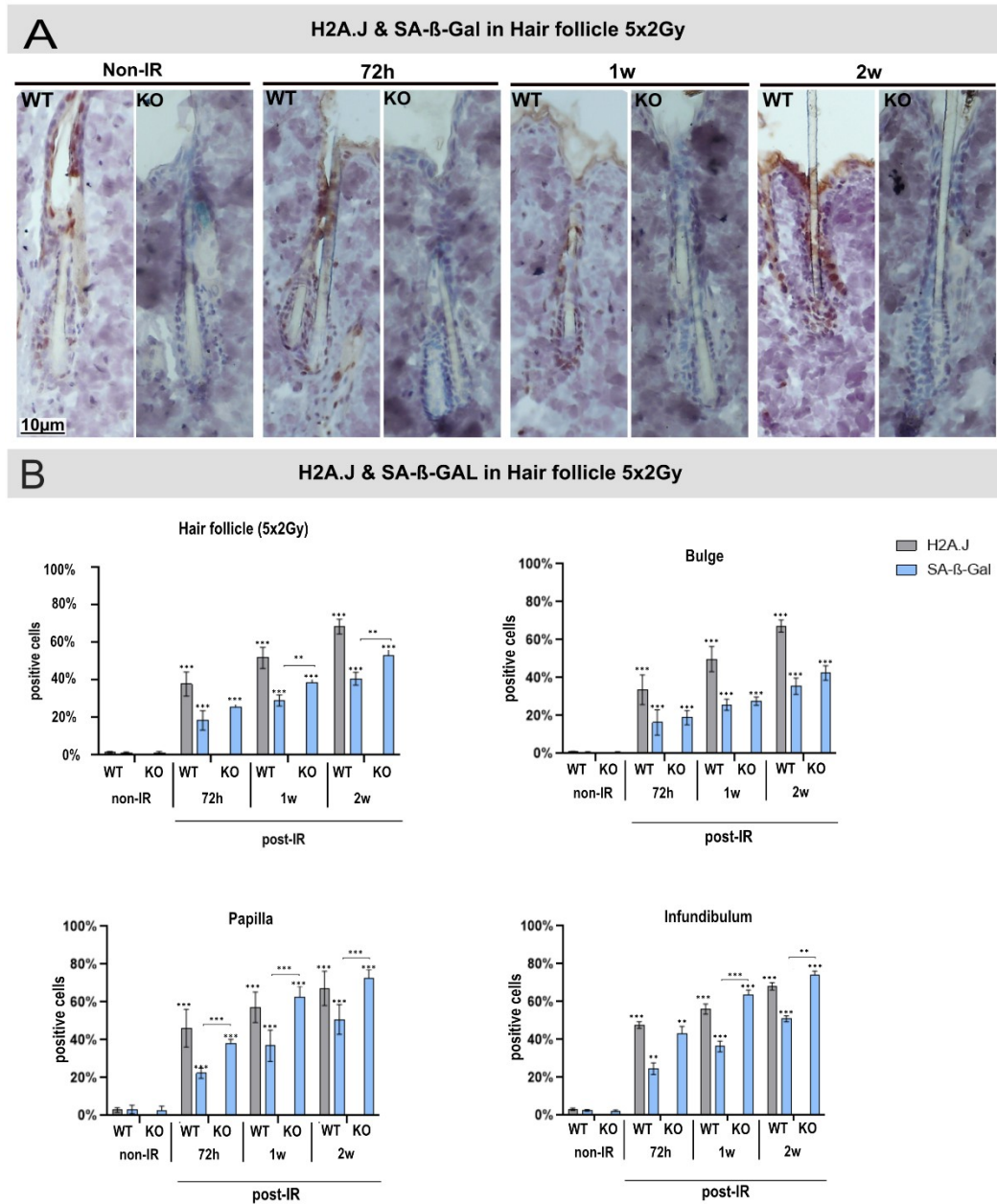
Figure 10. Quantitative analysis of H2A.J and SA-β-Gal after 5x2Gy irradiation. (A) Overview images of immunohistological stain for H2A.J (brown) and X-gal for senescence (blue) in different parts of the hair follicle after fractionated irradiation with 5x2Gy (magnification: 10x, scale bar = 10μm). (B) Quantification of H2A.J+ and SA-β-Gal+ cells in different parts of the hair follicle at different times after irradiation with 5x2Gy, compared to age-matched, non-irradiated controls. Shown are the mean values of the percentage of H2A.J+ and SA-β-Gal+ cells and the standard deviation for three biological and three technical replicates (n=3). Significant differences between irradiated and unirradiated groups were assessed using the Man-Whitney non-parametric unpaired t-test and presented as * p <0.05; ** p <0.01 and ***p <0.001.

The bulge of the hair follicle showed very less H2A.J accumulation in the non-IR WT mice 0.8 ± 0.2%, gradually increasing to 33.5 ± 7.8% of H2A.J + cells at 72h post-IR. Further increase was observed at 1w post-IR with 49.7 ± 6.5% of H2A.J + cells. Highest increase was observed at the 2w time point post-IR where the WT showed 67.2 ± 3.1% of H2A.J + cells.

In the dermal papilla of the hair follicle, the non-IR showed 2.9 ± 1.4% of H2A.J+ cells further increasing to 46.1 ± 9.9% of H2A.J + cells at 72h post-IR. The 1w post-IR showed 57.2 ± 8.07% of H2A.J + cells. Further increase with time was observed at 2w post-IR showing 67.2 ± 9.06% of H2A.J + cells.

In the infundibulum of the hair follicle 3.1 ± 1.8% of H2A.J + cells were observed in the non-IR WT mice. During 72h post-IR 47.7 ± 5.2 % of H2A.J + cells were observed. Further increase was observed at 1w post-IR which showed 56.1 ± 8.09% of H2A.J + cells. After 2w post-IR showed the highest number of H2A.J + cells that is 68.08 ± 5.9%.

To study the accumulation of senescent cells with increasing time point SA-β-Gal + cells were quantified in whole hair follicle and other regions that is the bulge, papilla and infundibulum.

In the hair follicle the non-IR mice showed very low amount of SA-β-Gal + cells 1.2 ± 0.4% in WT and 1.5 ± 0.3% in the KO showing very low percentage of senescent cells. A significant difference was observed in the 72h post-IR time point in the percentage of SA-β-Gal + cells where the WT showed 18.5 ± 5.2% and the KO showed higher that is 25.3± 1.8% of SA-β-Gal + cells. The 1w post-IR showed 29.05 ± 2.9% in WT and 38.5 ± 2.4% of senescent cells. At the 2w post-IR the highest percent of SA-β-Gal+ cells was observed in the WT showing 40.6 ± 3.4% and knock out showing 52.8 ± 4.4% SA-β-Gal + cells.

The bulge of the hair follicles showed 0.6± 0.3% of SA-β-Gal in WT and 0.7 ± 0.3% in the KO. After 72h post-IR 16.3 ± 6.6% SA-β-Gal+ cells were seen in the WT and 18.8 ± 3.02% cells were seen in the knock out showing no significant difference. In the 1w post-IR the WT showed 25.7 ± 2.9% of SA-β-Gal+ cells and the knock out showed 27.6 ± 1.7% of SA-β-Gal

+ cells thus showing no significant difference between them. After 2w post-IR a significant difference (p= 0.02) was seen between the WT and KO where the WT showed 35.4±. 4.3% and KO showed 42.4 ± 4.5% of SA-β-Gal + cells.

The dermal papilla of the hair follicle showed no significant differences between the non-IR WT mice that showed 3.1 ± 0.7% and KO that showed 4.01 ± 1.2% of SA-β-Gal + cells. After 72h post-IR the WT showed 22.3± 2.7% and the KO showed 37.8± 2.7% of SA-β-Gal+ showing a significant difference and increase in the senescent cells in KO skin tissue samples. After 1w post-IR the WT showed 36.8 ± 2.7% and the KO showed 62.7 ± 1.8%, thus showing significant difference and increase in the SA-β-Gal + cells in KO. After 2w post-IR the WT showed 50.7 ± 7.9% of senescent cells and the KO showed 72.6 ± 2.8% SA-β-Gal + cells.

In the infundibulum of the hair follicle showed no significant differences between the non-IR WT that showed 2.5 ± 1.3% and KO showed 3.2 ± 1.13% of SA-β-Gal + cells. After 72h post-IR the WT showed 24.6 ± 9.3% and the KO showed 43.2 ± 7.9% showing a significant difference and increase in the SA-β-Gal + cells in KO murine skin samples. After 1w post-IR the WT showed 36.3 ± 8.4% and the KO showed 63.7 ± 8.9% SA-β-Gal + cells, thus showing significant difference and increase in the senescent cells in KO. After 2w post-IR the WT showed 51.01 ± 4.6 % of SA-β-Gal+ cells and the KO showed 74.03 ± 7.1% of SA-β-Gal + cells.

Therefore, after 2Gy radiation low levels of H2A.J and SA-β-Gal + cells were observed in different part of the hair follicle. However, fractionated radiation of 5x2Gy clearly showed an elevating percentage of SA-β-Gal + cells with later time points. Additionally, the knock out murine skin tissue samples showed higher SA-β-Gal+ cells in comparison to WT thus indicating more radiosensitivity in comparison to WT mice therefore indicating more senescence induction.

While only minor differences in senescence induction were observed in the bulge region, highly significant differences in SA-ß-Gal+ cells between WT and KO were observed in the proliferative papilla and infundibulum segment (Fig. 1C). Despite increased senescence induction, no clinical skin changes were observed at these moderate doses.

4.3. Cytokine expression after 5x2Gy radiation

 In order to investigate the effects of fractionated radiation of 5x2Gy on the SASP, different cytokines (IL-6, GM-CSF, MCP-1) were studied at different time points post-IR, as shown in fig. 11.
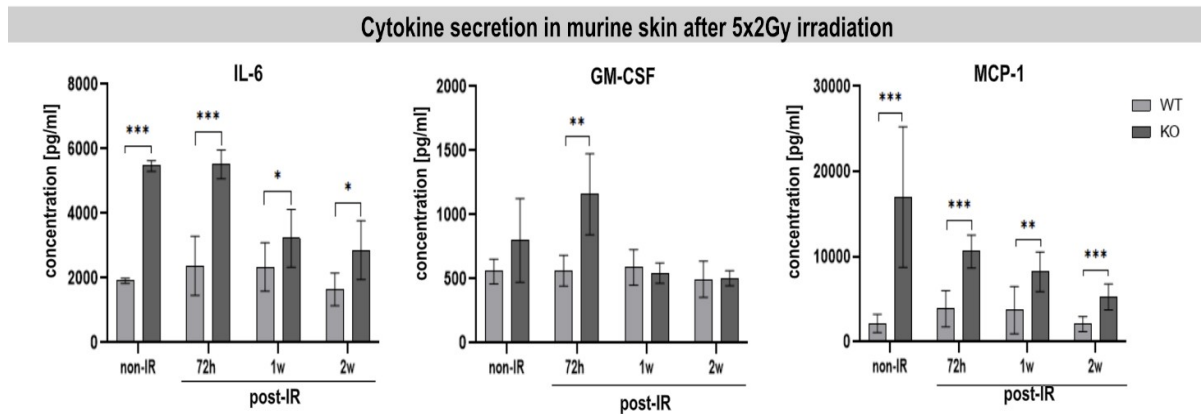
Figure 11. Cytokine /Chemokine analysis after fractionated irradiation with 5x2Gy. Quantification of IL-6, MCP-1 and GM-CSF by ELISA in the supernatant of mouse skin before (non-IR) and after fractionated irradiation with 5x 2Gy. Data are presented as mean concentration (pg/ml) with the standard deviation for three biological and three technical replicates (n=3). Significant differences between the irradiated and non-irradiated groups were assessed using the Man-whitney non-parametric unpaired t-test and presented by * p <0.05; **p <0.01 and *** p <0.001.

The IL-6 cytokine shows a pivotal role in response to inflammation. Referring to fig 11, non-irradiated WT skin showed 1913 pg/ml of IL-6, while the KO skin showed 5471 pg/ml of IL-6, thus showing significant difference between WT and KO skin. After 72h post-IR the WT skin showed 2378 pg /ml of IL-6, while the KO skin showed 5517 pg/ml of IL-6 , thus KO skin showed a higher level of IL-6 in response to radiation. After 1w post-IR the WT skin showed 2340 pg/ml and the KO skin showed 3227 pg/ml of IL-6, showing significantly higher levels of IL-6 in KO in comparison to WT skin. After 2w post-IR the WT skin showed

1645 pg/ ml of IL-6, while the KO skin showed 2526.25 pg/ ml of IL-6, again showing significantly higher levels of IL-6 in KO in comparison to WT skin.

Granulocyte-macrophage stimulating factor (GM-CSF) is an inflammatory cytokine which is primarily important for growth and differentiation of granulocytes and macrophages.

In reference to the fig. 12, the non-irradiated WT skin showed 557 pg/ ml while the non-irradiated KO skinsh owed 799 pg/ ml. After 72h post-IR the WT skin showed 564 pg/ml, while the KO skin 1160 pg/ml of GM-CSF, showing that the KO skin has significantly higher level of GM-CSF in comparison to the WT skin. After 1w post-IR the WT skin showed 589 pg /ml, while the KO skin showed 544 pg/ml, therefore showing no significant differences between WT and KO skin. At 2w post-IR the WT skin showed 496.3 pg/ml, while the KO skin showed 504 pg/ml of GM-CSF, thus idicating an initial increase at the early time point, but no significant change at later time points.

Monocyte-chemoattractant-protein-I (MCP-1) is a chemokine primarily involved in macrophage recruitment. The non-irradiated KO skin showed already very high amounts of MCP-1 (17008 pg/ml) compared to non-irradiated WT skin (2154 pg/ ml). After 72h post-IR the level of MCP-1 in KO skin decreased to 10619 pg/ml but still remained higher than in WT skin (3888 pg/ml). After 1w post-IR the level of MCP-1 was still higher in KO skin (8241 pg/ml) in comparison to WT skin (3729 pg/ml). A gradual reduction was observed in the level of MCP-1 at later timepoints (2w post-IR: 5271 pg/ml in KO versus 2097 pg/ml in WT skin).

Therefore, an elevation in cytokines was observed in early timepoints, which declined gradually at later time periods, with KO skin expressing higher levels of cytokines compared to WT skin.
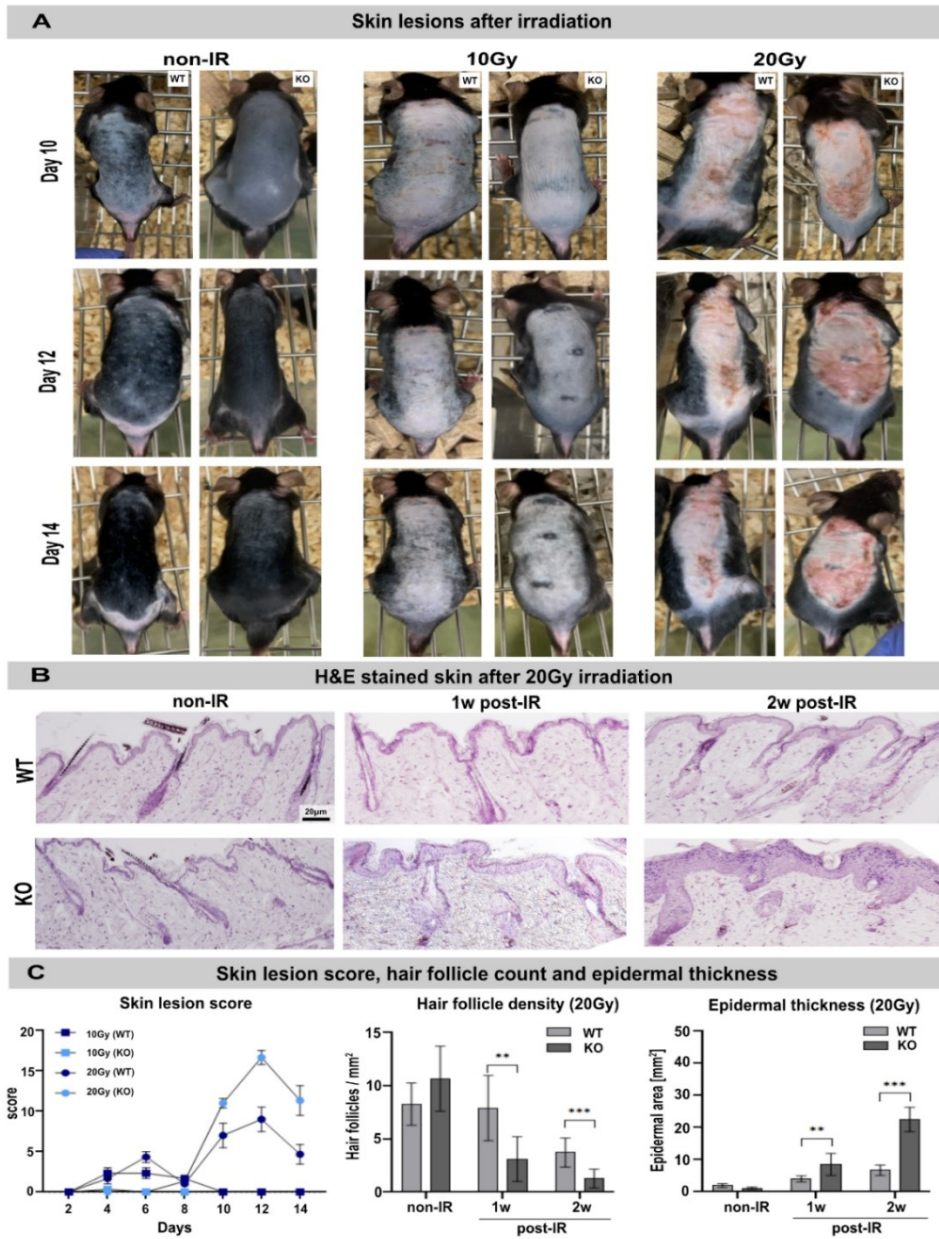
4.4. Skin lesions in response to high-dose radiation
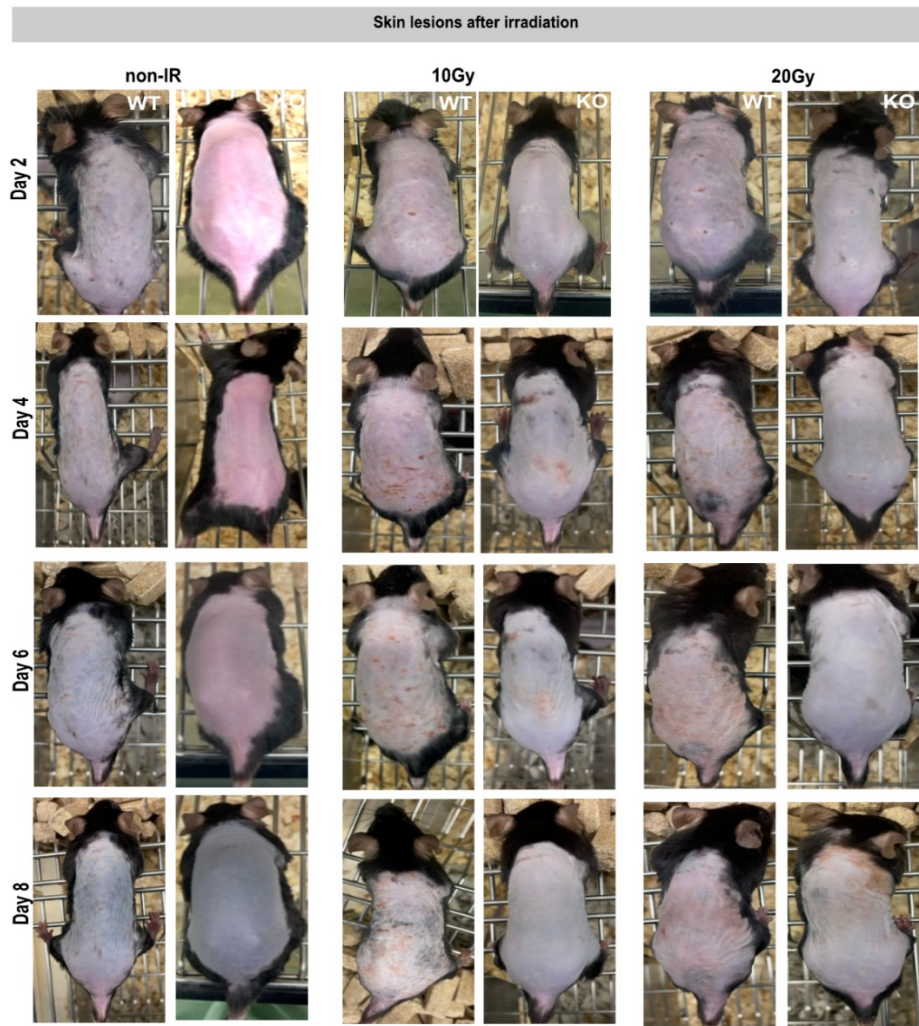
Figure 12. Visual inspection for skin lesion scoring during 1st week following 10Gy and 20Gy irradiation. Skin lesions were scored on a scale of 0-6 during the 2nd, 4th 6th and 8th day following IR exposure.

4.5. Epidermal thickness and hair follicle density after 20Gy radiation

Figure 13. Visual inspection, quantitative analysis of skin lesions, hair follicle density and epidermal thickness following 20Gy irradiation. (A) Skin lesions were scored on a scale of 0-6 during the 10th, 12th and 14th day following IR exposure. (B) Overview images of H&E-stained skin sections of (non-) irradiated WT and KO mice (magnification: 10x). (C) Graphic presentation of the skin lesion score, hair follicle density, epidermal thickness for WT and KO mice at different time points after irradiation. All data are shown as mean with standard deviation (n=3). Significant differences were assessed using the Man-whitney non-parametric unpaired t-test and presented by *p <0.05; **p <0.01 and ***p <0.001 given.

After exposure to high-dose radiation with 10Gy and 20Gy, respectively, the visual inspection was recorded and photo-documented. It was observed that after 10Gy only mild skin lesions

occurred in the WT mice by the 4th (2.3 ± 1.1) and 6th day (2.3 ± 1.1); in KO mice slight skin lesions occurred on the 4th day (0.3 ± 0.5), but on the 6th day no skin abrasions were observed. During the 8th day the WT skin had started healing, but still had some minor lesions (1.6 ± 0.5); KO skin, by contrast, had healed completely. The 10th day marked the onset of hair growth in both WT and KO mice, showing no skin lesions during the following days.

However in comparison to the non-IR WT and KO mice , the mice irradiated with 10Gy showed delayed hair growth in both WT and KO.

Referring to the fig. 12 and fig. 13, after exposure to 20Gy, the WT mice showed slight skin lesions on the 4th day (1.6 ± 1.1) and intense skin lesions on 6th day (4.3 ± 1.1), followed by dry desquamation but no signs of skin lesion on the 8th day (1 ± 0.0). However, the KO mice showed no signs of skin lesion or skin erythema until the 6th day, on the 8th day the KO skin started showing signs of erythema with dry desquamation around the neck area (1.3 ± 0.5). On the 10th day WT skin revealed high levels of dry and moist desquamation (7 ± 2.6), but these skin lesions were even more pronounced in the KO mice (11 ± 1). On the 12th day the WT mice showed signs of moist desquamated area and very few spots of excoration (9 ± 2.6). However, the KO mice showed elevated amounts of dry and moist desquamated areas along with high amounts of inflammed skin (16 ± 1.5). During the 14th day the WT mice showed some signs of recovery (4.6 ± 2.08), but still some regions of the dorsal skin was covered with dry and moist desquamation. The KO mice, by contrast, showed intensively inflamed doral skin with clearly more dry and moist desquamated areas (11.3 ± 3.2).

This macroscopic visible difference in skin toxicity was further investigated by histological analysis of H&E stained skin sections, collected at 1w and 2w after 20Gy post-IR. Accordingly, hair follicle density and epidermal thickness were measured in WT and KO skin at 1w and 2w post-IR.

In non-irrradiated mice , WT (8.2 ± 1.9 HF/mm^2) and KO skin (10.6 ± 3.05 HF/mm^2) showed no significant difference in hair follicle density. After 1w post-IR , WT skin showed 7.9 ±

3.06 HF/ mm^2 in contrast to KO skin that showed 3.1 ± 2.1 HF/ mm^2 (p=0.0012). At 2w post-IR, WT skin showed a further reduction in hair follicle density with 3.7 ± 1.3 HF/ mm^2 in WT and 1.2 ± 0.8 HF/mm^2 in KO skin (p= 0.0005). Accordingly, in KO versus WT skin, the hair follicle density is reduced by more than 50% after irradiation.

Non-irradiated skin of WT and KO mice displayed no significant difference in their epidermal thickness. After 1w post-IR WT skin showed an epidermal thickness of 4.04 ± 0.8 mm^2 and KO skin showed 8.5 ± 3.4 mm^2 (p= 0.0019), this means that the KO epidermis is significantly thicker than the WT epidermis. This trend which even strengthened after 2w post-IR weeks with WT skin showing 6.7 ± 1.5 mm^2 and KO skin showing 22.5 ± 3.8 (p=0.0004) mm^2 of epidermal thickness.

In summary, one can say that both the macroscopic and the microscopic skin damage after exposure to radiation with 20Gy were significantly more pronounced in the KO mice.

4.6. H2A.J, SA-β-Gal and lamin B1 expression after 20Gy radiation
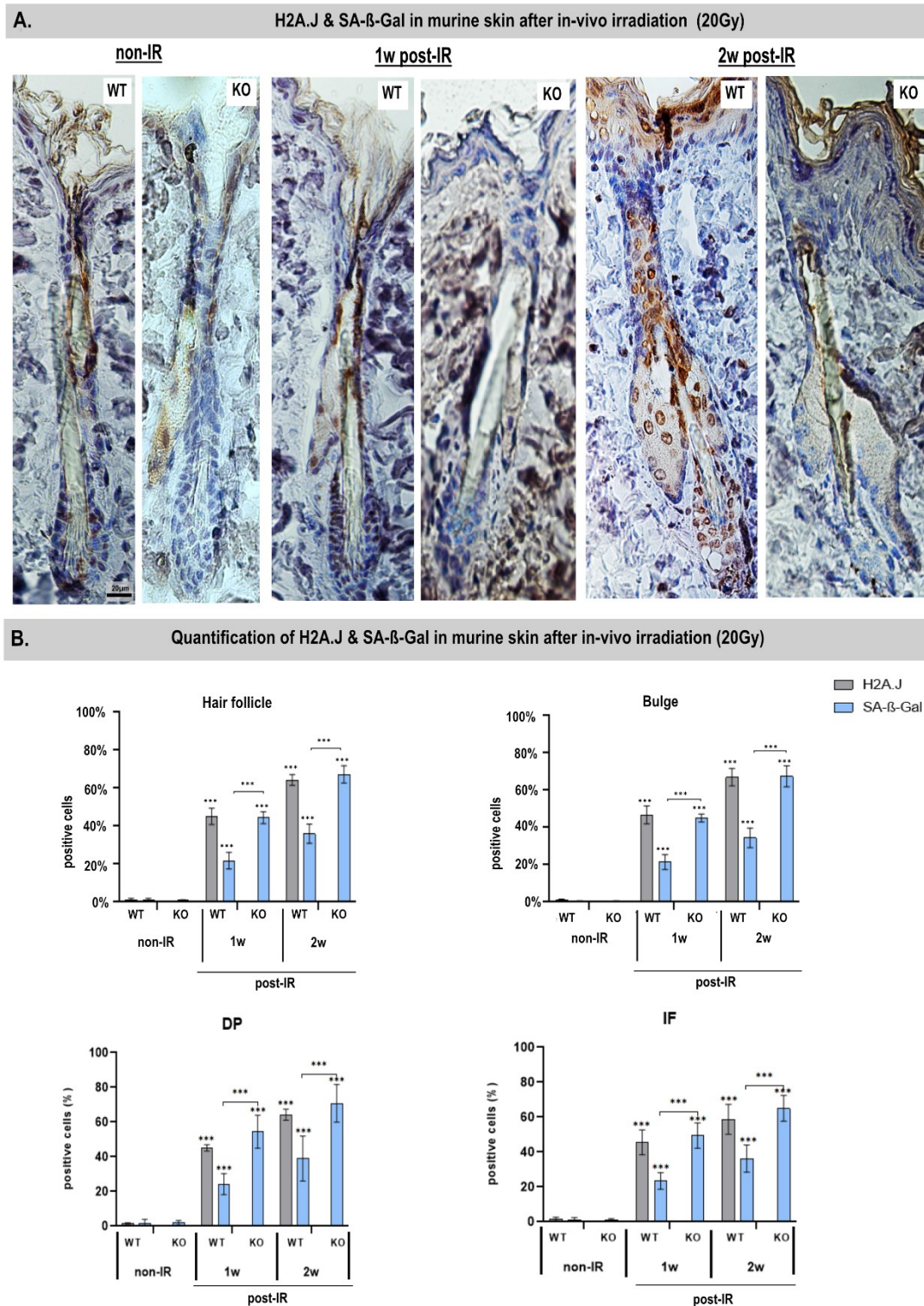
Figure 14. Quantitative analysis of H2A.J and SA-β-Gal after 20Gy irradiation (A) Overview of images of immunohistological stain for H2A.J (brown) and X-gal for senescence (blue) in different parts of the hair follicle after irradiation with 20Gy (magnification: 10x, scale bar = 20μm). (B) Quantification of H2A.J+ and SA-β-Gal+ cells in different parts of the hair follicle at different times after irradiation with 20Gy compared to age-matched, non-irradiated controls. Shown are the mean values of the percentage of H2A.J+ and SA-β-Gal+ cells and the standard error of mean for three biological and three technical replicates (n=3). Significance differences between the irradiated and unirradiated groups were assessed using the Man-Whitney non-parametric unpaired t-test and shown as *p <0.05; **p <0.01 and ***p <0.001.

After exposure to 20Gy, collected skin tissue samples were further analysed for expression of H2A.J and SA-β-Gal after 1w and 2w post-IR. Therefore H2A.J + and SA-β-Gal + cells were quantified in the different regions of the hair follicle (bulge, papilla, infundibulum) and the whole hair follicle.

In non-irradiated WT skin the hair follicle showed very low levels of H2A.J (1.2 ± 0.5%) . After 20Gy exposure the number of H2A.J + cells increased to 45 ± 4.3% at 1w post-IR, and 64 ± 2.8% at 2w post-IR, indicating a strong upregulation of H2A.J expression.

The bulge region in the hair follicle of non-irradiated skin showed 0.9 ± 0.2% of H2A.J + cells. However, after IR exposure the number of H2A.J + cells increased to 46.7± 4.7% at 1w post-IR and 66.9 ± 4.6% at 2w post-IR. of H2A.J + cells. Thus the bulge region showed an increase in the percentage H2A.J + cells over later time points.

Further the dermal papilla region showed 1.6 ± 1.0% of H2A.J + cells in WT non-IR thus showing very less level of H2A.J. After 1w post-IR it was seen to have 45.06 ± 5.4% of H2A.J + cells. Further gradual increase was observed after 2w post-IR which showed to have 64.2 ± 9.5% of H2A.J + cells.

Finally the infundibulum showed to to have 1.7±0.9% of H2A.J+ cells in the non-IR WT mice. Further gradual increase was observed during 1w post-IR showing 42.4 ± 10.0% of H2A.J+ cells. Further analysis 2w post-IR quantification showed 58.6 ± 8.5% of H2A.J + cells thus showing further increase in the percentage of H2A.J + cells.

Further during the analysis of SA-β-Gal, the hair follicle from non-IR mice showed to have 0.9 ± 0.8% in the WT and 0.8 ± 0.3% of H2A.J positive cells in KO showing no significant difference. After 1w post-IR the WT showed 21.7 ± 4.3% in WT and 44.4 ± 3.1% in the KO showing a gradual rise in the number of SA-β-Gal+ cells in the KO in comparison to WT. Further gradual increase was observed was seen after 2w post-IR where the WT which showed 35.9 ± 5.01% and the KO which showed 67.2 ± 4.6 % of SA-β-Gal + cells.

In the bulge region of the hair follicle, the WT non-IR showed to have 0.38 ± 0.3% of SA-β-Gal + cells in comparison to KO non-IR which showed 0.35 ± 0.3% SA-β-Gal+ cells therefore showing no significant difference. After 1w post-IR the WT showed 21.4 ± 3.9% SA-β-Gal + cells while the KO showed to have significantly higher percentage of SA-β-Gal + cells that is 45.0 ± 2.14%. After 2w post-IR the WT showed 34.37 ± 5.2% of SA-β-Gal + cells while the KO showed to have significantly greater percentage of SA-β-Gal + cells that is 67.4 ± 5.6%.

In the dermal papilla region of the hair follicle, the non-IR group showed to have 1.7 ± 2.1% SA-β-Gal cells while the non-IR group in the knock out showed to have 2.0 ± 1.3% SA-β-Gal + cells thus showing no significant difference between them. Further the 1w post-IR analysis in the WT showed to have 22.6 ± 5.2% of SA-β-Gal + cells which the knock out showed to have significantly higher percentage of SA-β-Gal+ cells that is 44.2 ± 6.8%. The 2w post-IR analysis showed to have 39.0 ± 12.9% SA-β-Gal + cells while the knock out showed to have significantly higher number of SA-β-gal + cells that is 70.7 ± 10.8% in comparison to WT.

In the infundibulum of the hair follicle, the WT non-IR group showed to have 1.2 ± 1.0% of SA-β-Gal+ cells in comparison to KO that showed to have 0.9 ± 0.8% of SA-β-Gal+ cells therefore showing no significant difference. During the 1w post-IR analysis the WT showed to have 22.8±7.04% SA-β-Gal + cells in comparison to KO that showed significantly higher percentage of SA-β-Gal + cells that is 44.5 ± 11.07%. The 2w post-IR analysis showed much gradual greater percentage of SA-β-Gal+ cells that is 36.2 ± 7.8% however the KO showed significantly much greater percentage of SA-β-Gal+ cells that is 64.9 ± 7.3%.

Therefore, after exposure to high radiation dose significant differences were observed in the SA-β-Gal activity between the WT and KO in different parts of the hair follicle where the KO showed more SA-β-Gal activity in comparison to WT. Additionally the WT also showed increased expression of H2A.J post-IR in different parts of hair follicle.

Nuclear Lamin B1 is a chief physical constituent of the nucleus. Previous studies have shown Lamin B1 expression decreases during cellular senescence (Freund et al., 2012).
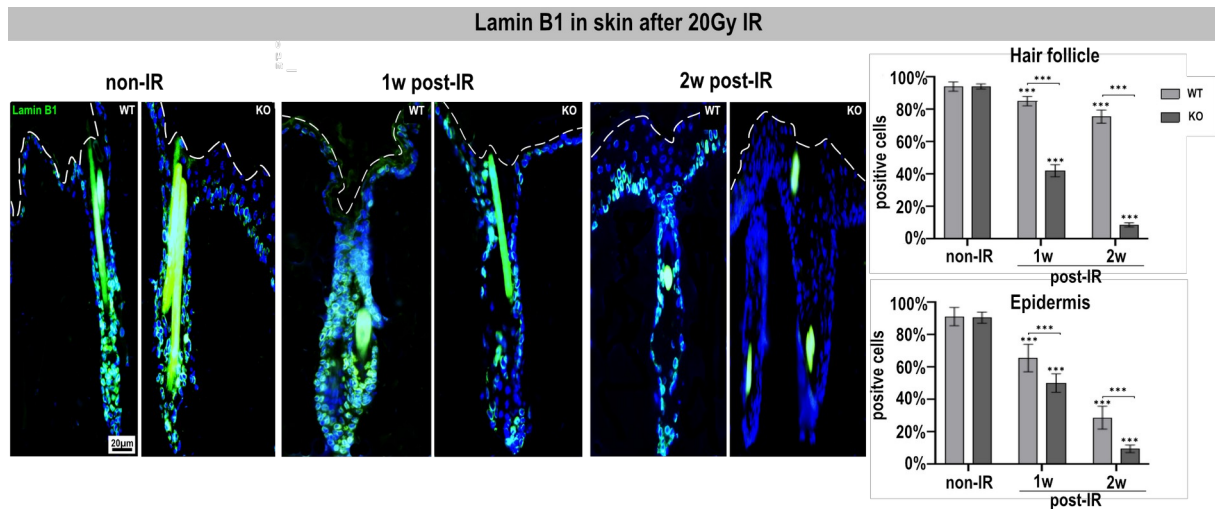
Figure 15. Quantitative analysis of Lamin B1 after 20Gy irradiation. Overview images of immunofluorescence labeling with Lamin B1 (green) in bulge of hair follicle and epidermis after irradiation (magnification: 20x, scale bar = 20µm)**.** the graphs shows quantification lamin B1 in bulge of hair follicle and epidermis at different times after irradiation with 20Gy compared to age-matched, non-irradiated controls. Shown are the mean percentage of lamin B1 and standard deviation for three biological and three technical replicates (n=3). The significance of the differences between the irradiated and nonirradiated groups was assessed using the Man Whitney, non-parametric , unpaired t-test and found to be *$p < 0.05$; **$p < 0.01$ and ***$p < 0.001$ given.

After 20Gy radiation referring to fig 15 in the hair follicle the non-IR group showed no variation in the levels of lamin B1 in WT 94.2 ± 2.8% and KO showing 94.2 ± 1.5% of lamin B1 expression in hair follicle bulge. A significant decrease was observed after 1w post-IR between WT which showed 85.1 ± 2.8% and KO which showed 42.2 ± 3.7% of Lamin B1+ cell. Thus it was observed that after 1w post-IR the percent of lamin B1+ cells in the KO reduced to nearly half in comparison to WT. After 2w post-IR the WT showed 75.6 ± 4.1% of lamin B1+ cells whereas the KO showed 8.7 ± 1.3% (p<0.0001) of lamin B1+ cells. Therefore, after 2w post-IR it was observed in the bulge of the hair significantly lower percentage of lamin B1+ cells in the KO in comparison to the WT.

In the epidermis the non-IR group of the WT showed 91.2 ± 5.6% of lamin B1+ cells and the KO showed 90.6 ± 3.4% of lamin B1+ cells in the hair follicle bulge, thus showing no significant difference. After 1w post-IR it was observed that the WT showed 65.6 ± 8.5% of

lamin B1+ cells while the KO showed 50.2 ± 5.7% of lamin B1+ cells. Therefore after 1w post-IR a significant reduction in the lamin B1 was observed in comparison to WT. After 2w post-IR the WT showed 28.7 ± 7.03% of lamin B1+ cells whicle the KO out showed 9.6 ± 2.3% (p< 0.0001) of lamin B1+ cells. Further, reduction on the percentage of lamin B1+ cells was observed in the epidermis of the KO in comparison to the WT after 2w post-IR.

Therefore, in the hair follicle bulge 1w post-IR WT showed less changes in the levels of lamin B1 in comparison to KO while 2w post-IR showed major changes where KO had very low lamin B1+ cells in comparison to WT. Similar pattern was noted in the epidermis as well where there was a decline in the expression levels of lamin B1 1w post-IR in the WT but KO showed comparitively lower levels. Further in 2w post-IR while there was further decline observed in the lamin B1 levels where KO showed very low levels of lamin B1 expression in comparison to WT.

4.7. Hair follicle stem cells in the bulge region after 20Gy radiation

The CD34+ HFSC's are multipotent stem cells that reside in the bulge of the hair follicle in murine epidermis and subsidize to wound repair. To understand the effect of high radiation exposure on CD34+ hair follicle stem cells in WT and H2A.J-/- KO mice. The CD34+ HFSC's were quantified in the hair follicle bulge at each time point.
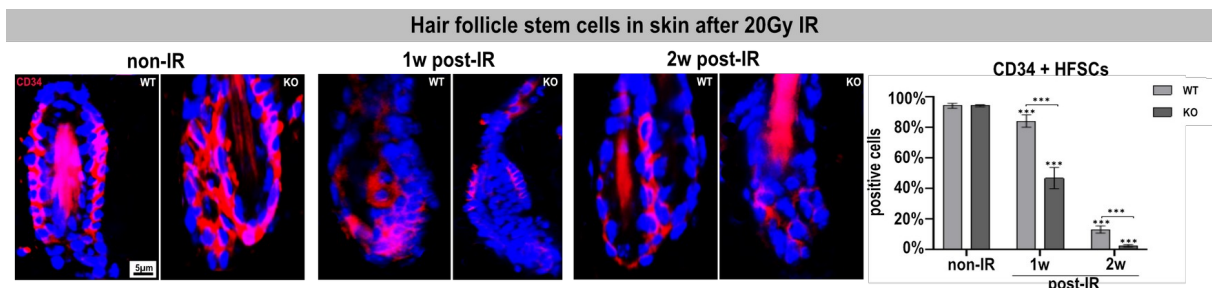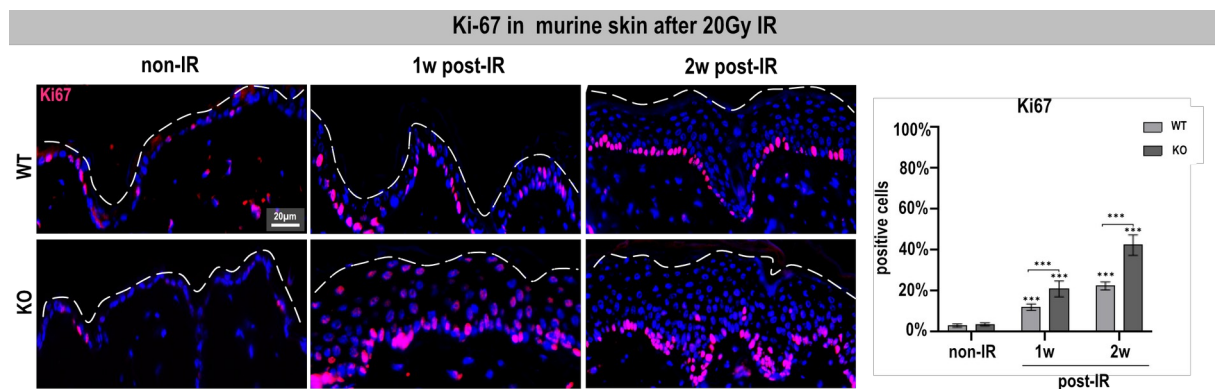

Figure 16. Quantitative analysis of CD34-positive hair follicle stem cells after 20Gy irradiation Overview images of immunofluorescence labeling with CD34 (red) in bulge of hair follicle after irradiation (magnification: 20x, scale bar = 5μm). the graph shows quantified CD34 in bulge of hair follicle at different times after irradiation with 20Gy compared to age-matched, non-irradiated controls. Shown are the mean percentage of CD34 and standard deviation for three biological and three technical replicates (n=3). The significance of the differences between the irradiated and nonirradiated groups was assessed using the Man Whitney, non-parametric , unpaired t-test and found to be *p < 0.05; **p < 0.01 and ***p < 0.001 given.

Referring to fig 16, the non-IR showed 94.6 ± 1.3% and the KO showed 94.17 ± 0.5% of CD34$^+$ cells therefore showing no significant difference. After 1w post-IR the WT showed 85.4 ± 2.6% of hair follicle stem cells thus showing a slight reduction in the percentage, while the KO showed 48.1 ± 6.02% of CD34$^+$ HFSC's. Therefore, a substantial reduction was observed in the KO in comparison to the WT after 1 week. After 2w post-IR the WT showed 13.0± 2.4% of CD34$^+$ HFSC's while knock out showed 2.7 ± 0.7% (p<0.0001) of CD34$^+$ HFSC's thus showing further reduction in the levels of hair follicle stem cells in the WT in comparison to the KO.

Therefore, 1w post-IR WT showed slight reduction in the CD34$^+$ HFSC's while it reduced to almost half in KO. Further decline was observed 2w post-IR where there was extremely low levels of CD34$^+$ HFSC's in KO in comparison to WT.

4.8. Ki-67 expression in epidermal skin after 20Gy radiation

The Ki-67 protein is a widely used proliferation marker. Inflated number of Ki-67+ cells in the epidermis indicates increased epidermal hyperplasia, a characterisitic which is associated with various inflammatory skin diseases.

Figure 17. Quantitative analysis of Ki-67 positive proliferative cells after 20Gy irradiation Overview images of immunofluorescence labeling with Ki-67 (red) in epidermis of murine skin after irradiation (magnification: 20x, scale bar = 20μm). The graph shows quantified Ki-67 in epidermis at different times after irradiation with 20Gy compared to age-matched, non-irradiated controls. Shown are the mean percentage of Ki-67 positive cells and standard deviation for three biological and three technical replicates (n=3). The significance of the differences between the irradiated and non-irradiated groups was assessed using the Man Whitney, non-parametric , unpaired t-test and found to be *p < 0.05; **p < 0.01 and ***p < 0.001 given.

While the non-IR group showed very low levels of Ki-67+ cells in the epidermis in the WT that is 3.08 ± 0.7% and the KO showed 3.6 ± 0.7% of Ki-67+ cells with no significant difference. Referring to the fig 17 significant difference in the levels Ki-67+ cells was observed where the WT showed 12.1 ± 1.5% of Ki-67+ cells and the KO showed 21.03 ± 3.8% of ki-67 + cells. After 2w post-IR the WT showed 22.4 ± 1.9% of Ki-67+ cells while the KO showed 42.3 ± 4.9% (p<0.0001) of Ki-67+ cells. Therefore, it was observed that 2w post-IR the percentage of Ki-67+ cells nearly doubled in KO in comparison to the WT.

Although significant differences were also observed during 1w post-IR between WT and KO, Ki-67 showed more expression in KO 2w post-IR in comparison to WT.

4.9. JunB expression in epidermal skin after 20Gy radiation

JunB is a transcription factor that is one of the central members of activator protein-1. It is known to play a pivotal part in cell proliferation and differentiation (Farràs et al., 2008). In general the Jun proteins are regarded as positive regulator of keratinocyte proliferation/differentiation during development (Singh et al., 2018).
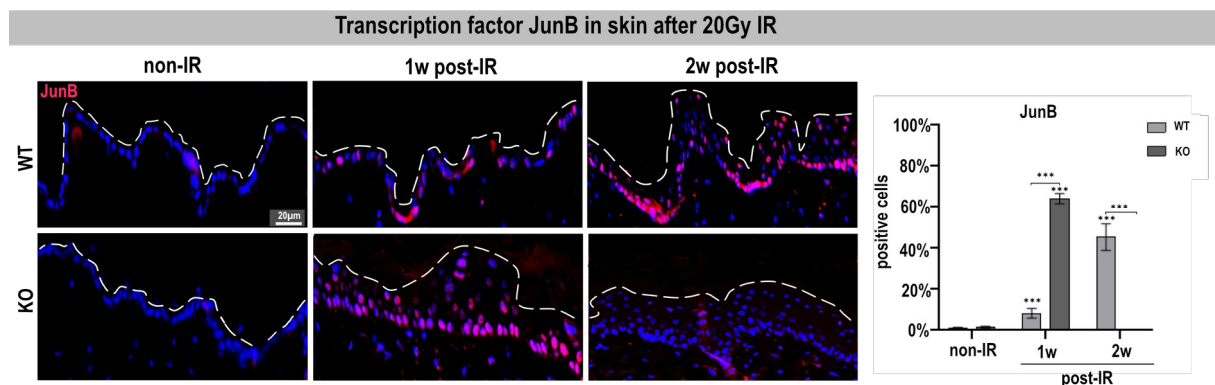
Figure 18. Quantitative analysis of transcription factor JunB after 20Gy irradiation. Overview of images of immunofluorescence labeling with transcription factor JunB (red) in epidermis of murine skin after irradiation (magnification: 20x, scale bar = 20μm). The graph shows quantified JunB in epidermis at different times after irradiation with 20Gy compared to age-matched, non-irradiated controls. Shown are the mean percentage of JunB positive cells and standard deviation for three biological and three technical replicates (n=3). The significance of the differences between the irradiated and non-irradiated groups was assessed using the Man Whitney, non-parametric , unpaired t-test and found to be *p < 0.05; **p < 0.01 and ***p < 0.001 given.

To understand the role JunB in response to high radiation exposure in WT and H2A.J KO mice, JunB was quantified in the epidermis at different time point. The non-IR showed very

less expression of JunB+ cells in WT 1.08 ± 0.3% of JunB+ cells while the KO showed 1.5 ± 0.3% of JunB+ cells thus showing no significant difference between the two. After 1w post-IR the WT showed 8.2 ± 2.4% of JunB+ cells and the KO showed 64.12 ± 2.49% of JunB+ cells thus showing a very high significant increase in the KO in comparison to the WT. After 2w post-IR the WT showed 45.4 ± 6.4% of JunB+ cells while the KO showed 0.15 ± 0.2% ($p<0.0001$) of JunB+ cells thereby showing a significant difference in the level of JunB+ cells in the WT and KO.

Thus, 1w post–IR the WT showed very low expression of JunB in comparison to KO however, low levels of JunB+ cells were seen in KO after 2w post-IR indicating loss of differentiation in KO in comparison to WT.

4.10. Expression of myeloperoxidase in dermal skin after 20Gy radiation

Myeloperoxidase is a major constitutent of neutrophils which are recruited to the site of inflammation where they inactivate foreign microoorganisms. To study the response to high dose radiation dose in WT and KO mice skin , the accumulation of myeloperoxidase (MPO) was studied by quantifying at different time points in the epidermis.
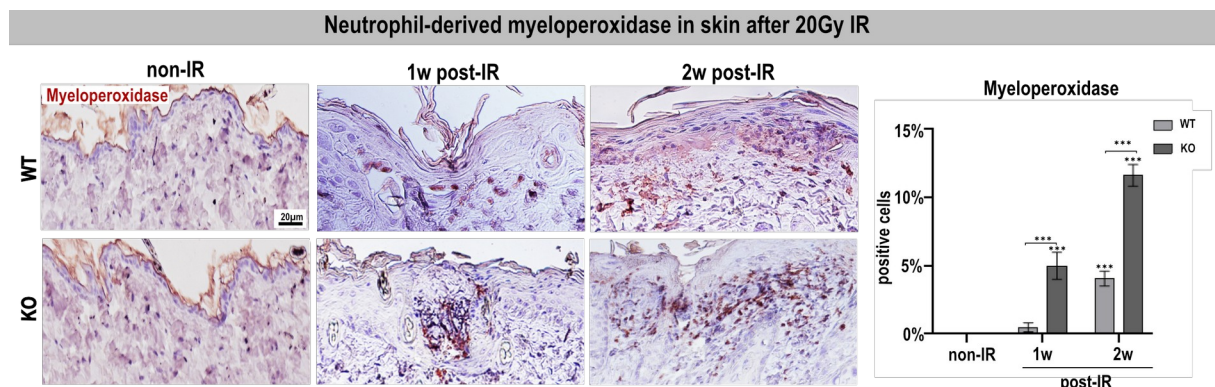
Figure 19. Quantitative analysis of MPO after 20Gy irradiation. Overview of images of immunohistological labeling of myeloperoxidase (brown) in epidermis of murine skin after irradiation (magnification: 10x, scale bar = 20µm). The graph shows quantified myeloperoxidase in epidermis at different times after irradiation with 20Gy compared to age-matched, non-irradiated controls. Shown are the mean percentage of myeloperoxidase positive cells and standard deviation for three biological and three technical replicates (n=3). The significance of the differences between the irradiated and non-irradiated groups was assessed using the Man-Whitney, non-parametric , unpaired t-test and found to be *$p < 0.05$; **$p < 0.01$ and ***$p < 0.001$.

Referring to figure 19, the control showed no signs of MPO. After 1w post-IR the WT 0.49 ± 0.3% of MPO+ cells in the epidermis while the KO showed 4.9 ± 0.9% of MPO+ cells in the

knock out thus indicating onset of inflammation in response to radiation exposure. After 2w post-IR the WT showed $4.06 \pm 0.5\%$ of MPO+ cells while the KO showed $11.6 \pm 0.7\%$ ($p<0.0001$) of MPO+ cells thus indicating more radiosensitivity in the KO in comparison to the WT.

Thus, 1w post-IR the WT showed very low expression of MPO in comparison to KO. However, 2w post-IR higher expression of MPO was observed in KO compared to WT indicating more neutrophilic accumulation in KO in comparison to WT.

5. <u>Discussion</u>

In vivo studies have revealed that H2A.J collects in mice and human skin not only with aging but also in response to ionizing radiation (Contrepois et al., 2017; Rübe et al., 2021). In murine skin H2A.J showed accumulation in undifferentiated keratinocytes in the hair follicle in response to ionizing radiation exposure (Hippchen et al., 2022). In addition, H2A.J has shown to play an imperative role in modulation of SASP and cellular senescence thereby playing a key role in radiation induced inflammation (Contrepois et al., 2017; Isermann et al., 2020).

In this preclinical in-vivo study with H2A.J WT and KO mice we identified an epigenetic key mechanism that via reorganization of damaged chromatin leads to altered gene regulation and modulated SASP secretion after IR exposure.

5.1 Visual observation in skin and hair in response to radiation

The skin is an organ which has the capacity to continuously renew itself overtime. However, exposure to high doses of ionizing radiation disturbs the normal proliferation and maturation, of germinative epidermal and hair matrix cells (Hymes et al., 2006). Following exposure to 10Gy (section 4.4 & 4.5) the WT and KO mice showed delayed hair growth for a duration of 2 weeks in comparison to the control group. This confirms that the hair follicles are highly sensitive to ionizing radiation (Song & Lambert, 1999 ;Hymes et al., 2006).

Previous studies have shown that DNA is the prior target of ionizing radiation, and radiation exposure leads to the loss of reproductive ability (Ji et al., 2017) when cells are unable to repair damaged DNA. Proliferating cells are generally more radiosensitive than highly differentiated, non-proliferating cells (Driskell et al., 2015). Thus, depletion of HFSCs residing in the bulge region of the hair follicles may result in delayed hair growth (Ansell et al., 2017).

On the other hand, exposure to a high dose of 20Gy showed slight to intense erythema with dry and moist desquamation indicative of radiation dermatitis (Ryan,2012). Interestingly the KO mice showed more skin damage at 1w and 2w post-IR in comparison to the WT mice. Radiation -induced skin injury refers to the immediate damage of basal keratinocytes and hair follicle stem cells, leading to the compensatory hyperproliferation of keratinocytes and hair follicle atrophy (McQuestion, 2011; Mendelsohn et al).

5.1.1. Changes in epidermal thickness in relation to radiation exposure

Acute radiation skin damage primarily involves cellular changes and inflammation in the epidermal and dermal layer of the skin (Schmuth et al.). Following IR exposure with 20Gy, the histological analysis showed an increased epidermal thickening and reduced hair follicle density in the KO versus WT skin. These findings could be stated as a consequential event as a result of increased acute radiation injury in the KO in contrast to WT. Moreover it has been observed that radiation induces acute skin toxicity (Fodor et al., 2022). This fits with our study that showed increased epidermal thickness and decreased hair follicle density in the KO is also an explanation of more skin lesions and wounds in KO more than WT that was observed during visual inspection.

5.2. Time- and dose-dependent H2A.J accumulation

H2A.J has been shown to be highly expressed in the epithelial cells of multiple glands i.e mammary, prostrate pancreatic and salivary gland (Redon et al., 2021). Previous studies have shown that H2A.J accumulates in skin tissue specific manner with ageing and also in human skin (Rübe et al., 2021) H2A.J showed an accumulating trend in the in the hair follicle stem cells and interfollicular epidermal cells in young (8 week) mice following irradiation by a fractionated low dose of 50x100mGy (Contrepois et al., 2017a). Similar trend was observed in this study where H2A.J was seen to accumulate after single dose of 2Gy. Previous studies show that following fractionated dose of 5x2Gy, accumulation of H2A.J is enhanced in

largely epidermal cell population in the murine hair follicle (Hippchen et al., 2022). In this study, H2A.J seemed to drastically increase and accumulates in different parts of the hair follicle with increasing time points when exposed to fractionated dose of 5x2Gy, and single dose of 20Gy. Therefore, it can be presumed that differential H2A.J expression in various epidermal populations and elevated H2A.J expression in various epidermal cell populations might reflect towards epigenetic regulation mechanisms involved in the induction of differentiation and maturation of keratinocytes (Hippchen et al., 2022). Moreover, in reference to previous studies H2A.J accumulation was found to be increased 4-folds in epidermis of old human skin (60 yr) in comparison to epidermis of young human skin (17yr) (Contrepois et al., 2017a; Rübe et al., 2021). Therefore, in this study accumulation of H2A.J may be indicative towards accelerated epidermal ageing in response to increase exposure to high dose of ionizing radiation.

5.2.1. H2A.J and SA-β-Gal accumulation following radiation exposure

In this study, we studied the expression of H2A.J accumulation with SA-β-Gal post radiation exposure of 2Gy, fractionated dose of 5x2Gy and dorsal skin radiation of 20Gy using IHC for different time points. Cellular senescence has often been investigated as a response to stresses that can damage DNA and destabilize the genome (Campisi, 2013; Rodier et al., 2009). Earlier studies have shown that H2A.J accumulates in mouse epidermal cells in a model of RAS-induced senescence.(Contrepois et al., 2017a). An increasing trend was observed in the percentage of SA-β-Gal and H2A.J with increasing time point in different parts of the murine hair follicle which might reveal the primary initiation of differentiation processes in response to DNA damage. Moreover, it was observed that H2A.J-KO murine epidermis exhibit more expression of SA-β-Gal which could indicate towards more radiosensitivity which may further explain DNA damaged immunomodulatory response in the skin homeostasis in response to IR exposure (Campisi, 2013; Contrepois et al., 2017a; Hippchen et al., 2022) this

might reflect further to be an explanation for chronic inflammation and radiation-induced dermatitis in this study.

5.3. DNA damage response in keratinocytes following radiation

After exposure to dose of 2Gy, the DNA damage response was analysed in different parts of the hair follicle in the epidermis of the murine skin.

An increase in the levels in the 53BP1 was observed 24h post-IR which gradually decreased with increasing time point in all parts of the hair follicle in both WT and KO mice. This could be related to the fact that timely signalling to recognize damage and initiate cellular repair of double strand breaks with appropriate fidelity took place as it is of extreme importance for genomic maintenance (Pfeiffer et al., 2000).

However, 1week post-IR it was found that 53BP1 foci levels were still above control levels in all parts of the hair follicle in both WT and KO mice. This could indicate towards presence of the persistent 53BP1 foci present at the site DNA damage which indicated towards persistent chromatin lesions bearing the hallmarks of DNA DSB's (Rodier et al., 2009).

Since the bulge of the hair follicle is known to be a reservoir for multipotent stem cells (Arita et al., 2004), Existence of such persistent DNA damage might be a cause of reduction of proliferative potential of stem and progenitor cells (Schuler & Rübe, 2013).

5.4. Depletion of nuclear lamin B1 in response to high-dose radiation

The nuclear lamina is known to be closely opposed to the inner membrane of nuclear envelope and therefore contributes to the shape, size and mechanical stability of the nucleus (Shimi et al., 2011). After exposure to a high dose of 20Gy, influence of ionizing radiation was studied on nuclear membrane by focusing on the expression of nuclear laminB1 in the epidermis and bulge of the hair follicle.

The controls showed no change in the expression of Lamin B1+ cells. However, 1w post-IR the lamin B1 declined drastically in the KO skin and almost diminished at 2w post-IR. On the

other hand, in the WT skin the levels of lamin B1 showed comparatively less reduction post-IR. It has been observed that the absence of lamin B1 expression slows down the proliferation of cells and induces premature senescence (Shimi et al., 2011).

Additionally, the nuclear lamin B1 has been shown to play an important role in DNA replication and repair, RNA polymerase transcription and epigenetic control of chromatin remodelling (Moir et al., 2000; Shimi et al., 2008; Shumaker et al., 2008; Spann et al., 2002).

Following exposure to high doses of ionizing radiation the cells lose their nuclear stability by the fast depletion of their lamin B1, thus affecting the mechanical strength of the cells, which may result in the progression to premature senescence. (Moir et al., 2000; Shimi et al., 2011). Moreover, the elevated loss of nuclear stability in KO versus WT skin may indicate a higher radiosensitivity of KO versus WT mice.

5.5. Ki-67 expression in response to high- dose radiation.

An interesting aspect was to study the expression of Ki-67 which is a widely known nuclear protein that is expressed only in the proliferating cells. Following exposure to 20Gy, increasing levels of Ki-67+ cells were observed along with increasing epidermal thickening. This was observed to be higher in KO skin versus WT skin. Ki-67 is known to be an extremely important proliferation marker (Sun & Kaufman, 2018).

High levels of Ki-67 in addition to increased epidermal thickening indicates epidermal hyperplasia as consequence of acute radiation injury. (Sezer et al., 2015). Previous studies have shown an inverse correlation between H2A.J and Ki-67, where Ki-67 was not expressed in the cells expressing H2A.J and vice versa. In human skin Ki-67+ cells decreased and H2A.J+ keratinocytes increased with increasing age of the donors (Rübe et al., 2021).

Thus, increased expression levels of Ki-67+ cells in KO versus WT skin indicate increased proliferation of keratinocytes as cell replenishment as a result of increased radiation damage.

 (Calonje et al., 2012; Sezer et al., 2015; Sun & Kaufman, 2018)

5.6. Depletion of hair follicle stem cells in response to high-dose radiation

The cell surface marker CD34 marks the murine hair follicle stem cell (HFSCs) in the bulge region, which have the characteristics of stem cells including quiescence and multipotency (Trempus et al., 2007). Moreover, these HFSCs monitor and regulate the regenerative capacity of the epidermis, when the skin is damaged by external stress factors, such as ionizing radiation (Levy et al.).These HFSCs not only play a essential role in maintaining the epidermal homeostasis and normal follicular growth (Cotsarelis et al., n.d.; R. Morris et al.), but also contribute to wound repair (Claudinot et al., 2005; Levy et al).

Following exposure to a high dose of 20Gy, the number of CD34+ HFSCs decreased more in WT versus KO skin with increasing time, suggesting an increased vulnerability of KO versus WT HFSCs with an elevated risk of developing radiation-induced alopecia (Nanashima et al., 2012).

Exogenous agents such as ionizing radiation led to a variety of DNA damage, of which double strand breaks are known to be the most toxic (Roos & Kaina, 2012). Proliferative stem cells are known to be more susceptible to DNA damage in response to ionizing radiation. Therefore, even though these cells manage to survive and maintain the stem cell pool, the consequential compositional changes may lead to the impairment of long-term functionality of skin tissue, possibly stimulating premature ageing (Greubel et al., 2008; Ward, 1991).

Decreased numbers of HFSCs may therefore contribute to disturbed epidermal structure in KO skin, thus failing to contribute to epidermal homeostasis following IR exposure.

5.7. Regulation of transcription factor JunB in response to high-dose radiation

Activator protein (AP-1) is a family of dimeric transcription factors which are well known for their involvement in proliferation, inflammation, differentiation, and apoptosis (Shaulian, 2010). JunB is a member of the AP-1 family and is known as a positive regulator of

keratinocyte proliferation and differentiation in response to multiple stressors (Zenz R & Wagner E.F 2005).

In KO mice following irradiation with 20Gy, the level of JunB was increased at 1w post-IR, but declined drastically at 2w post-IR showing. Earlier studies have shown that JunB deficiency in basal progenitor cells results in a dermatitis like syndrome, that resembles seborrheic dermatitis, a condition that harbours structurally and functionally impaired sebaceous glands, (Farràs et al., 2008; Singh et al., 2018).

Tissue homeostasis needs stable cell proliferation and differentiation with the fine-tuned regulation of stem cells which have the capacity to self-renew and differentiate in distinct lineages (Iglesias-Bartolome & Gutkind, 2010). It has been shown, that skin-specific JunB deficiency in mice is associated with skin pathologies such as ulcerative skin lesions, prolonged inflammation with delayed tissue remodelling (Florin et al., 2006; Pflegerl et al., 2009).

A hyperplastic thickened epidermis with enhanced inflammation was observed in KO versus WT skin, suggesting an unreported influence of H2A.J on the transcription factor JunB in monitoring keratinocytes and their progenitors during repair and regeneration of skin (Florin et al., 2006; Singh et al., 2018).

Moreover, it has been found that JunB plays an essential role in signalling of Notch genes. Deficiency of JunB has shown to cause an upregulation of Notch signalling, leading to aberrant epidermal differentiation (Singh et al., 2018). Additionally it has been observed that JunB deficiency could also be modulated by the upregulation of Wnt family genes, which are major elements of epidermal stemness in skin tissue (Singh et al., 2018).

5.8. Modulation of cytokine secretion in response to high-dose radiation

After high-dose IR exposure, a cascade of cytokines is induced in the various skin cells, which persists over the long period of acute and chronic radiation reactions

(Borish & Steinke, 2003). Cytokines are identified to play a substantial role in the cell-to-cell signalling, thereby mediating interactions between different cell types's within skin tissue and with distant organs (Müller & Meineke, 2007; L. Wang et al., 2022).

IL-6 is a pluripotent cytokine responsible acute inflammatory response in response to ionizing radiation (Takashima & Bergstresser, 1996; Xu et al., 1995). This finding fits with our observation, where following fractionated IR IL-6 was found to be elevated in both WT and KO skin, but KO versus WT skin showed higher IL-6 levels, indicating a stronger inflammatory response.

Similar findings were observed for the hematopoetic growth factor GM-CSF; KO versus WT skin showed higher GM-CSF levels following IR exposure, potentially indicating the stimulation and upregulation of myeloid progenitor cells in the bone marrow (Hachiya et al.). MCP-1 a chemokine important for macrophage recruitment showed a similar radiation response. MCP-1 is known to activate and induce the expression of pro-inflammatory cytokines IL-6 and IL1-β and upregulate TGF-β (Becker, 2005; Cranford et al., 2015). Increased MCP-1 expression in KO versus WT skin may indicate the stronger upregulation of these cytokines following IR exposure. The increased cytokine expression is associated with more pronounced skin inflammation and a greater risk of radiation-induced skin tissue complications

(Deorukhkar et al., n.d.; Multhoff & Radons, 2012).

5.9. Neutrophil-derived myeloperoxidase in response to high- dose radiation

The protein MPO is known to be a major constituent of neutrophils (Arnhold, 2020). Neutrophils are play an significant role at the site of inflammation where they recognize,

phagocytose and inactivate microorganisms (Paquet et al., 2010). Therefore, in freshly formed phagosomes, MPO plays a pivotal role in the creation and conservation of an alkaline milieu, optimal for combating microbes by providing neutrophil extracellular traps (Arnhold, 2020; Paquet et al., 2010).

In response to IR exposure with 20Gy, the KO versus WT skin showed a stronger staining for MPO, likely reflecting the degranulation of accumulated neutrophils.

Thus, the absence of H2A.J leads to the increased accumulation of inflammatory cells following high-dose IR exposure, likely reflecting the increased radiation-induced injury in KO versus WT skin (Arnhold & Flemmig, 2010; van der Veen et al., 2009).

Collectively, in this study we can show that following high-dose IR exposure H2A.J KO versus WT skin has stronger radiation reactions with more skin inflammation and increased hair follicle loss. Significant differences were observed in senescence induction between various keratinocyte populations, with HFSCs in bulge regions of KO skin being particularly badly damaged at high doses, leading to an increased loss of hair follicle density. Elevated Ki-67 levels caused excessive proliferation and abnormal differentiation of keratinocytes, leading to more epidermal hyperplasia.

6. <u>Conclusion</u>

This study shows that even though histone variant H2A.J has no impact on the acute DSB repair process, the absence of H2A.J leads to enhanced radiation induced senescence. As a result the enforced SASP activation of immune responses leads to enhanced recruitment of inflammatory cells, particularly neutrophils, and thereby elevates the inflammatory phase of radiation-induced skin reactions.

Future studies have to clarify the function and importance of H2A.J in chronic inflammation and radiation-induced fibrosis.

7. <u>References</u>

1. AA Goodarzi, P. J. (2013). The repair and signaling responses to DNA double-strand breaks. *Adv. Genet.*, *82*, 1–45.

2. Almendral, J. M., Sommer, D., Macdonald-Bravo, H., Burckhardt, J., Perera, J., & Bravo, R. (1988). Complexity of the early genetic response to growth factors in mouse fibroblasts. *Molecular and Cellular Biology*, *8*(5), 2140–2148. https://doi.org/10.1128/MCB.8.5.2140

3. Ansell, D. M., Garcin, C. L., David, |, & Ansell, M. (2017). The battle of the bulge: re-evaluating hair follicle stem cells in wound repair. *Experimental Dermatology*, *26*(2), 101–104. https://doi.org/10.1111/EXD.13184

4. Arita, K., Akiyama, M., Tsuji, Y., McMillan, J. R., Eady, R. A. J., & Shimizu, H. (2004). Gap junction development in the human fetal hair follicle and bulge region. *British Journal of Dermatology*, *150*(3), 429–434. https://doi.org/10.1046/J.1365-2133.2004.05775.X

5. Arnhold, J. (2020). The Dual Role of Myeloperoxidase in Immune Response. *International Journal of Molecular Sciences 2020, Vol. 21, Page 8057*, *21*(21), 8057. https://doi.org/10.3390/IJMS21218057

6. Arnhold, J., & Flemmig, J. (2010). Human myeloperoxidase in innate and acquired immunity. *Archives of Biochemistry and Biophysics*, *500*(1), 92–106. https://doi.org/10.1016/J.ABB.2010.04.008

7. Becker, L. C. (2005). Yin and Yang of MCP-1. *Circulation Research*, *96*(8), 812–814. https://doi.org/10.1161/01.RES.0000165652.82726.d9

8. Birch, J., & Gil, J. (2020). Senescence and the SASP: many therapeutic avenues. *Genes & Development*, *34*(23–24), 1565–1576. https://doi.org/10.1101/GAD.343129.120

9. Bolderston, A., Lloyd, N. S., Wong, R. K. S., Holden, L., & Robb-Blenderman, L. (2006). The prevention and management of acute skin reactions related to radiation therapy: a systematic review and practice guideline. *Support Care Cancer*, *14*(8), 802–817. https://doi.org/10.1007/s00520-006-0063-4

10. Borish, L. C., & Steinke, J. W. (2003). 2. Cytokines and chemokines. *Journal of Allergy and Clinical Immunology*, *111*(2), S460–S475. https://doi.org/10.1067/MAI.2003.108

11. Bray, F. N., Simmons, B. J., Wolfson, A. H., & Nouri, K. (2016). Acute and Chronic Cutaneous Reactions to Ionizing Radiation Therapy. *Dermatology and Therapy 2016 6:2*, *6*(2), 185–206. https://doi.org/10.1007/S13555-016-0120-Y

12. Bunting, S. (2010). 53BP1 inhibits homologous recombination in Brca1-deficient cells by blocking resection of DNA breaks. *Cell*, *141*, 243–254.

13. Callen, E. (2013). 53BP1 mediates productive and mutagenic DNA repair through distinct phosphoprotein interactions. *Cell*, *153*, 1266–1280.

14. Calonje, E., Brenn, T., Lazar, A., & McKee, P. (2012). *McKee's pathology of the skin: with clinical correlations*. https://www.research.ed.ac.uk/en/publications/mckees-pathology-of-the-skin-with-clinical-correlations

15. Campisi, J. (2013). Aging, cellular senescence, and cancer. *Annu. Rev. Physiol.*, *75*, 685–705. https://doi.org/10.1146/annurev-physiol-030212-183653

16. Celeste, A., Fernandez-Capetillo, O., Kruhlak, M. J., Pilch, D. R., Staudt, D. W., Lee, A., Bonner, R. F., Bonner, W. M., & Nussenzweig, A. (2003). Histone H2AX phosphorylation is dispensable for the initial recognition of DNA breaks. *Nature Cell Biology*, *5*(7), 675–679. https://doi.org/10.1038/NCB1004

17. Chang, D. W., Cheetham, L., te Marvelde, L., Bressel, M., Kron, T., Gill, S., Tai, K. H., Ball, D., Rose, W., Silva, L., & Foroudi, F. (2014). Risk factors for radiotherapy incidents and impact of an online electronic reporting system. *Radiotherapy and Oncology*, *112*(2), 199–204. https://doi.org/10.1016/J.RADONC.2014.07.011

18. Chen, Z., Cao, K., Xia, Y., Li, Y., Hou, Y., Wang, L., Li, L., Chang, L., & Li, W. (2019). Cellular senescence in ionizing radiation (Review). *Oncology Reports*, *42*(3), 883–894. https://doi.org/10.3892/OR.2019.7209/HTML

19. Chu, C. N., Hu, K. C., Wu, R. S. C., & Bau, D. T. (2021). Radiation-irritated skin and hyperpigmentation may impact the quality of life of breast cancer patients after whole breast radiotherapy. *BMC Cancer*, *21*(1). https://doi.org/10.1186/S12885-021-08047-5

20. Claudinot, S., Nicolas, M., Oshima, H., Rochat, A., & Barrandon, Y. (2005). Long-term renewal of hair follicles from clonogenic multipotent stem cells. *Proceedings of the National Academy of Sciences of the United States of America*, *102*(41), 14677–14682. https://doi.org/10.1073/PNAS.0507250102

21. Contrepois, K., Coudereau, C., Benayoun, B. A., Schuler, N., Roux, P. F., Bischof, O., Courbeyrette, R., Carvalho, C., Thuret, J. Y., Ma, Z., Derbois, C., Nevers, M. C., Volland, H., Redon, C. E., Bonner, W. M., Deleuze, J. F., Wiel, C., Bernard, D., Snyder, M. P., … Mann, C. (2017a). Histone variant H2A.J accumulates in senescent cells and promotes inflammatory gene expression. *Nature Communications 2017 8:1*, *8*(1), 1–18. https://doi.org/10.1038/ncomms14995

22. Contrepois, K., Coudereau, C., Benayoun, B. A., Schuler, N., Roux, P. F., Bischof, O., Courbeyrette, R., Carvalho, C., Thuret, J. Y., Ma, Z., Derbois, C., Nevers, M. C., Volland, H., Redon, C. E., Bonner, W. M., Deleuze, J. F., Wiel, C., Bernard, D., Snyder, M. P., … Mann, C. (2017b). Histone variant H2A.J accumulates in senescent cells and promotes inflammatory gene expression. *Nature Communications 2017 8:1*, *8*(1), 1–18. https://doi.org/10.1038/ncomms14995

23. Cotsarelis, G. (2006). Epithelial stem cells: A folliculocentric view. *Journal of Investigative Dermatology*, *126*(7), 1459–1468. https://doi.org/10.1038/sj.jid.5700376

24. Cotsarelis, G., Sun, T., Cell, R. L.-, & 1990, undefined. (n.d.). Label-retaining cells reside in the bulge area of pilosebaceous unit: implications for follicular stem cells, hair cycle, and skin carcinogenesis. *Elsevier*. Retrieved December 8, 2022, from https://www.sciencedirect.com/science/article/pii/009286749090696C

25. Cotsarelis, G., Sun, T. T., & Lavker, R. M. (1990). Label-retaining cells reside in the bulge area of pilosebaceous unit: Implications for follicular stem cells, hair cycle, and skin carcinogenesis. *Cell*, *61*(7), 1329–1337. https://doi.org/10.1016/0092-8674(90)90696-C

26. Cranford, T. L., Enos, R. T., Velázquez, K. T., McClellan, J. L., Davis, J. M., Singh, U. P., Nagarkatti, M., Nagarkatti, P. S., Robinson, C. M., & Murphy, E. A. (2015). Role of MCP-1 on inflammatory processes and metabolic dysfunction following high-fat feedings in the FVB/N strain. *International Journal of Obesity 2016 40:5*, *40*(5), 844–851. https://doi.org/10.1038/ijo.2015.244

27. Deorukhkar, A., pharmacology, S. K.-B., & 2010, undefined. (n.d.). Targeting inflammatory pathways for tumor radiosensitization. *Elsevier*. Retrieved December 9, 2022, from https://www.sciencedirect.com/science/article/pii/S0006295210004739

28. Difilippantonio, S. (2008). 53BP1 facilitates long-range DNA end-joining during V(D)J recombination. *Nature*, *456*, 529–533.

29. Ding, L. H., Shingyoji, M., Chen, F., Hwang, J. J., Burma, S., Lee, C., Cheng, J. F., & Chen, D. J. (2005). Gene Expression Profiles of Normal Human Fibroblasts after Exposure to Ionizing Radiation: A Comparative Study of Low and High Doses. *Https://Doi.Org/10.1667/RR3354*, *164*(1), 17–26. https://doi.org/10.1667/RR3354

30. Ditullio, R. (2002). 53BP1 functions in an ATM-dependent checkpoint pathway that is constitutively activated in human cancer. *Nature Cell Biol.*, *4*, 998–1002.

31. Dormand, E. L., Banwell, P. E., & Goodacre, T. E. E. (2005). Radiotherapy and wound healing. *International Wound Journal*, *2*(2), 112–127. https://doi.org/10.1111/J.1742-4801.2005.00079.X

32. Dowling, K., Barrett, S., Mullaney, L., & Poole, C. (2017). A nationwide investigation of radiation therapy event reporting-and-learning systems: Can standards be improved? *Radiography*, *23*(4), 279–286. https://doi.org/10.1016/j.radi.2017.06.004

33. Downs, J. A., Allard, S., Jobin-Robitaille, O., Javaheri, A., Auger, A., Bouchard, N., Kron, S. J., Jackson, S. P., & Côté, J. (2004). Binding of chromatin-modifying activities to phosphorylated histone H2A at DNA damage sites. *Molecular Cell*, *16*(6), 979–990. https://doi.org/10.1016/J.MOLCEL.2004.12.003

34. Driskell, I., Oeztuerk-Winder, F., Humphreys, P., & Frye, M. (2015). Genetically induced cell death in bulge stem cells reveals their redundancy for hair and epidermal regeneration. *Stem Cells*, *33*(3), 988–998. https://doi.org/10.1002/STEM.1910

35. Eriksson, D., & Stigbrand, T. (2010). Radiation-induced cell death mechanisms. *Tumor Biology*, *31*(4), 363–372. https://doi.org/10.1007/S13277-010-0042-8/FIGURES/4

36. Farràs, R., Baldin, V., Gallach, S., Acquaviva, C., Bossis, G., Jariel-Encontre, I., & Piechaczyk, M. (2008). JunB breakdown in mid-/late G2 is required for down-regulation of cyclin A2 levels and proper mitosis. *Molecular and Cellular Biology*, *28*(12), 4173–4187. https://doi.org/10.1128/MCB.01620-07

37. Fernandez-Capetillo, O., Lee, A., Nussenzweig, M., & Nussenzweig, A. (2004). H2AX: The histone guardian of the genome. *DNA Repair*, *3*(8–9), 959–967. https://doi.org/10.1016/J.DNAREP.2004.03.024

38. Florin, L., Knebel, J., Zigrino, P., Vonderstrass, B., Mauch, C., Schorpp-Kistner, M., Szabowski, A., & Angel, P. (2006). Delayed wound healing and epidermal hyperproliferation in mice lacking JunB in the skin. *The Journal of Investigative Dermatology*, *126*(4), 902–911. https://doi.org/10.1038/SJ.JID.5700123

39. Ford, E., & Dieterich, S. (2017). Safety Considerations in Stereotactic Body Radiation Therapy. *Seminars in Radiation Oncology*, *27*(3), 190–196. https://doi.org/10.1016/j.semradonc.2017.02.003

40. Freund, A., Laberge, R. M., Demaria, M., & Campisi, J. (2012). Lamin B1 loss is a senescence-associated biomarker. *Molecular Biology of the Cell*, *23*(11), 2066–2075. https://doi.org/10.1091/mbc.E11-10-0884

41. Friedman, E. J. (2005). Immune Modulation by Ionizing Radiation and its Implications for Cancer Immunotherapy. *Current Pharmaceutical Design*, *8*(19), 1765–1780. https://doi.org/10.2174/1381612023394089

42. Fuchs, E. (2008). Skin stem cells: rising to the surface. *The Journal of Cell Biology*, *180*(2), 273–284. https://doi.org/10.1083/JCB.200708185

43. Fuchs, E., & Segre, J. A. (2000). Stem cells: A new lease on life. *Cell*, *100*(1), 143–155. https://doi.org/10.1016/S0092-8674(00)81691-8

44. Gallet, P., Phulpin, B., Merlin, J. L., Leroux, A., Bravetti, P., Mecellem, H., Tran, N., & Dolivet, G. (2011). Long-term alterations of cytokines and growth factors expression in irradiated tissues and relation with histological severity scoring. *PLoS ONE*, *6*(12). https://doi.org/10.1371/JOURNAL.PONE.0029399

45. Greubel, C., Hable, V., Drexler, G., Hauptner, A., & Dietzel, S. (2008). Competition effect in DNA damage response. *Radiat Environ Biophys*, *47*.

46. Guarino, M., Tosoni, A., & Nebuloni, M. (2009). Direct contribution of epithelium to organ fibrosis: epithelial-mesenchymal transition. *Human Pathology*, *40*(10), 1365–1376. https://doi.org/10.1016/J.HUMPATH.2009.02.020

47. Gupta, A., Hunt, C. R., Chakraborty, S., Pandita, R. K., Yordy, J., Ramnarain, D. B., Horikoshi, N., & Pandita, T. K. (2014). Role of 53BP1 in the Regulation of DNA Double-Strand Break Repair Pathway Choice. *Radiation Research*, *181*(1), 1. https://doi.org/10.1667/RR13572.1

48. Hachiya, M., Suzuki, G., Koeffler, H., research, M. A.-E. cell, & 1994, undefined. (n.d.). Irradiation increases expression of GM-CSF in human fibroblasts by transcriptional

and post-transcriptional regulation. *Elsevier*. Retrieved December 9, 2022, from https://www.sciencedirect.com/science/article/pii/S0014482784712663

49. Hayflick, L., & Moorhead, P. S. (1961). The serial cultivation of human diploid cell strains. *Experimental Cell Research*, *25*(3), 585–621. https://doi.org/10.1016/0014-4827(61)90192-6

50. Hippchen, Y., Tewary, G., Jung, D., Schmal, Z., Meessen, S., Palm, J., & Rübe, C. E. (2022). Cultured Human Foreskin as a Model System for Evaluating Ionizing Radiation-Induced Skin Injury. *Undefined*, *23*(17). https://doi.org/10.3390/IJMS23179830

51. Hu, A., Zhou, W., Wu, Z., Zhang, H., Li, J., & Qiu, R. (2022). Modeling of DNA Damage Repair and Cell Response in Relation to p53 System Exposed to Ionizing Radiation. *International Journal of Molecular Sciences*, *23*(19). https://doi.org/10.3390/ijms231911323

52. Hymes, S. R., Strom, E. A., & Fife, C. (2006a). Radiation dermatitis: Clinical presentation, pathophysiology, and treatment 2006. *Journal of the American Academy of Dermatology*, *54*(1), 28–46. https://doi.org/10.1016/J.JAAD.2005.08.054

53. Hymes, S. R., Strom, E. A., & Fife, C. (2006b). Radiation dermatitis: Clinical presentation, pathophysiology, and treatment 2006. *Journal of the American Academy of Dermatology*, *54*(1), 28–46. https://doi.org/10.1016/J.JAAD.2005.08.054

54. Iglesias-Bartolome, R., & Gutkind, J. S. (2010). Keeping the epidermal stem cell niche in shape. *Cell Stem Cell*, *7*(2), 143–145. https://doi.org/10.1016/J.STEM.2010.07.008

55. IM Ward, K. M. J. van D. J. and C. (2003). p53 Binding protein 53BP1 is required for DNA damage responses and tumor suppression in mice. *Mol. Cell. Biol.*, *23*, 2556–2563.

56. Isermann, A., Mann, C., & Rübe, C. E. (2020). Histone Variant H2A.J Marks Persistent DNA Damage and Triggers the Secretory Phenotype in Radiation-Induced Senescence. *Undefined*, *21*(23), 1–20. https://doi.org/10.3390/IJMS21239130

57. Janko, M., Ontiveros, F., Fitzgerald, T. J., Deng, A., Decicco, M., & Rock, K. L. (2012). IL-1 Generated Subsequent to Radiation-Induced Tissue Injury Contributes to the Pathogenesis of Radiodermatitis. *Https://Doi.Org/10.1667/RR3097.1*, *178*(3), 166–172. https://doi.org/10.1667/RR3097.1

58. Jaschke, W., Schmuth, M., Trianni, A., & Bartal, G. (2017). Radiation-Induced Skin Injuries to Patients: What the Interventional Radiologist Needs to Know. *CardioVascular and Interventional Radiology*, *40*(8), 1131–1140. https://doi.org/10.1007/S00270-017-1674-5

59. Ji, J., Ho, B. S. Y., Qian, G., Xie, X. M., Bigliardi, P. L., & Bigliardi-Qi, M. (2017). Aging in hair follicle stem cells and niche microenvironment. *Journal of Dermatology*, *44*(10), 1097–1104. https://doi.org/10.1111/1346-8138.13897

60. Karagiannis, T. C., & El-Osta, A. (2007). Chromatin modifications and DNA double-strand breaks: The current state of play. *Leukemia*, *21*(2), 195–200. https://doi.org/10.1038/SJ.LEU.2404478

61. Kaur, P. (2006). Interfollicular epidermal stem cells: Identification, challenges, potential. *Journal of Investigative Dermatology*, *126*(7), 1450–1458. https://doi.org/10.1038/sj.jid.5700184

62. Khare, S. P., Habib, F., Sharma, R., Gadewal, N., Gupta, S., & Galande, S. (2012). HIstome—a relational knowledgebase of human histone proteins and histone modifying enzymes. *Nucleic Acids Research*, *40*(Database issue), D337. https://doi.org/10.1093/NAR/GKR1125

63. Kuilman, T., Michaloglou, C., Mooi, W. J., & Peeper, D. S. (2010). The essence of senescence. *Genes and Development*, *24*(22), 2463–2479. https://doi.org/10.1101/GAD.1971610

64. L Anderson, C. H. Y. A. (2001). Phosphorylation and rapid relocalization of 53BP1 to nuclear foci upon DNA damage. *Mol. Cell. Biol.*, *21*, 1719–1729.

65. LB Schultz, N. C. A. M. T. H. (2000). p53 binding protein 1 (53BP1) is an early participant in the cellular response to DNA double-strand breaks. *J. Cell Biol.*, *151*, 1381–1390.

66. Levy, V., Lindon, C., Harfe, B., cell, B. M.-D., & 2005, undefined. (n.d.). Distinct stem cell populations regenerate the follicle and interfollicular epidermis. *Elsevier*. Retrieved December 8, 2022, from https://www.sciencedirect.com/science/article/pii/S1534580705004259

67. Liao, W., Hei, T. K., & Cheng, S. K. (2017). Radiation-Induced Dermatitis is Mediated by IL17-Expressing γδ T Cells. *Radiation Research*, *187*(4), 454. https://doi.org/10.1667/RR007CC.1

68. Lieber, M. (2010). The mechanism of double-strand DNA break repair by the nonhomologous DNA end-joining pathway. *Annu. Rev. Biochem.*, *79*, 181–211.

69. Li, M., You, L., Xue, J., & Lu, Y. (2018a). Ionizing radiation-induced cellular senescence in normal, non-transformed cells and the involved DNA damage response: A mini review. *Frontiers in Pharmacology*, *9*(MAY), 522. https://doi.org/10.3389/FPHAR.2018.00522/BIBTEX

70. Li, M., You, L., Xue, J., & Lu, Y. (2018b). Ionizing radiation-induced cellular senescence in normal, non-transformed cells and the involved DNA damage response: A mini review. *Frontiers in Pharmacology*, *9*(MAY), 522. https://doi.org/10.3389/FPHAR.2018.00522/BIBTEX

71. Malicki, J., Bly, R., Bulot, M., Godet, J. L., Jahnen, A., Krengli, M., Maingon, P., Martin, C. P., Przybylska, K., Skrobała, A., Valero, M., & Jarvinen, H. (2014). Patient safety in external beam radiotherapy - Guidelines on risk assessment and analysis of adverse error-events and near misses: Introducing the ACCIRAD project. *Radiotherapy and Oncology*, *112*(2), 194–198. https://doi.org/10.1016/j.radonc.2014.08.011

72. Manis, J. (2004). 53BP1 links DNA damage-response pathways to immunoglobulin heavy chain class-switch recombination. *Nature Immunol.*, *5*, 481–487.

73. Martin, M. T., Vulin, A., & Hendry, J. H. (2016). Human epidermal stem cells: Role in adverse skin reactions and carcinogenesis from radiation. *Mutation Research - Reviews in Mutation Research*, *770*, 349–368. https://doi.org/10.1016/J.MRREV.2016.08.004

74. Mazeron, R., Aguini, N., Rivin, E., Baudré, A., Bour, M. S., Dumas, I., Hubert, F., Lopes, S., Desroches, A., Deutsch, E., Lefkopoulos, D., & Bourhis, J. (2014). Improving safety in radiotherapy: The implementation of the Global Risk Analysis method. *Radiotherapy and Oncology*, *112*(2), 205–211. https://doi.org/10.1016/j.radonc.2014.08.037

75. McCart, E. A., Thangapazham, R. L., Lombardini, E. D., Mog, S. R., Panganiban, R. A. M., Dickson, K. M., Mansur, R. A., Nagy, V., Kim, S. Y., Selwyn, R., Landauer, M. R., Darling, T. N., & Day, R. M. (2017). Accelerated senescence in skin in a murine model of radiation-induced multi-organ injury. *Journal of Radiation Research*, *58*(5), 636. https://doi.org/10.1093/JRR/RRX008

76. McQuestion, M. (2011). Evidence-Based Skin Care Management in Radiation Therapy: Clinical Update. *Seminars in Oncology Nursing*, *27*(2), e1–e17. https://doi.org/10.1016/J.SONCN.2011.02.009

77. Mendelsohn, F., Divino, C., … E. R.-A. in skin &, & 2002, undefined. (n.d.). Wound care after radiation therapy. *Journals.Lww.Com*. Retrieved December 7, 2022, from https://journals.lww.com/aswcjournal/Fulltext/2002/09000/Wound_Care_After_Radiation_Therapy.7.aspx

78. Moir, R. D., Spann, T. P., Herrmann, H., & Goldman, R. D. (2000). Disruption of Nuclear Lamin Organization Blocks the Elongation Phase of DNA Replication. *The Journal of Cell Biology*, *149*(6), 1179. https://doi.org/10.1083/JCB.149.6.1179

79. Mongiardi, M. P., Pellegrini, M., Pallini, R., Levi, A., & Falchetti, M. L. (2021). Cancer Response to Therapy-Induced Senescence: A Matter of Dose and Timing. *Cancers 2021, Vol. 13, Page 484*, *13*(3), 484. https://doi.org/10.3390/CANCERS13030484

80. Morris, R. J., Liu, Y., Marles, L., Yang, Z., Trempus, C., Li, S., Lin, J. S., Sawicki, J. A., & Cotsarelis, G. (2004). Capturing and profiling adult hair follicle stem cells. *Nature Biotechnology 2004 22:4*, *22*(4), 411–417. https://doi.org/10.1038/nbt950

81. Morris, R., Liu, Y., Marles, L., Yang, Z., … C. T.-N., & 2004, undefined. (n.d.). Capturing and profiling adult hair follicle stem cells. *Nature.Com*. Retrieved December 8, 2022, from https://idp.nature.com/authorize/casa?redirect_uri=https://www.nature.com/articles/nbt950&casa_token=USZv7k9iemcAAAAA:XQjT95nHtsweBtXy_f5YneIikDxZmv-ugD8bqUXFp8qQvW5jv-9rrmK1nt-nv46aus3cpKJP4IScrfeIvA

82. Müller, K., hematology, V. M.-E., & 2007, undefined. (n.d.). Radiation-induced alterations in cytokine production by skin cells. *Elsevier*. Retrieved December 9, 2022, from https://www.sciencedirect.com/science/article/pii/S0301472X07000203

83. Müller, K., & Meineke, V. (2007). Radiation-induced alterations in cytokine production by skin cells. *Experimental Hematology*, *35*(4 SUPPL.), 96–104. https://doi.org/10.1016/j.exphem.2007.01.017

84. Müller, K., & Meineke, V. (2011). Radiation-induced mast cell mediators differentially modulate chemokine release from dermal fibroblasts. *Journal of Dermatological Science*, *61*(3), 199–205. https://doi.org/10.1016/j.jdermsci.2011.01.003

85. Müller, K., science, V. M.-J. of dermatological, & 2011, undefined. (n.d.). Radiation-induced mast cell mediators differentially modulate chemokine release from dermal fibroblasts. *Elsevier*. Retrieved December 9, 2022, from https://www.sciencedirect.com/science/article/pii/S0923181111000247

86. Multhoff, G., & Radons, J. (2012). Radiation, inflammation, and immune responses in cancer. *Frontiers in Oncology*, *2 JUN*. https://doi.org/10.3389/FONC.2012.00058/FULL

87. Myung, P., & Ito, M. (2012). Dissecting the bulge in hair regeneration. *The Journal of Clinical Investigation*, *122*(2), 448–454. https://doi.org/10.1172/JCI57414

88. Nagineni, C. N., Naz, S., Choudhuri, R., Chandramouli, G. V. R., Krishna, M. C., Brender, J. R., Cook, J. A., & Mitchell, J. B. (2021). Radiation-induced senescence reprograms secretory and metabolic pathways in colon cancer hct-116 cells. *International Journal of Molecular Sciences*, *22*(9). https://doi.org/10.3390/IJMS22094835/S1

89. Nanashima, N., Ito, K., Ishikawa, T., Nakano, M., & Nakamura, T. (2012). Damage of hair follicle stem cells and alteration of keratin expression in external radiation-induced acute alopecia. *International Journal of Molecular Medicine*, *30*(3), 579–584. https://doi.org/10.3892/IJMM.2012.1018/HTML

90. N Dimitrova, Y.-C. C. D. S. T. de L. (2008). 53BP1 promotes non-homologous end joining of telomeres by increasing chromatin mobility. *Nature*, *456*, 524–528.

91. Ohyama, M., Terunuma, A., Tock, C. L., Radonovich, M. F., Pise-Masison, C. A., Hopping, S. B., Brady, J. N., Udey, M. C., & Vogel, J. C. (2006). Characterization and isolation of stem cell–enriched human hair follicle bulge cells. *The Journal of Clinical Investigation*, *116*(1), 249–260. https://doi.org/10.1172/JCI26043

92. Okunieff, P., Xu, J., Hu, D., Liu, W., Zhang, L., Morrow, G., Pentland, A., Ryan, J. L., & Ding, I. (2006). Curcumin protects against radiation-induced acute and chronic cutaneous toxicity in mice and decreases mRNA expression of inflammatory and fibrogenic cytokines. *International Journal of Radiation Oncology Biology Physics*, *65*(3), 890–898. https://doi.org/10.1016/j.ijrobp.2006.03.025

93. Oshima, H., Rochat, A., Kedzia, C., Kobayashi, K., & Barrandon, Y. (2001). Morphogenesis and renewal of hair follicles from adult multipotent stem cells. *Cell*, *104*(2), 233–245. https://doi.org/10.1016/S0092-8674(01)00208-2

94. Ota, T., Suzuki, Y., Nishikawa, T., Otsuki, T., Sugiyama, T., Irie, R., Wakamatsu, A., Hayashi, K., Sato, H., Nagai, K., Kimura, K., Makita, H., Sekine, M., Obayashi, M., Nishi, T., Shibahara, T., Tanaka, T., Ishii, S., Yamamoto, J. ichi, … Sugano, S. (2004). Complete sequencing and characterization of 21,243 full-length human cDNAs. *Nature Genetics*, *36*(1), 40–45. https://doi.org/10.1038/NG1285

95. Paldor, M., Levkovitch-Siany, O., Eidelshtein, D., Adar, R., Enk, C. D., Marmary, Y., Elgavish, S., Nevo, Y., Benyamini, H., Plaschkes, I., Klein, S., Mali, A., Rose-John, S., Peled, A., Galun, E., & Axelrod, J. H. (2022). Single-cell transcriptomics reveals a senescence-associated IL-6/CCR6 axis driving radiodermatitis. *EMBO Molecular Medicine*, *14*(8). https://doi.org/10.15252/EMMM.202115653

96. Panier, S., & Boulton, S. J. (2013). Double-strand break repair: 53BP1 comes into focus. *Nature Reviews Molecular Cell Biology 2013 15:1*, *15*(1), 7–18. https://doi.org/10.1038/nrm3719

97. Panteleyev, A. A. (2018). Functional anatomy of the hair follicle: The Secondary Hair Germ. *Experimental Dermatology*, *27*(7), 701–720. https://doi.org/10.1111/EXD.13666

98. Paquet, P., de Groote, D., & Piérard, G. E. (2010). Functionally active macrophage-derived myeloperoxidase in the skin of drug-induced toxic epidermal necrolysis. *Dermatology (Basel, Switzerland)*, *220*(3), 201–207. https://doi.org/10.1159/000284592

99. Paus, R., van der Veen, C., Eichmüller, S., Kopp, T., Hagen, E., Müller-Röver, S., & Hofmann, U. (1998). Generation and cyclic remodeling of the hair follicle immune system in mice. *The Journal of Investigative Dermatology*, *111*(1), 7–18. https://doi.org/10.1046/J.1523-1747.1998.00243.X

100. Peng, X., Wu, Y., Brouwer, U., van Vliet, T., Wang, B., Demaria, M., Barazzuol, L., & Coppes, R. P. (2020). Cellular senescence contributes to radiation-induced hyposalivation by affecting the stem/progenitor cell niche. *Cell Death & Disease*, *11*(10). https://doi.org/10.1038/S41419-020-03074-9

101. Pfeiffer, P., Goedecke, W., Mutagenesis, G. O.-, & 2000, undefined. (2000). Mechanisms of DNA double-strand break repair and their potential to induce chromosomal aberrations. *Academic.Oup.Com*, *15*(4), 289–302. https://academic.oup.com/mutage/article-abstract/15/4/289/1143400

102.   Pflegerl, P., Vesely, P., Hantusch, B., Schlederer, M., Zenz, R., Janig, E., Steiner, G., Meixner, A., Petzelbauer, P., Wolf, P., Soleiman, A., Egger, G., Moriggl, R., Kishimoto, T., Wagner, E. F., & Kenner, L. (2009). Epidermal loss of JunB leads to a SLE phenotype due to hyper IL-6 signaling. *Proceedings of the National Academy of Sciences of the United States of America*, *106*(48), 20423–20428. https://doi.org/10.1073/PNAS.0910371106

103.   Piechaczyk, M., & Farràs, R. (2008). Regulation and function of JunB in cell proliferation. *Biochemical Society Transactions*, *36*(Pt 5), 864–867. https://doi.org/10.1042/BST0360864

104.   Potten, C. S. (1974). THE EPIDERMAL PROLIFERATIVE UNIT: THE POSSIBLE ROLE OF THE CENTRAL BASAL CELL. *Cell Proliferation*, *7*(1), 77–88. https://doi.org/10.1111/J.1365-2184.1974.TB00401.X

105.   Potten, C. S. (2009). Cell Death (Apoptosis) in Hair Follicles and Consequent Changes in the Width of Hairs after Irradiation of Growing Follicles. *Http://Dx.Doi.Org/10.1080/09553008514551351*, *48*(3), 349–360. https://doi.org/10.1080/09553008514551351

106.   Rando, T. A. (2006). Stem cells, ageing and the quest for immortality. *Nature 2006 441:7097*, *441*(7097), 1080–1086. https://doi.org/10.1038/nature04958

107.   Redon, C. E., Schmal, Z., Tewary, G., Mangelinck, A., Courbeyrette, R., Thuret, J. Y., Aladjem, M. I., Bonner, W. M., Rübe, C. E., & Mann, C. (2021). Histone variant h2a.J is enriched in luminal epithelial gland cells. *Genes*, *12*(11), 1665. https://doi.org/10.3390/GENES12111665/S1

108.   Revenco, T., Lapouge, G., Moers, V., Brohée, S., & Sotiropoulou, P. A. (2017). Low Dose Radiation Causes Skin Cancer in Mice and Has a Differential Effect on Distinct Epidermal Stem Cells. *Stem Cells (Dayton, Ohio)*, *35*(5), 1355–1364. https://doi.org/10.1002/STEM.2571

109.   Rodier, F., Coppé, J. P., Patil, C. K., Hoeijmakers, W. A. M., Muñoz, D. P., Raza, S. R., Freund, A., Campeau, E., Davalos, A. R., & Campisi, J. (2009). Persistent DNA damage signaling triggers senescence-associated inflammatory cytokine secretion. *Nature Cell Biology*, *11*(8), 973. https://doi.org/10.1038/NCB1909

110.   Roos, W., & Kaina, B. (2012). *DNA damage-induced apoptosis: From specific DNA lesions to the DNA damage response and apoptosis.*

111.   Rossetto, D., Avvakumov, N., & Côté, J. (2012). Histone phosphorylation. *Http://Dx.Doi.Org/10.4161/Epi.21975*, *7*(10), 1098–1108. https://doi.org/10.4161/EPI.21975

112.   Rossetto, D., Truman, A. W., Kron, S. J., & Côté, J. (2010). Epigenetic modifications in double-strand break DNA damage signaling and repair. *Clinical Cancer Research*, *16*(18), 4543–4552. https://doi.org/10.1158/1078-0432.CCR-10-0513

113.   Rübe, C. E., Bäumert, C., Schuler, N., Isermann, A., Schmal, Z., Glanemann, M., Mann, C., & Scherthan, H. (2021). Human skin aging is associated with increased expression of the histone variant H2A.J in the epidermis. *Undefined*, *7*(1). https://doi.org/10.1038/S41514-021-00060-Z

114.   Rübe, C. E., Rodemann, H. P., & Rübe, C. (2004). [The relevance of cytokines in the radiation-induced lung reaction. Experimental basis and clinical significance]. *Strahlentherapie Und Onkologie : Organ Der Deutschen Rontgengesellschaft ... [et Al]*, *180*(9), 541–549. https://doi.org/10.1007/S00066-004-1279-1

115.   Ryan, J. L. (2012a). Ionizing Radiation: The Good, the Bad, and the Ugly. *Journal of Investigative Dermatology*, *132*(3), 985–993. https://doi.org/10.1038/JID.2011.411

116.   Ryan, J. L. (2012b). Ionizing Radiation: The Good, the Bad, and the Ugly. *Journal of Investigative Dermatology*, *132*(3), 985–993. https://doi.org/10.1038/JID.2011.411

117.   Salminen, A., Kauppinen, A., & Kaarniranta, K. (2012). Emerging role of NF-κB signaling in the induction of senescence-associated secretory phenotype (SASP). *Cellular Signalling*, *24*(4), 835–845. https://doi.org/10.1016/J.CELLSIG.2011.12.006

118.   Sándor, N., Schilling-Tóth, B., Kis, E., Benedek, A., Lumniczky, K., Sáfrány, G., & Hegyesi, H. (2015). Growth Differentiation Factor-15 (GDF-15) is a potential marker of radiation response and radiation sensitivity. *Mutation Research/Genetic Toxicology and Environmental Mutagenesis*, *793*, 142–149. https://doi.org/10.1016/J.MRGENTOX.2015.06.009

119.   Schaue, D., Kachikwu, E. L., & McBride, W. H. (2012). Cytokines in Radiobiological Responses: A Review. *Radiation Research*, *178*(6), 505. https://doi.org/10.1667/RR3031.1

120.   Schmuth, M., Sztankay, A., … G. W.-A. of, & 2001, undefined. (n.d.). Permeability barrier function of skin exposed to ionizing radiation. *Jamanetwork.Com*. Retrieved December 7, 2022, from https://jamanetwork.com/journals/jamadermatology/article-abstract/478469

121.   Schuler, N., & Rübe, C. E. (2013). Accumulation of DNA Damage-Induced Chromatin Alterations in Tissue-Specific Stem Cells: The Driving Force of Aging? *PLOS ONE*, *8*(5), e63932. https://doi.org/10.1371/JOURNAL.PONE.0063932

122.   Sezer, E., Böer-Auer, A., Cetin, E., Tokat, F., Durmaz, E., Sahin, S., & Ince, U. (2015). Diagnostic utility of Ki-67 and Cyclin D1 immunostaining in differentiation of psoriasis vs. other psoriasiform dermatitis. *Dermatology Practical & Conceptual*, *5*(3), 7–13. https://doi.org/10.5826/DPC.0503A02

123.   Shaulian, E. (2010). AP-1--The Jun proteins: Oncogenes or tumor suppressors in disguise? *Cellular Signalling*, *22*(6), 894–899. https://doi.org/10.1016/J.CELLSIG.2009.12.008

124.   Shibata, A., & Jeggo, P. A. (2020). Roles for 53BP1 in the repair of radiation-induced DNA double strand breaks. *DNA Repair*, *93*. https://doi.org/10.1016/J.DNAREP.2020.102915

125.   Shimi, T., Butin-Israeli, V., Adam, S. A., Hamanaka, R. B., Goldman, A. E., Lucas, C. A., Shumaker, D. K., Kosak, S. T., Chandel, N. S., & Goldman, R. D. (2011). The role of nuclear lamin B1 in cell proliferation and senescence. *Genes & Development*, *25*(24), 2579. https://doi.org/10.1101/GAD.179515.111

126.   Shimi, T., Pfleghaar, K., Kojima, S. I., Pack, C. G., Solovei, I., Goldman, A. E., Adam, S. A., Shumaker, D. K., Kinjo, M., Cremer, T., & Goldman, R. D. (2008). The A- and B-type nuclear lamin networks: microdomains involved in chromatin organization and transcription. *Genes & Development*, *22*(24), 3409. https://doi.org/10.1101/GAD.1735208

127.   Shumaker, D. K., Solimando, L., Sengupta, K., Shimi, T., Adam, S. A., Grunwald, A., Strelkov, S. v., Aebi, U., Cardoso, M. C., & Goldman, R. D. (2008). The highly conserved nuclear lamin Ig-fold binds to PCNA: its role in DNA replication. *The Journal of Cell Biology*, *181*(2), 269. https://doi.org/10.1083/JCB.200708155

128.   Singh, K., Camera, E., Krug, L., Basu, A., Pandey, R. K., Munir, S., Wlaschek, M., Kochanek, S., Schorpp-Kistner, M., Picardo, M., Angel, P., Niemann, C., Maity, P., &

Scharffetter-Kochanek, K. (2018). JunB defines functional and structural integrity of the epidermo-pilosebaceous unit in the skin. *Nature Communications*, *9*(1). https://doi.org/10.1038/S41467-018-05726-Z

129.   Song, S., & Lambert, P. F. (1999). Different Responses of Epidermal and Hair Follicular Cells to Radiation Correlate with Distinct Patterns of p53 and p21 Induction. *The American Journal of Pathology*, *155*(4), 1121. https://doi.org/10.1016/S0002-9440(10)65215-7

130.   Spałek, M. (2016). Chronic radiation-induced dermatitis: Challenges and solutions. *Clinical, Cosmetic and Investigational Dermatology*, *9*, 473–482. https://doi.org/10.2147/CCID.S94320

131.   Spann, T. P., Goldman, A. E., Wang, C., Huang, S., & Goldman, R. D. (2002). Alteration of nuclear lamin organization inhibits RNA polymerase II–dependent transcription. *The Journal of Cell Biology*, *156*(4), 603. https://doi.org/10.1083/JCB.200112047

132.   Strahl, B. D., & Allis, C. D. (2000). The language of covalent histone modifications. *Nature*, *403*(6765), 41–45. https://doi.org/10.1038/47412

133.   Strausberg, R. L., Feingold, E. A., Grouse, L. H., Derge, J. G., Klausner, R. D., Collins, F. S., Wagner, L., Shenmen, C. M., Schuler, G. D., Altschul, S. F., Zeeberg, B., Buetow, K. H., Schaefer, C. F., Bhat, N. K., Hopkins, R. F., Jordan, H., Moore, T., Max, S. I., Wang, J., … Marra, M. A. (2002). Generation and initial analysis of more than 15,000 full-length human and mouse cDNA sequences. *Proceedings of the National Academy of Sciences of the United States of America*, *99*(26), 16899. https://doi.org/10.1073/PNAS.242603899

134.   Suganuma, T., & Workman, J. L. (2011). Signals and combinatorial functions of histone modifications. *Annual Review of Biochemistry*, *80*, 473–499. https://doi.org/10.1146/ANNUREV-BIOCHEM-061809-175347

135.   Sun, X., & Kaufman, P. D. (2018). Ki-67: more than a proliferation marker. *Chromosoma 2018 127:2*, *127*(2), 175–186. https://doi.org/10.1007/S00412-018-0659-8

136.   Suomela, S., Kariniemi, A.-L., Impola, U., Karvonen, S.-L., Snellman, E., Uurasmaa, T., Peltonen, J., & Saarialho-Kere, U. (n.d.). Matrix metalloproteinase-19 is expressed by keratinocytes in psoriasis. *Researchgate.Net*. Retrieved December 8,

2022, from https://www.researchgate.net/profile/Juha-Peltonen-2/publication/10769395_Matrix_Metalloproteinase-19_is_Expressed_by_Keratinocytes_in_Psoriasis/links/0fcfd50c84344d3383000000/Matrix-Metalloproteinase-19-is-Expressed-by-Keratinocytes-in-Psoriasis.pdf

137.   Takashima, A., & Bergstresser, P. R. (1996). Cytokine-mediated communication by keratinocytes and Langerhans cells with dendritic epidermal T cells. *Seminars in Immunology*, *8*(6), 333–339. https://doi.org/10.1006/smim.1996.0044

138.   Tamburini, B. A., & Tyler, J. K. (2005). Localized Histone Acetylation and Deacetylation Triggered by the Homologous Recombination Pathway of Double-Strand DNA Repair. *Molecular and Cellular Biology*, *25*(12), 4903–4913. https://doi.org/10.1128/MCB.25.12.4903-4913.2005

139.   TA Mochan, M. V. R. D. T. H. (2004). 53BP1, an activator of ATM in response to DNA damage. *DNA Repair*, *3*, 945–952.

140.   Tanaka, H., Sato, S., Koyama, M., Kujirai, T., & Kurumizaka, H. (2020). Biochemical and structural analyses of the nucleosome containing human histone H2A.J. *The Journal of Biochemistry*, *167*(4), 419–427. https://doi.org/10.1093/JB/MVZ109

141.   Trempus, C. S., Morris, R. J., Bortner, C. D., Cotsarelis, G., Faircloth, R. S., Reece, J. M., & Tennant, R. W. (2003). Enrichment for living murine keratinocytes from the hair follicle bulge with the cell surface marker CD34. *Journal of Investigative Dermatology*, *120*(4), 501–511. https://doi.org/10.1046/j.1523-1747.2003.12088.x

142.   Trempus, C. S., Morris, R. J., Ehinger, M., Elmore, A., Bortner, C. D., Ito, M., Cotsarelis, G., Nijhof, J. G. W., Peckham, J., Flagler, N., Kissling, G., Humble, M. M., King, L. C., Adams, L. D., Desai, D., Amin, S., & Tennant, R. W. (2007). CD34 Expression by Hair Follicle Stem Cells Is Required for Skin Tumor Development in Mice. *Cancer Research*, *67*(9), 4173. https://doi.org/10.1158/0008-5472.CAN-06-3128

143.   van Attikum, H., & Gasser, S. M. (2005). The histone code at DNA breaks: A guide to repair? *Nature Reviews Molecular Cell Biology*, *6*(10), 757–765. https://doi.org/10.1038/NRM1737

144. van der Veen, B. S., de Winther, M. P. J., & Heeringa, P. (2009). Myeloperoxidase: Molecular mechanisms of action and their relevance to human health and disease. *Antioxidants and Redox Signaling*, *11*(11), 2899–2937. https://doi.org/10.1089/ARS.2009.2538

145. Vidanes, G. M., Bonilla, C. Y., & Toczyski, D. P. (2005). Complicated tails: Histone modifications and the DNA damage response. *Cell*, *121*(7), 973–976. https://doi.org/10.1016/J.CELL.2005.06.013

146. Wang, B. (2002). 53BP1, a mediator of the DNA damage checkpoint. *Science*, *298*, 1435–1438.

147. Wang, L., Jiang, J., Chen, Y., Jia, Q., & Chu, Q. (2022). The roles of CC chemokines in response to radiation. *Radiation Oncology 2022 17:1*, *17*(1), 1–12. https://doi.org/10.1186/S13014-022-02038-X

148. Ward, J. (1991). *DNA damage and repair.*

149. Woodhouse, K. D., Hashemi, D., Betcher, K., Doucette, A., Weaver, A., Monzon, B., Rosenthal, S. A., & Vapiwala, N. (2018). Safety practices, perceptions, and behaviors in radiation oncology: A national survey of radiation therapists. *Practical Radiation Oncology*, *8*(1), 48–57. https://doi.org/10.1016/j.prro.2017.06.003

150. Xiao, Y., Mo, W., Jia, H., Yu, D., Qiu, Y., Jiao, Y., Zhu, W., Koide, H., Cao, J., & Zhang, S. (2020). Ionizing radiation induces cutaneous lipid remolding and skin adipocytes confer protection against radiation-induced skin injury. *Journal of Dermatological Science*, *97*(2), 152–160. https://doi.org/10.1016/J.JDERMSCI.2020.01.009

151. Xue, J., Yu, C., Sheng, W., Zhu, W., Luo, J., Zhang, Q., Yang, H., Cao, H., Wang, W., Zhou, J., Wu, J., Cao, P., Chen, M., Ding, W. Q., Cao, J., & Zhang, S. (2017). The Nrf2/GCH1/BH4 Axis Ameliorates Radiation-Induced Skin Injury by Modulating the ROS Cascade. *Journal of Investigative Dermatology*, *137*(10), 2059–2068. https://doi.org/10.1016/J.JID.2017.05.019

152. Xu, S., Ariizumi, K., Edelbaum, D., Bergstresser, P. R., & Takashima, A. (1995). Cytokine-dependent regulation of growth and maturation in murine epidermal dendritic cell lines. *European Journal of Immunology*, *25*(4), 1018–1024. https://doi.org/10.1002/eji.1830250424

153.   Yang, X., Ren, H., Guo, X., Hu, C., & Fu, J. (2020). Radiation-induced skin injury: pathogenesis, treatment, and management. *Aging (Albany NY)*, *12*(22), 23379. https://doi.org/10.18632/AGING.103932

154.   Yang, X., Yan, H., Zhai, Z., Hao, F., Ye, Q., Zhong, B., & Fei Hao, C. (2010). Pharmacology and therapeutics: Neutrophil elastase promotes proliferation of HaCaT cell line and transwell psoriasis organ culture model. *Wiley Online Library*, *49*(9), 1068–1074. https://doi.org/10.1111/j.1365-4632.2010.04500.x

155.   Yun, M., Wu, J., Workman, J. L., & Li, B. (2011). Readers of histone modifications. *Cell Research*, *21*(4), 564–578. https://doi.org/10.1038/CR.2011.42

8. <u>Acknowledgment</u>

First of all i would like to extend my heartfelt gratitude to Prof. Claudia Rübe for believing in me and giving me the opportunity to work in her Lab as a PhD candidate. Thank you so much for being so kind and patient with me throughout my PhD journey. You provided a very interesting project for my dissertation. I have clearly learned a lot and grown as a scientist under your supervision. I will forever be grateful for the trust and faith you have bestowed upon me.

I would also like to extend special thanks to Prof. Dr. med. Christian Rübe, director of the department for Radiation Therapy and Radiation Oncology, for providing all his support and for the use of clinics accelerator. Additionally, i would also like to thank all the staff, from planners to technicians, in the clinic who have helped and supported through each of the numerous mice irradiations over the years.

I would like to further extend my gratitude Prof. Klaus Römer for his kind guidance, time and support throughout my PhD work. I would especially like to be thankful to you for your kind cooperation and understanding and for supporting my ideas.

A special thanks to Carl Mann for providing us the H2A.J antibody and H2A.J KO mice, without your support this project would not have been possible.

I would like to further extend my thanks to my colleagues Zoe Schmal and Anna Issermann for guiding me in the initial phase of my PhD journey. A special thank you to our lab technician Daniela Jung thank you for always being there and for providing me with all the lab essentials required in time of need.

Speaking of "A friend in need, a friend indeed", i cannot thank you enough Mutaz (aka Gandalf the Grey). My PhD journey was surely one hell of a ride and i wouldn't have made it without you. Not only have i gained experience and grown as person throughout my PhD journey, but i have also earned a friend for life who has been my constant moral support and

my pillar through all my thick and thin with me. Thank you for making me laugh through all my cries and cheering me up when i felt at my lowest. Your pippins has learned a lot from you (I am not centrifuging balance anymore...!). In addition to have made so many memories i feel lucky to have gotten a friend and colleague like you. Thank you for making me not miss my family so much...!!!.

A special thank you to my colleague Julia von der lippe for helping with the german translation for summary of my dissertation (i owe you gebrannte mandeln...!).

Last but not least my heart full thank you to my parents, thank you so much Mum and dad for walking through all my stress and frustrations with me in my PhD journey. Thank you for making me look on the bright side when i couldn't see light at the end of the tunnel.

I cannot forget to thank my childhood best friends and family Krisha and Nisha for tolerating all my complaints and frustrations. Even if u guys were so far you never made me feel like it. Thank you for making me feel like home when i missed it the most...!!!!.. Thank you for tolerating me throughout my PhD journey would not have been the same without you people.

9. <u>List of tables</u>

10. <u>List of Figures</u>

The curriculum vitae was removed from electronic version of the doctoral thesis for reasons of data protection.

Article

Cultured Human Foreskin as a Model System for Evaluating Ionizing Radiation-Induced Skin Injury

Yanick Hippchen [1,†], Gargi Tewary [1,†], Daniela Jung [1], Zoé Schmal [1], Stephan Meessen [2], Jan Palm [1] and Claudia E. Rübe [1,*]

[1] Department of Radiation Oncology, Saarland University Medical Center, 66421 Homburg, Germany
[2] Department of Urology, Klinikum Saarbrücken, 66119 Saarbrücken, Germany
[*] Correspondence: claudia.ruebe@uks.eu
[†] These authors contributed equally to this work.

Abstract: Purpose: Precise molecular and cellular mechanisms of radiation-induced dermatitis are incompletely understood. Histone variant H2A.J is associated with cellular senescence and modulates senescence-associated secretory phenotype (SASP) after DNA-damaging insults, such as ionizing radiation (IR). Using ex vivo irradiated cultured foreskin, H2A.J was analyzed as a biomarker of radiation-induced senescence, potentially initiating the inflammatory cascade of radiation-induced skin injury. Methods: Human foreskin explants were collected from young donors, irradiated ex vivo with 10 Gy, and cultured in air-liquid interphase for up to 72 h. At different time-points after ex vivo IR exposure, the foreskin epidermis was analyzed for proliferation and senescence markers by immunofluorescence and immunohistochemical staining of sectioned tissue. Secretion of cytokines was measured in supernatants by ELISA. Using our mouse model with fractionated in vivo irradiation, H2A.J expression was analyzed in epidermal stem/progenitor cell populations localized in different regions of murine hair follicles (HF). Results: Non-vascularized foreskin explants preserved their tissue homeostasis up to 72 h (even after IR exposure), but already non-irradiated foreskin epithelium expressed high levels of H2A.J in all epidermal layers and secreted high amounts of cytokines. Unexpectedly, no further increase in H2A.J expression and no obvious upregulation of cytokine secretion was observed in the foreskin epidermis after ex vivo IR. Undifferentiated keratinocytes in murine HF regions, by contrast, revealed low H2A.J expression in non-irradiated skin and significant radiation-induced H2A.J upregulations at different time-points after IR exposure. Based on its staining characteristics, we presume that H2A.J may have previously underestimated the importance of the epigenetic regulation of keratinocyte maturation. Conclusions: Cultured foreskin characterized by highly keratinized epithelium and specific immunological features is not an appropriate model for studying H2A.J-associated tissue reactions during radiation-induced dermatitis.

Keywords: cultured foreskin; ionizing radiation; radiation-induced dermatitis; histone variant H2A.J; cellular senescence; senescence-associated secretory phenotype (SASP)

1. Introduction

Radiotherapy is an important oncological treatment modality whereby ionizing radiation (IR) is locally delivered to eradicate cancer. Even with the technological advancement in radiotherapy planning and application, high percentages of patients receiving fractionated radiotherapy still suffer from radiation-induced skin toxicity, ranging from mild erythema and dry desquamation to more severe moist desquamation and up to skin ulceration [1]. However, the precise mechanism of radiation-induced skin injury at therapeutically relevant doses remains incompletely understood.

Healthy skin provides a protective barrier between the body and its environment for one's entire life [2]. The outermost <u>epidermis</u> is stratified into four layers, with keratinocytes being the predominant cell type. The *stratum basale* represents a single-cell layer attached to the basal lamina and comprises epidermal stem/progenitor cells. Basal cells and deep cells within the *stratum spinosum* undergo mitosis, thereby forming new keratinocytes that migrate into more superficial layers and complete their physiological maturation. By the time keratinocytes reach the *stratum granulosum*, they flatten and produce more keratin filaments and lipid-filled membrane-coated vesicles, thereby forming water-resistant barriers. The *stratum corneum* consists of numerous layers of flattened, dead corneocytes lacking nuclei. During their constant differentiation, keratinocytes migrate from basal to cornified layers and finally desquamate from the skin surface. Epidermal homeostasis depends on the regenerative capacity of stem/progenitor cells and on epigenetic mechanisms that regulate the differentiation and maturation processes in keratinocytes. The <u>dermis</u> comprises the superficial papillary layer and the deep, thicker reticular layer. The primary cell type in the dermis are fibroblasts, which produce extracellular structural proteins, such as collagen and elastin. The dermis contains hair follicles, sweat, sebaceous and apocrine glands, and blood vessels, providing nourishment and waste removal for both dermal and epidermal cells [3]. Even if the basic histological structure is identical, the composition of human skin is generally adapted to the particular requirements of the anatomical regions [4]. Foreskin consists of a double-sided layer of stratified squamous epithelium, with thickened and more keratinized epidermal layer and increased immune cell densities compared to other skin tissues, providing a robust physical barrier to mechanical and other environmental stress [5].

Since neither 3D-tissue organization nor multiple cell-type composition is reproduced in monolayer single cell-type cultures, our laboratory pioneered the use of foreskin biopsies to study the skin tissue response after ex vivo IR exposure [6]. Cellular stress responses induced by IR are highly complex. Increasing evidence suggests that senescent cells accumulate in the skin after IR exposure and may contribute to radiation-induced skin pathologies [7]. Senescent cells are characterized by their inability to proliferate, their resistance to apoptosis, and the secretion of factors that promote inflammation and tissue deterioration [8,9]. Previous studies have shown that histone variant H2A.J accumulates in human fibroblasts during replicative and radiation-induced senescence and modulates the secretion of inflammatory cytokines [10,11]. Our previous research shows that H2A.J is a sensitive marker of senescent keratinocytes in the human epidermis in the context of skin aging [12]. Here, we aimed to analyze radiation-induced senescence in human skin by establishing cultured foreskin explants for ex vivo IR exposure to mimic the complex radiation responses.

2. Results

2.1. H2A.J and Ki67 Expression in Foreskin Explants after Ex Vivo Irradiation

To test histone variant H2A.J as a biomarker for radiation-induced senescence, cultured foreskin samples were stained for H2A.J to analyze keratinocyte senescence (Figure 1). Already in the non-irradiated foreskin, the majority of keratinocytes were highly positive for H2A.J by IHC staining; after ex vivo irradiation, there was a tendency for stronger H2A.J staining intensity (Figure 1A). However, immunofluorescence microscopy of non-irradiated foreskin explants showed different H2A.J expression levels in the various epidermis layers (Figure 1B). Accordingly, relative proportions of H2A.J+ keratinocytes were analyzed in the different epidermal layers (Figure 1A). Independently of IR exposure, we observed the highest proportions of H2A.J+ keratinocytes (≈80%) in granular layers, where epidermal keratinocytes are transformed from living cells into corneocytes (Figure 1C). Compared to the granular layer, we observed clearly lower H2A.J expression levels in the *stratum spinosum* and *basale* (≈50%), reflecting epidermal layers with less differenti-

ated keratinocytes. To explore the role of H2A.J for induction of cellular senescence, cultured foreskin samples were exposed to IR (10Gy) and analyzed 24h after ex vivo exposure. Unexpectedly, our results revealed no radiation-dependent increase in H2A.J+ cells in the different epidermal layers (Figure 1C). Accordingly, our findings suggest that tissue-specific H2A.J expression in the foreskin is independent of senescence induction after IR exposure. Using the proliferation marker Ki67, we examined the regenerative capacity in human foreskin samples in relation to IR exposure (Figure 1B). In non-irradiated foreskin, Ki67+ cells were most abundant in the *stratum spinosum* (6% ± 0.1%), less frequent in the *stratum basale* (2% ± 0.1%) and completely absent in the *stratum granulosum* (Figure 1C). After IR exposure with 10Gy, the Ki67+ cell fractions in the different epidermal layers remained stable, suggesting that the proliferative capacity of the foreskin epidermis is not affected by these IR doses. Moreover, using Ki67 in direct combination with H2A.J, we constantly observed an inverse correlation between Ki67+ and H2A.J+ cells (Figure 1B). The fact that Ki67-H2A.J immunostaining was mutually exclusive strongly suggests that cells expressing H2A.J have lost their ability to proliferate.
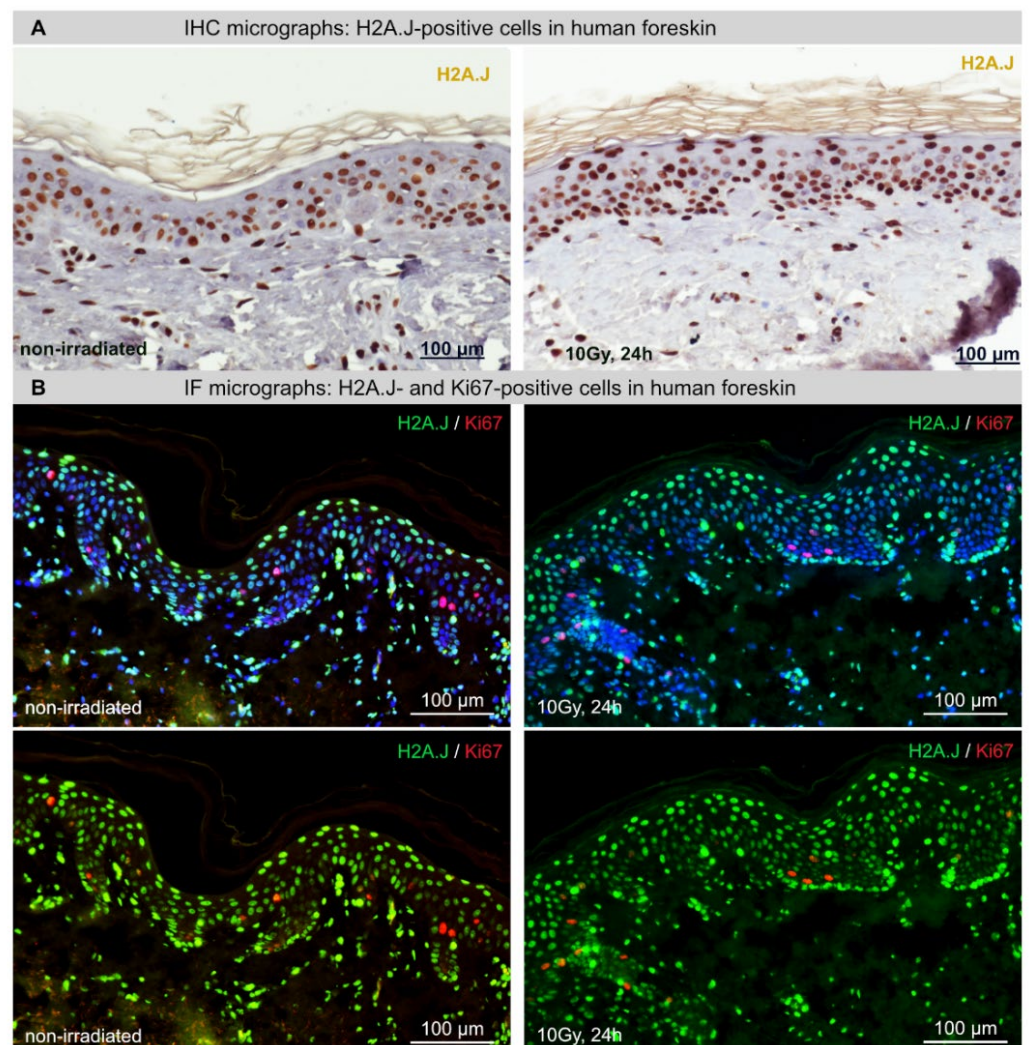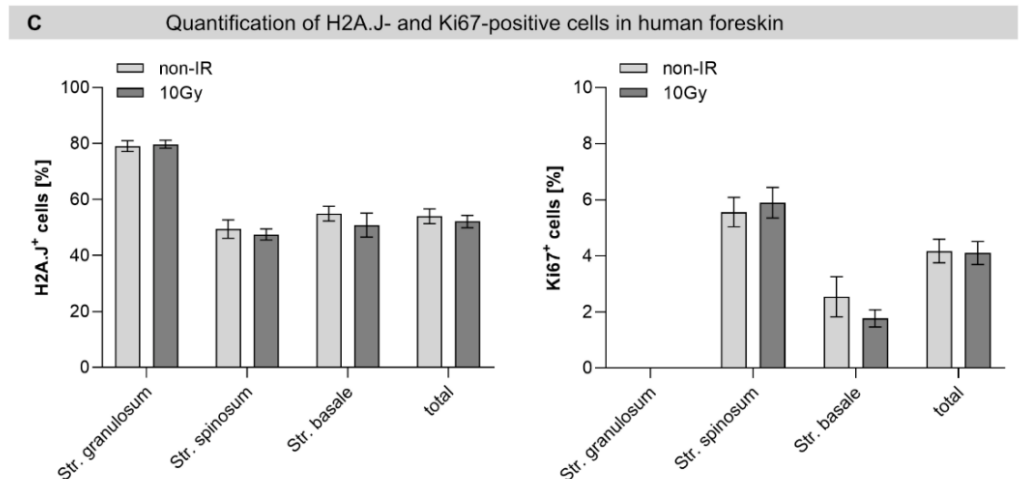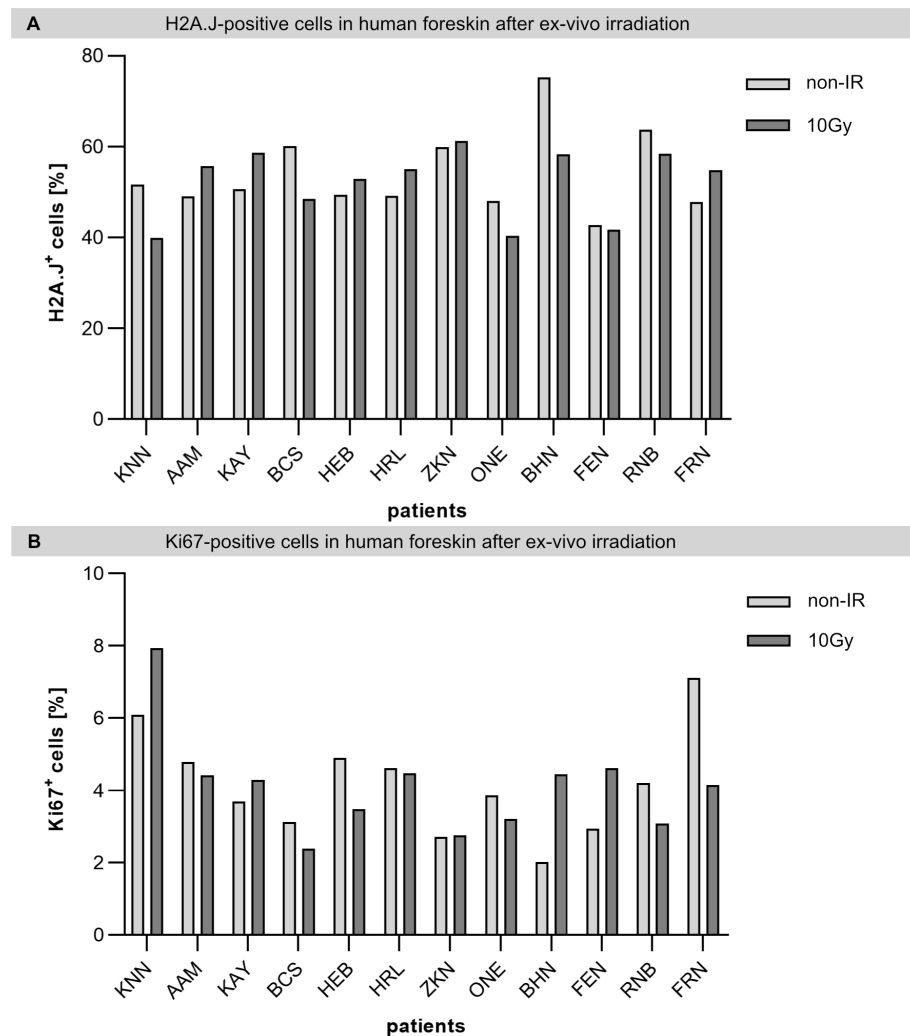
Figure 1. H2A.J and Ki67 expression in foreskin explants after ex vivo IR exposure. (**A**) IHC micrographs of H2A.J staining in foreskin explants after IR exposure (10 Gy; 24 h post-IR) compared to non-irradiated control. (**B**) IF micrographs of H2A.J and Ki67 double-staining in foreskin explants after IR exposure (10 Gy; 24 h post-IR) compared to non-irradiated control. Top photos contain DAPI signals, and bottom photos show the same photos but without corresponding DAPI signals so that the different H2A.J staining intensities (green signal) in the epidermis become more visible. (**C**) Graphic presentation of the quantification of H2A.J+ and Ki67+ cells in epidermis of foreskin explants. Data are presented as mean ± SD (n = 12).

2.2. Individual H2A.J Expression in Foreskin Explants after Ex Vivo Irradiation

The possibility of identifying patient-related factors that are associated with individual radiosensitivity would optimize adjuvant treatment by radiotherapy, limiting the severity of normal tissue reactions. In this study, we aimed to test whether H2A.J-associated inflammation could serve as a possible biomarker of individual radiosensitivity. Accordingly, a larger number of foreskin specimens was screened without any differences in H2A.J expression being observed. Only specimens from young donors were quantitatively evaluated, as we assumed that foreskin samples from children would have very low baseline H2A.J expression due to their young age. In Figure 2, the H2A.J+ and Ki67+ cells before and following IR exposure are shown for each individual donor in order to detect possible inter-individual differences. However, our cohort of young donors showed no differences in terms of either baseline or radiation-induced H2A.J expression (Figure 2A). Moreover, p21 staining of non-irradiated and irradiated foreskin explants revealed only very low levels of p21-positive cells, suggesting that at this dose and examination time, there is no induction of premature senescence in foreskin keratinocytes (Supplementary Figure S3).

Figure 2. Patient-to-patient variability of H2A.J and Ki67 expression in foreskin explants before and after ex vivo IR exposure. Graphic presentation of the quantification of H2A.J+ (**A**) and Ki67+ keratinocytes (**B**) in the epidermis of foreskin explants before and after IR exposure (10Gy; 24 h post-IR) for the individual donors (listed with the initials of their names) (*n* = 12).

2.3. Individual Cytokine Secretion in Foreskin Explants after Ex Vivo Irradiation

Recent progress in molecular radiobiology has improved the mechanistic understanding of normal-tissue effects and shifted the focus from initial-damage induction to the concerted biological response at cell and tissue levels affected by early activation of cytokine cascades. Radiation-induced skin inflammation is characterized by an almost immediate upregulation of pro-inflammatory cytokines, thereby recruiting inflammatory cells from the surrounding tissue. Here, we measured cytokine expression levels in foreskin supernatants for interleukins 6 and 8 (IL-1 and IL-6) and monocyte chemoattractant protein-1 (MCP-1), representing H2A.J-associated signature cytokines [10,11]. Our findings suggest that foreskin samples from young donors vary in their inflammatory response to IR exposure (Figure 3). For the donor KNN, we observed significantly elevated cytokine expression levels for IL-6, IL-8, and MCP-1 following IR exposure (Figure 3); this finding may suggest that this individual develops stronger inflammatory reactions in response to radiotherapy.
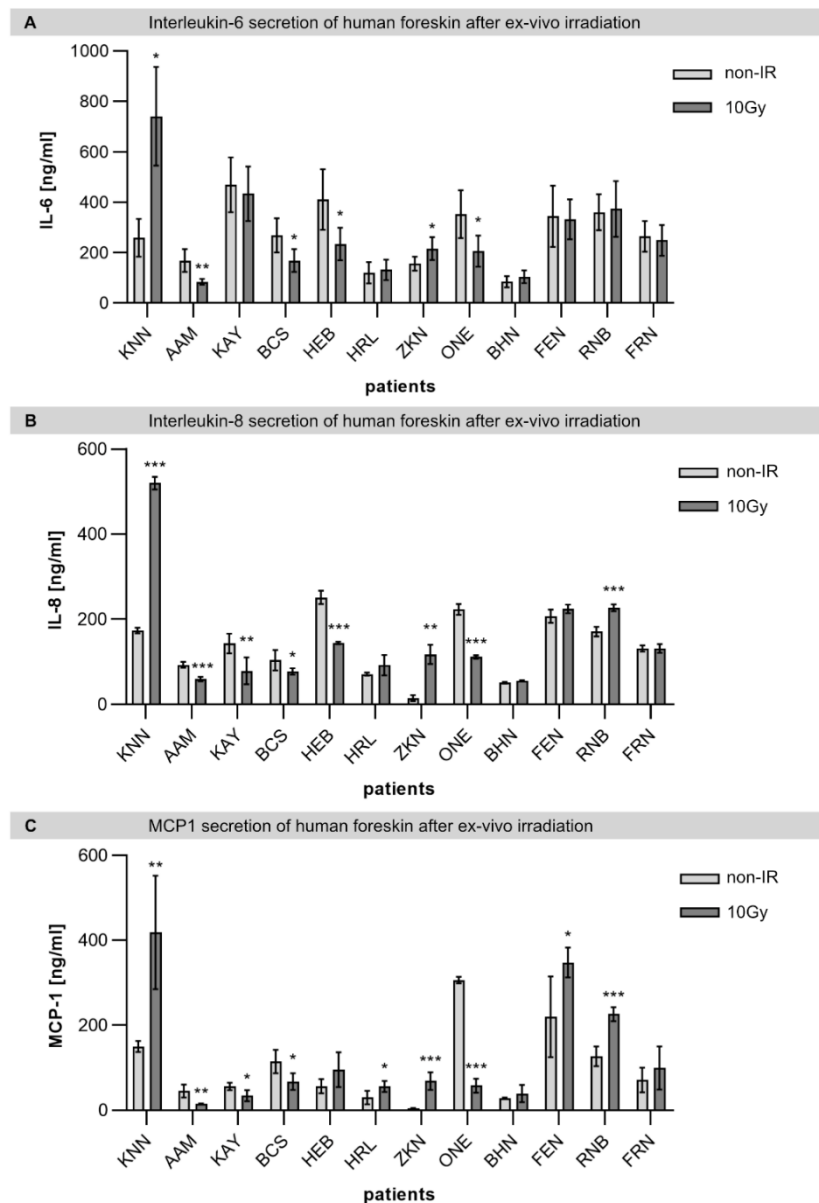
Figure 3. Patient-to-patient variability of cytokine expression in foreskin explants before and after ex vivo IR exposure. Graphic presentation of the quantification of IL-6 (**A**), IL-8 (**B**), and MCP-1 (**C**) measured by ELISA in the supernatant of foreskin explants before (non-IR) and after IR exposure (10 Gy; 24 h post-IR) for individual donors ($n = 12$). * $p < 0.1$; ** $p < 0.01$; *** $p < 0.001$

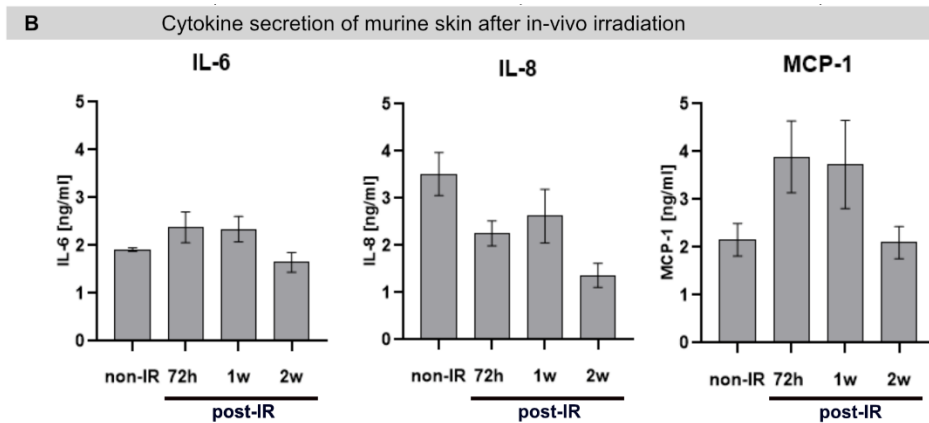### 2.4. H2A.J Expression in Murine Skin after Fractionated In Vivo Irradiation

The long-term function of non-vascularized skin explants during in vitro culturing is particularly limited by the maintenance of epidermal stem cell compartments. Human skin regions from different anatomical locations are characterized by the same basic histological structure but vary considerably in the thickness of their layers and their specific adnexal structures. After injury, skin appendages such as hair follicles (containing hair follicle stem cells in bulge regions) are capable of re-epithelialization via the migration of keratinocytes from the adnexal epithelium to the surface of the epidermis [13]. Upon skin injury, multiple stem cell populations in hair follicles and interfollicular epidermis make distinct contributions to the regenerating epithelium over time [13,14]. To overcome tissue-culture-associated limitations, we used our mouse model of fractionated in vivo irradiation to investigate H2A.J and cytokine expression in murine skin over a longer period,

ultimately to recapitulate radiation-induced skin toxicities more closely. Accordingly, laboratory mice were exposed to fractionated irradiation (5 × 2 Gy) and at defined time-points (72 h, 1, and 2 weeks) after the last in vivo exposure, the back-skin epidermis was harvested for analysis of H2A.J expression and cytokine secretion. Figure 4A shows representative pictures of H2A.J- and SA-ß-Gal expression in hair follicles in non-irradiated versus irradiated dorsal skin (1w post-IR). Subsequently, H2A.J+ and Sa-ß-Gal+ cells were quantified in different regions (infundibulum, bulge, papilla) of hair follicles in murine skin sections. While non-irradiated skin revealed very low numbers of H2A.J+ cells (≈2%), the percentage of H2A.J+ cells increased significantly after fractionated in vivo irradiation, from ≈40% at 72 h post-IR to ≈70% at 2 w post-IR. The number of SA-ß-Gal+ cells also increased significantly after IR exposure, but to clearly lower levels, from ≈1% in non-irradiated skin to ≈16% at 72 h post-IR and ≈40% at 2 w post-IR. These findings suggest that H2A.J expression in different regions of hair follicles cannot be equated with senescent keratinocytes. However, we observed slight differences in radiation-induced H2A.J expression between the different hair follicle regions, with the lowest expression in bulge regions as putative hair follicle stem cells niche. Hair follicles stem cells are characterized by their long-term potential for hair follicle regeneration. Previous studies have unraveled the specific role of histone modifications in maintaining the epigenetic control between stem cell quiescence and differentiation in skin homeostasis [15,16]. Based on our findings, we presume that differential H2A.J expression in different epidermal cell populations and the increased H2A.J expression after IR exposure may reflect an epigenetic regulation mechanism inducing an epidermal differentiation process in keratinocytes.

To evaluate the inflammatory effects of fractionated in vivo irradiation, we analyzed the secretion of different cytokines in skin supernatants by ELISA. Cytokines analysis of IL-6 and MCP-1 revealed slightly higher expression levels at 72 h and 1 w post-IR compared to non-irradiated controls, suggesting transient inflammatory effects after this fractionated in vivo irradiation, inducing no major damage in epidermal keratinocytes. Interleukin-8 has important functions in initiating inflammation in humans, attracting immune cells such as neutrophils, thereby contributing to chronic inflammation. However, mice normally do not have the IL-8 gene [17]; thus, our IL-8 measurements may reflect non-specific detection of other components.
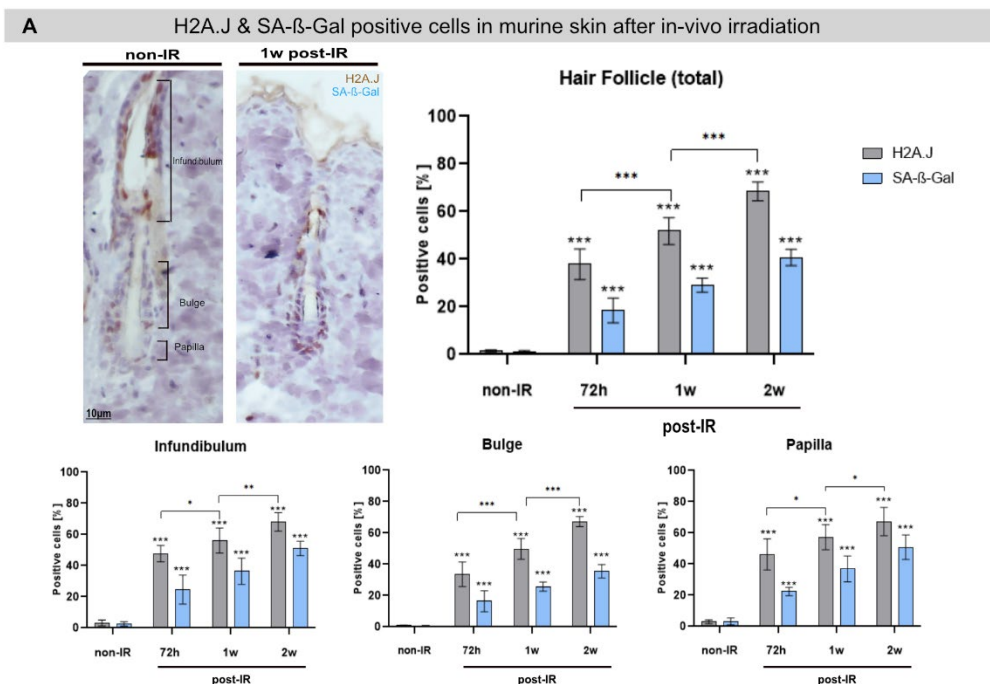
Figure 4. H2A.J and SA-ß-Gal expression in murine skin before and after fractionated in vivo IR exposure. (**A**) Graphic presentation of the quantification of H2A.J+ and SA-ß-Gal+ cells in different regions of murine hair follicles (infundibulum, bulge, papilla) before (non-IR) and at different time-points after fractionated in vivo irradiation (72 h, 1 w, and 2 w post-IR). * $p < 0.1$; ** $p < 0.01$; *** $p < 0.001$ (**B**) Graphic presentation of the quantification of IL-6, IL-8, and MCP-1 measured by ELISA in the supernatant of murine skin before (non-IR) and after fractionated in vivo irradiation (5 × 2Gy; 72 h, 1 w, and 2 w post-IR). Data are presented as mean ± SD ($n = 3$).

3. Discussion

The foreskin serves as the primary barrier to many pathogens and therefore has a very characteristic epidermal structure with specific immunological properties [18]. The thickened and more cornified foreskin epithelium is associated with highly increased H2A.J expression (even without IR exposure), potentially reflecting stronger differentiation and maturation processes to build up trans-epithelial resistance. The natural state of the male foreskin is characterized by chronic inflammatory milieu; this is in line with our observation of clearly increased secretion of inflammatory cytokines (already without IR exposure) [5]. In largely undifferentiated epidermal cell populations of murine hair follicles, by contrast, the basic expression of H2A.J was very low and only enhanced with increasing time after IR exposure. Direct comparison with SA-ß-Gal staining in different skin areas suggests that H2A.J is not a specific marker for cellular senescence but rather a marker for epithelial differentiation [19]. Based on our findings, we presume that differential H2A.J expression in various epidermal cell populations and increased H2A.J expression after IR exposure may reflect epigenetic regulation mechanisms inducing differentiation and maturation processes in keratinocytes.

Over recent years, 3D co-culturing methodologies of skin equivalents have been developed to mimic human skin pathology more accurately than commonly used 2D monolayer cell cultures [6]. Moreover, the possibility of generating cultured explants from patient-derived skin opened a new perspective to investigate individual radiation-induced skin reactions, thereby improving efficient translational research and personalized treatments [20]. Skin explants can be feasible solutions to address the missing link between the conditions in vivo and oversimplified 2D monolayer or 3D co-culturing models (such as spheroids or organoids) in vitro. Here, we used human foreskin explants to test H2A.J as a biological marker to measure senescent keratinocytes after IR exposure.

Predictive assays testing individual radiosensitivity would greatly help to establish personalized risk specifications for radiotherapy, with the perspective of modifying the treatment in radiosensitive individuals. However, our findings suggest that H2A.J expression is not a feasible marker for radiation-induced senescence in foreskin explants and cannot predict radiation-induced skin toxicity.

Previous in vitro studies indicate that H2A.J incorporation into the chromatin of senescent cells leads to epigenetic modifications and is associated with the secretion of inflammatory cytokines, collectively known as SASP [10,11]. In previous studies investigating abdominal skin biopsies from adult donors before and after ex vivo IR exposure, we

could show that the H2A.J expression was significantly increased in keratinocytes of irradiated skin, suggesting that H2A.J may be a promising marker for radiation-induced senescence and may predict radiotherapy responses [12]. Here, analyzing foreskin explants from young donors (1–9 years), we observed extremely high H2A.J expression levels in all epidermal layers, even without genotoxic stress by IR exposure. This observation is in sharp contrast to our previous results, showing only low H2A.J expression levels ($\approx$20%) in the abdominal epidermis of young donors ($\leq$20 years) but highly increased H2A.J expression levels ($\approx$70%) in aged donors ($\geq$60 years)[12]. Moreover, analyzing foreskin explants, we found no radiation-induced increase in H2A.J or cytokine expression levels. Collectively, H2A.J expression and cytokine secretion in keratinocytes of human foreskin explants were dramatically higher -before and after IR exposure- than in other human body skin or in undifferentiated keratinocytes of murine hair follicles. Based on these findings, we presume that histone variant H2A.J is associated with the epigenetic regulation of epidermal keratinocytes during their progression from the undifferentiated basal to the differentiated state. Moreover, increased H2A.J expression in relatively undifferentiated keratinocytes after IR exposure may reflect the early activation of differentiation processes in response to DNA damage. Genotoxic stress triggers cascades of inflammatory signaling pathways, leading to the release of pro-inflammatory factors and thereby modulating immune responses [21]. Further mechanistic understanding of DNA damage-induced immunomodulatory responses on skin homeostasis after IR exposure might shed light on the complex pathophysiology of radiation-induced dermatitis.

Dynamic epigenetic changes allow keratinocytes to regulate their gene expression programs to fulfill specialized cellular functions within different epidermal layers. Upon their maturation process, differentiated keratinocytes exit the cell cycle and migrate from the basal layer through the more superficial spinous and granular layers, culminating in their cornification and cell death. How keratinocytes dynamically govern the hierarchy of self-renewal, differentiation, and maturation to finely balance proliferation and differentiation processes is still poorly understood [13,22,23]. Keratinocyte function depends on complex gene regulatory networks that ultimately determine gene expression changes and guide the transition from basal to differentiated keratinocyte states. Epigenetic modifications such as the incorporation of histone variant H2A.J may impact the transcriptional regulation of keratinocytes and are likely coupled to the spatial organization of the epidermis. We observed substantial differences between the abdominal and foreskin epidermis in terms of thickness and level of keratinization, likely reflecting their skin-specific exposures to mechanical stress and environmental stimuli [5]. Based on the characteristic staining patterns in different epidermal keratinocytes, we presume that H2A.J expression may have a previously unappreciated role in epigenetic regulation of keratinocyte transition from basal to differentiated states.

In radiotherapy, the threshold range for transient erythema of the skin is 3–5 Gy, and prolonged erythema has threshold ranges of 5–10 Gy. We intended the application of a dose that evokes an inflammatory response but does not damage the foreskin explant too much by radiation-induced apoptosis or necrosis. In the mouse model, fractionated irradiation was carried out in vivo in accordance with the clinical conditions of patients in radiotherapy. This prolonged irradiation schedule is only possible in vascularized mouse skin in vivo but not in non-vascularized foreskin explants in vitro since its cultivation period is limited to a few days. The biological effect of a single dose of 10 Gy and fractionated irradiation of 5 × 2 Gy (=10 Gy) is indeed very different. Despite this lower biological effect, we observed the radiation-induced upregulation of H2A.J in the largely undifferentiated keratinocytes of the hair follicles of mouse skin during fractionated irradiation.

In addition to providing a physical barrier to the outside world, the skin is also an active immune organ, comprised of highly complex networks of innate and adaptive immune cells, whereby different anatomical skin areas have specific immunologic features [13]. The foreskin may develop microtrauma during sexual activity, with disrupted epi-

thelial barriers permitting the entry of pathogens. Previous studies on foreskin pathophysiology described clear differences to normal body skin regarding the cornified envelope, structures of tight junctions, densities of infiltrating immune cells, and secretion of inflammatory cytokines [5]. Together these different features regulate the barrier function of the pluri-stratified foreskin and may explain its increased epithelial resistance upon IR exposure.

Communication between damaged or senescent keratinocytes and their microenvironment plays an important role in the pathophysiology of skin inflammation [21]. However, complex tissue organization with the interaction between the epidermal and dermal compartment and their specific immune responses cannot faithfully be reproduced using foreskin explants. Skin reconstructs mimicking epidermis and dermis similar to in vivo conditions have to be developed to study the pathophysiology of radiation-induced skin injury. However, challenges remain in the manufacturing of skin reconstructs that recreate physiologically relevant microenvironments and encompass main skin cells, incorporate perfused vasculature and skin appendages, as well as components of the immune system.

4. Materials and Methods

4.1. Human Foreskin Collection

Foreskin samples were collected from young, healthy volunteers (1–9 years, n = 12) with medical indications for circumcision. Protocol procedures were approved by local ethics committee ("Ethikkommission der Ärztekammer des Saarlandes"). The parents of study participants provided written informed consent for the collection and analysis of normally discarded foreskin tissues.

4.2. Ex Vivo Irradiation of Cultured Foreskin Explants

Foreskin explants were rinsed with PBS and divided into small pieces (0.5 cm²). Foreskin samples were incubated dermal side down on polyethylene membranes and epidermal side exposed to air in 6-well plates (each well filled with 2 mL medium) at 37 °C under 5% CO_2. The culture medium consisted of DMEM, 10,000 units of penicillin, 10 mg/mL streptomycin, and 200 mM/L glutamine. After air-medium interface cultivation for 24 h, foreskin explants were exposed to IR with 10Gy (6-MV photons, 2 Gy/min) using the linear accelerator Artiste™ (Siemens, Munich, Germany). Twenty-four hours after IR exposure, foreskin tissue samples were embedded for microscopic analysis, and the supernatant was used for cytokine measurement (Supplementary Figure S1A). Histopathological studies confirmed the viability and functionality of our foreskin culture method (Supplementary Figure S1B). Moreover, for different culture periods, we observed no variations in H2A.J+ cell numbers, suggesting that foreskin keratinocytes maintain their epigenetic status (Supplementary Figure S2).

4.3. Immunohistochemistry (IHC)

Formalin-fixed foreskin samples were embedded in paraffin and sectioned at 4 μm thickness. After dewaxing in xylene and rehydration in decreasing concentrations of alcohol, antigen retrieval was performed in citrate buffer, and sections were incubated with anti-H2A.J-antibody (Active Motif, 61793, Carlsbad, CA, USA) followed by biotin-labeled antibodies (Dako, Glostrup, Denmark). Staining was completed by incubation with 3,3′-diaminobenzidine and substrate chromogen. Finally, sections were counterstained with hematoxylin and mounted with Aqueous Mounting Medium (Dako, Glostrup, Denmark). For the visualization of connective tissue, the Masson-Goldner trichromic staining technique was carried out according to the manufacturer's instructions (Masson-Goldner staining kit, Merck, Darmstadt, Germany).

4.4. Immunofluorescence Microscopy (IFM)

Formalin-fixed foreskin tissues were embedded in paraffin and sectioned to 4 μm thickness. After dewaxing in xylene and rehydration in decreasing concentrations of alcohol, sections were boiled in citrate buffer and blocked with 2% goat serum (Carl Roth, Karlsruhe, Germany). Sections were incubated with primary antibodies (anti-H2A.J, Active Motive; anti-Ki67, Abcam, Berlin, Germany), followed by AlexaFluor-488 or AlexaFluor-568 secondary antibodies (Invitrogen Waltham, MA, USA). Finally, sections were mounted in VECTAshield™ with 4′,6-diamidino-2-phenylindole (DAPI; Vector Laboratories, Burlingame, CA, USA). For quantitative analysis ≥1000 epidermal cells were registered for each sample, and H2A.J+ and Ki67+ cells were counted using Nikon E600 epifluorescent microscope (Nikon, Düsseldorf, Germany). To analyze the distribution of H2A.J in different epidermal layers, H2A.J+ cells were enumerated separately in *stratum granulosum spinosum/basale*, and the relative amounts of H2A.J+ cells were depicted per layer.

4.5. Fractionated In Vivo Irradiation of Mice

Eight-week-old male C57BL/6 mice (Charles River Laboratories, Sulzfeld, Germany) were housed in groups in IVC cages under standard laboratory conditions. Whole-body irradiation with 5 fractions of 2 Gy (daily IR exposure from Monday to Friday) was performed at the linear accelerator (Artiste™, Siemens), as described previously [24]. Then, 72 h, 1, and 2 weeks after the last IR exposure (sham-)irradiated animals ($n = 3$ per time-point and treatment-group, 18 animals in total) were anesthetized intraperitoneally using Ketamine and Rompun prior to tissue collection. Experimental studies were approved by the Medical Sciences Animal Care and Use Committee of Saarland.

4.6. SA-β-Gal Staining

Skin samples were dissected from the back of mice, fixed, and stained overnight with X-Gal solution according to the manufacturer's instructions (Merck Millipore, MA, USA). After overnight incubation, skin samples were washed, fixed in 4% PFA, and embedded in paraffin. Embedded skin tissue was further processed as already described above for IHC. Senescent cells were identified as blue-stained cells under light microscopy.

4.7. Enzyme-Linked ImmunoSorbent Analysis (ELISA)

Supernatants (2mL per well) were collected from cultured (non-irradiated and irradiated) human foreskin or murine skin samples (sized 0.5 cm^2) and were frozen at −80 °C until analysis. ELISA kits available for purchase (human: Invitrogen, KHC-0061, KHC-0081, BMS281, Carlsbad, CA, USA; murine: Abcam, ab100713, ab208979, Cambridge, UK; MyBioSource, MBS7606860, San Diego, CA, USA) were used to screen the SASP factors IL-6, IL-8, and MCP-1 with standard ELISA plate reader, according to the supplier's protocol.

4.8. Statistical Analysis

Statistical analyses were performed by unpaired t-test using Graphpad Prism software (Version 8, GraphPad Software, San Diego, CA, USA). Statistical significance was presented as * $p < 0.05$, ** $p < 0.01$, and *** $p < 0.001$.

Author Contributions: Y.H. and S.M. acquired the human foreskin samples and evaluated patient data. G.T. performed animal experiments and analyzed murine skin. Y.H., G.T., D.J., and Z.S. performed IHC, IFM, and ELISA experiments. Z.S. and J.P. prepared the data visualization and presentation. C.E.R. planned, managed, and coordinated the research activities, acquired the funding for

the project, and wrote the manuscript. All authors edited the manuscript. All authors have read and agreed to the published version of the manuscript.

References

1. Yee, C.; Wang, K.; Asthana, R.; Drost, L.; Lam, H.; Lee, J.; Vesprini, D.; Leung, E.; DeAngelis, C.; Chow, E. Radiation-induced Skin Toxicity in Breast Cancer Patients: A Systematic Review of Randomized Trials. *Clin. Breast Cancer* **2018**, *18*, e825–e840.
2. Lee, H.; Hong, Y.; Kim, M. Structural and Functional Changes and Possible Molecular Mechanisms in Aged Skin. *Int. J. Mol. Sci.* **2021**, *22*, 12489.
3. Watt, F.M. Mammalian skin cell biology: At the interface between laboratory and clinic. *Science* **2014**, *346*, 937–940.
4. Johansson, J.A.; Headon, D.J. Regionalisation of the skin. *Semin. Cell Dev. Biol.* **2014**, *25–26*, 3–10.
5. Lemos, M.P.; Lama, J.R.; Karuna, S.T.; Fong, Y.; Montano, S.M.; Ganoza, C.; Gottardo, R.; Sanchez, J.; McElrath, M.J. The inner foreskin of healthy males at risk of HIV infection harbors epithelial CD4+ CCR5+ cells and has features of an inflamed epidermal barrier. *PLoS ONE* **2014**, *9*, e108954.
6. Liu, H.; Tuchinda, P.; Fishelevich, R.; Harberts, E.; Gaspari, A.A. Human in vitro skin organ culture as a model system for evaluating DNA repair. *J. Dermatol. Sci.* **2014**, *74*, 236–241.
7. Wang, A.S.; Dreesen, O. Biomarkers of Cellular Senescence and Skin Aging. *Front. Genet.* **2018**, *9*, 247.
8. Sharpless, N.E.; Sherr, C.J. Forging a signature of in vivo senescence. *Nat. Rev. Cancer* **2015**, *15*, 397–408.
9. Tchkonia, T.; Zhu, Y.; Van Deursen, J.; Campisi, J.; Kirkland, J.L. Cellular senescence and the senescent secretory phenotype: Therapeutic opportunities. *J. Clin. Investig.* **2013**, *123*, 966–972.
10. Contrepois, K.; Coudereau, C.; Benayoun, B.A.; Schuler, N.; Roux, P.-F.; Bischof, O.; Courbeyrette, R.; Carvalho, C.; Thuret, J.-Y.; Ma, Z.; et al. Histone variant H2A.J accumulates in senescent cells and promotes inflammatory gene expression. *Nat. Commun.* **2017**, *8*, 14995.
11. Isermann, A.; Mann, C.; Rübe, C. Histone Variant H2A.J Marks Persistent DNA Damage and Triggers the Secretory Phenotype in Radiation-Induced Senescence. *Int. J. Mol. Sci.* **2020**, *21*, 9130.
12. Rübe, C.E.; Bäumert, C.; Schuler, N.; Isermann, A.; Schmal, Z.; Glanemann, M.; Mann, C.; Scherthan, H. Human skin aging is associated with increased expression of the histone variant H2A.J in the epidermis. *npj Aging Mech. Dis.* **2021**, *7*, 7.
13. Hsu, Y.-C.; Li, L.; Fuchs, E. Emerging interactions between skin stem cells and their niches. *Nat. Med.* **2014**, *20*, 847–856.
14. Liu, N.; Matsumura, H.; Kato, T.; Ichinose, S.; Takada, A.; Namiki, T.; Asakawa, K.; Morinaga, H.; Mohri, Y.; De Arcangelis, A.; et al. Stem cell competition orchestrates skin homeostasis and ageing. *Nature* **2019**, *568*, 344–350.
15. Avgustinova, A.; Benitah, S.A. Epigenetic control of adult stem cell function. *Nat. Rev. Mol. Cell Biol.* **2016**, *17*, 643–658.
16. Kang, S.; Chovatiya, G.; Tumbar, T. Epigenetic control in skin development, homeostasis and injury repair. *Exp. Dermatol.* **2019**, *28*, 453–463.
17. Asfaha, S.; Dubeykovskiy, A.N.; Tomita, H.; Yang, X.; Stokes, S.; Shibata, W.; Friedman, R.A.; Ariyama, H.; Dubeykovskaya, Z.A.; Muthupalani, S.; et al. Mice That Express Human Interleukin-8 Have Increased Mobilization of Immature Myeloid Cells, Which Exacerbates Inflammation and Accelerates Colon Carcinogenesis. *Gastroenterology* **2013**, *144*, 155–166.
18. Pasparakis, M.; Haase, I.; Nestle, F.O. Mechanisms regulating skin immunity and inflammation. *Nat. Rev. Immunol.* **2014**, *14*, 289–301.
19. Ho, C.Y.; Dreesen, O. Faces of cellular senescence in skin aging. *Mech. Ageing Dev.* **2021**, *198*, 111525.

20. Albrecht, H.; Durbin-Johnson, B.; Yunis, R.; Kalanetra, K.M.; Wu, S.; Chen, R.; Stevenson, T.R.; Rocke, D.M. Transcriptional Response of Ex Vivo Human Skin to Ionizing Radiation: Comparison Between Low- and High-Dose Effects. *Radiat. Res.* **2012**, *177*, 69–83.

21. Mansfield, K.; Naik, S. Unraveling Immune-Epithelial Interactions in Skin Homeostasis and Injury. *Yale J. Biol. Med.* **2020**, *93*, 133–143.

22. Aragona, M.; Dekoninck, S.; Rulands, S.; Lenglez, S.; Mascre, G.; Simons, B.D.; Blanpain, C. Defining stem cell dynamics and migration during wound healing in mouse skin epidermis. *Nat. Commun.* **2017**, *8*, 14684.

23. Hsu, Y.-C.; Fuchs, E. A family business: Stem cell progeny join the niche to regulate homeostasis. *Nat. Rev. Mol. Cell Biol.* **2012**, *13*, 103–114.

24. Schmal, Z.; Isermann, A.; Hladik, D.; von Toerne, C.; Tapio, S.; Rübe, C.E. DNA damage accumulation during fractionated low-dose radiation compromises hippocampal neurogenesis. *Radiother. Oncol.* **2019**, *137*, 45–54.